TAMPEREEN TEKNILLINEN YLIOPISTO
TAMPERE UNIVERSITY OF TECHNOLOGY
Julkaisu 636 • Publication 636

Robert Herda

Semiconductor Mirrors for Ultrafast Fiber Technology

Tampere 2006

Tampereen teknillinen yliopisto. Julkaisu 636
Tampere University of Technology. Publication 636

Robert Herda

Semiconductor Mirrors for Ultrafast Fiber Technology

Thesis for the degree of Doctor of Technology to be presented with due permission for public examination and criticism in Sähkötalo Building, Auditorium S1, at Tampere University of Technology, on the 1st of December 2006, at 12 noon.

Tampereen teknillinen yliopisto - Tampere University of Technology
Tampere 2006

ISBN 952-15-1684-4 (printed)
ISBN 952-15-1720-4 (PDF)
ISSN 1459-2045

ABSTRACT

This thesis studies the design of Semiconductor Saturable Absorber Mirrors (SESAMs) and their properties in mode-locked fiber lasers. The recovery times of SESAMs were controlled by ion bombardment and metamophoric growth. Quantum-dot structures enabled fast absorber recovery. In resonant saturable absorbers the modulation depth is enhanced, while the saturation fluence is decreased. The strong self-starting mechanism of high-modulation-depth and low-saturation-energy absorbers was used to achieve reliable mode locking without the need for dispersion compensation, while maintaining stability against Q-switched mode locking. It was shown that the two-photon absorption can become the dominant nonlinear mechanism in resonant SESAMs. Two-photon absorbtion in resonant absorbers can improve the stability against Q-switching instabilities; however, excessive two-photon absorption can decrease the modulation depth of a saturable absorber and, therefore, prevent mode locking.

The influence of the SESAM recovery time on the pulse quality was investigated. A fast absorber is preferable in order to avoid instabilities in the pulse shapes and to generate highly compressible pulses. We studied the effect of the recovery time on the self-starting operation of a mode-locked fiber laser. It was shown that amplified spontaneous emission can saturate a slow absorber and, therefore, degrade the modulation depth and prevent self-starting operation. Finally, we demonstrated synchronized operation of a mode-locked 1.55 μm erbium fiber laser to a mode-locked 1.05 μm ytterbium fiber laser using a semiconductor mirror as an optically driven modulator.

ACKNOWLEDGMENTS

The work presented in this thesis has been carried out at the Optoelectronics Research Centre (ORC) at the Tampere University of Technology from 2003 to 2006. I gratefully acknowledge the financial support provided by a Marie Curie Scholarship, by the European Commission through the URANUS project, and by the Academy of Finland through the Tule-QUEST project.

I would like to thank my supervisor Prof. Oleg Okhotnikov for his energetic support of me and my research. His enthusiasm and passion for the work in ultrafast fiber lasers helped me to achieve a high standard of research. I am also thankful for Prof. Markus Pessa's encouragement and support. Thanks to Antti Isomäki, Antti Härkönen, Dionísio Pereira, Esa Saarinen, Lasse Orsila, Luis Gomes and Dr. Mircea Guina for valuable help and discussions. Special thanks to Matei Rusu for sharing his great expertise on research equipment and his sense of humor throughout the laboratory work. I would like to thank Samuli Kivistö for producing a countless number of fiber couplers and Tommi Hakulinen for characterizing a countless number of absorbers. I would like to thank the MBE group, in particular Soile Suomalainen and Anne Vainionpää, for growing these absorbers. My work has also benefited from the cooperation with Prof. Edik Rafailov from the University of Dundee and Maria Ana Cataluna from the University of St. Andrews. I would like to express my gratitude to Anne Viherkoski and Kerttu Marttila for helping me in administrative issues.

Above all I would like to thank my colleagues from the Ultrafast and Intense Optics group who have made my stay in Finland enjoyable. Special thanks to Katrina Wendel for helping me to improve the style of this thesis, for being there for me, and for giving me encouragement during my time in Tampere. I would like to thank my brother for the fun times we had. Finally, I would like to thank my parents for their support and giving me the freedom to pursue my goals. Without them I would not have found the inspiration to keep up my studies.

Tampere, Finland, November 2006

Robert Herda

TABLE OF CONTENTS

LIST OF PUBLICATIONS

This thesis contains some unpublished material but is mainly based on the following publications, which are included as appendices. In the text, these publications are referred to as [P1]...[P5].

[P1] R. Herda and O. G. Okhotnikov, "Dispersion Compensation-Free Fiber Laser Mode-Locked and Stabilized by High-Contrast Saturable Absorber Mirror," *IEEE Journal of Quantum Electronics*, vol. 40, 2004, pp. 893–899.

[P2] R. Herda and O. G. Okhotnikov, "Effect of amplified spontaneous emission and absorber mirror recovery on the dynamics of mode-locked fiber lasers," *Applied Physics Letters*, vol. 86, 2005, pp. 0111131–0111133.

[P3] R. Herda, M. Rusu, A. Vainionpää, S. Suomalainen, O. Tengvall, and O. G. Okhotnikov, "Semiconductor All-Optical Modulator for Synchronization of Independent Fiber Laser Oscillators and Active Mode-Locking," *IEEE Journal of Quantum Electronics*, vol. 41, 2005, pp. 774–778.

[P4] R. Herda, T. Hakulinen, S. Suomalainen, and O. G. Okhotnikov, "Cavity-enhanced saturable and two-photon absorption in semiconductors," *Applied Physics Letters*, vol. 87, 2005, pp. 21111051–21111053.

[P5] R. Herda, O. G. Okhotnikov, E. U. Rafailov, W. Sibbett, P. Crittenden, and A. Starodumov, "Semiconductor Quantum-Dot Saturable Absorber Mode-Locked Fiber Laser," *IEEE Photonics Technology Letters*, vol. 18, 2006, pp. 157–159.

The following supplementary papers are related to this work but are not appended to this dissertation. In the text, these publications are referred to as [S1]...[S9].

[S1] S. Suomalainen, A. Vainionpää, O. Tengvall, T. Hakulinen, R. Herda, S. Karirinne, and O. G. Okhotnikov, "Long wavelength semiconductor saturable absorber mirrors using metamophoric InP grown on GaAs by Molecular Beam Epitaxy," *Journal of Vacuum Science and Technology B*, vol. 24, 2006, pp. 1496–1499.

[S2] T. Hakkarainen, E. Pavelescu, K. Arstila, V. Dhaka, T. Hakulinen, R. Herda, J. Kontinnen, N. Katchenko, H. Lemmetyinen, and J. Keinonen, "Optical properties of ion irradiated and annealed InGaAs/GaAs quantum wells and semiconductor saturable absorber mirrors," *Journal of Physics D*, vol. 38, 2005, pp. 985–989.

[S3] M. Rusu, R. Herda, and O. G. Okhotnikov, "Passively synchronized Erbium (1550 nm) and Ytterbium (1040 nm) mode-locked fiber lasers sharing the cavity," *Optics Letters*, vol. 29, 2004, pp. 2246–2248.

[S4] M. Rusu, R. Herda, and O. G. Okhotnikov, "Passively synchronized two-color mode-locked fiber system based on master-slave lasers geometry," *Optics Express*, vol. 12, 2004, pp. 4719–4724.

[S5] M. Rusu, R. Herda, and O. G. Okhotnikov, "1.05-m mode-locked Ytterbium fiber laser stabilized with the pulse train from a 1.54-m laser diode," *Optics Express*, vol. 12, 2004, pp. 5258–5262.

[S6] R. Herda and O. G. Okhotnikov, "All-fiber soliton source tunable over 500 nm," *CLEO 2005*, poster JWB39, Baltimore, USA.

[S7] M. Rusu, E. U. Rafailov, R. Herda, O. G. Okhotnikov, S. M. Saltiel, P. Battle, S. McNeil, A. B. Grudinin, and W. Sibbett, "Efficient generation of green and UV light in a single PP-KTP waveguide pumped by a compact all-fiber system," *Applied Physics Letters* vol. 88, 2006, pp. 121105-1–121105-3.

[S8] M. Rusu, R. Herda, S. Kivistö, and O. G. Okhotnikov,"Fiber taper for dispersion management in a mode-locked ytterbium fiber laser," *Optics Letters*, vol. 31, 2006, pp. 2257–2259.

[S9] R. Herda, A. Isomäki, and O. G. Okhotnikov, "Soliton sidebands in photonic bandgap fiber lasers," *Electronics Letters*, vol. 42, 2006, pp. 19–20.

AUTHOR'S CONTRIBUTION

This thesis includes 5 papers published in international peer-reviewed journals. It also contains material from supplementary publications and new unpublished results.

The work presented here is the result of teamwork. I have been directly responsible for the mode-locking experiments presented in this thesis and the implementation of the numerical simulations.

A summary of my contribution to the included papers is listed in Table 1 below.

Paper	Contribution in research work	Contribution in writing the paper
[P1]	Group work (60%)	Main author
[P2]	Group work (80%)	Main author
[P3]	Group work (40%)	Main author
[P4]	Group work (60%)	Main author
[P5]	Group work (60%)	Main author

Table 1: *Author's contribution to the papers and to the research work.*

LIST OF ABBREVIATIONS

ASE	Amplified Spontaneous Emission
cw	continuous wave
DBR	Distributed Bragg Reflector
NLSE	Nonlinear Schrödinger equation
QSML	Q-Switched Mode Locking
QW	Quantum Well
RTA	Rapid Thermal Annealing
SEMM	SEmiconductor Modulator Mirror
SESAM	SEmiconductor Saturable Absorber Mirror
SPM	Self-Phase Modulation
TPA	Two-Photon Absorption

LIST OF SYMBOLS

β_2	second order dispersion
β_3	third order dispersion
γ	nonlinear parameter
ω	optical frequency
ω_G	gain bandwidth
ω_M	modulation frequency
τ_A	absorber recovery time
τ_G	gain recovery time
τ_P	pulse duration
$E_{sat,A}$	absorber saturation energy
$E_{sat,G}$	gain saturation energy
E_2	inverse slope of two photon absorption
E_P	pulse energy
g	gain
l	loss
$P_{sat,A}$	absorber saturation power
$P_{sat,G}$	gain saturation power
q_0	modulation depth
t	time
T_R	round-trip time

1. INTRODUCTION

"Light can be gentle, dangerous, dreamlike, bare, living, dead, misty, clear, hot, dark, violet, springlike, falling, straight, sensual, limited, poisonous, calm and soft." - Sven Nykvist

Since the invention of the ruby laser [1], the range of available lasers and the range of applications spread widely. Due to their low cost, diode lasers have conquered a vast range of applications and can be found in every household CD and DVD player. In contrast to these low-cost systems, ultrashort pulse lasers are mainly used in scientific research and highly specialized areas in industry. These lasers are mostly solid state lasers since they are superior to fiber lasers when short high-energy pulses have to be provided directly from the laser; however, solid state lasers do not meet the conventional requirements of simplicity, maintenance, and reliability.

Today, fiber lasers are superior to solid state lasers in terms of maintenance requirements, compactness and costs. Ultrafast high-energy pulse fiber laser systems could replace solid state lasers in different areas and extend the application range of short pulse fiber lasers. Ytterbium-doped fiber lasers cover a wavelength range that makes them suitable to replace Nd:YAG lasers and long-wavelength Ti:Sapphire lasers. Fiber lasers cover the whole visible spectrum when using nonlinear frequency conversion. Using chirped pulse amplification in fibers, a few-hundred femtosecond pulses can be amplified to microjoule pulse energy [2]. With the advent of novel, reliable, cost-effective pulsed fiber sources, ultrafast lasers could be widely used as medical instruments in eye surgery [3] and dental surgery [4], tissue welding [5], and micromachining [6]. This thesis investigates short-pulse fiber lasers in order to extend their operation range eventually into these application areas.

Semiconductor Saturable Absorber Mirrors (SESAMs) are efficient triggers for pulsed operation. The goal of this thesis is to optimize the use of SESAMs in fiber lasers to work towards reliable, short pulse sources.

Chapter 2 reviews the mode-locking theory, both active and passive, and the modeling of fiber lasers. The theory of self-starting and Q-switched mode locking is presented.

Chapter 3 introduces different methods to change the parameters of saturable absorbers. Several methods to shorten the recovery time are presented. The properties of resonant SESAMs are discussed.

Chapter 4 investigates the influence of the absorber parameters of modulation depth, saturation energy, and recovery time on the pulse quality and the self-starting properties of a mode-locked fiber laser. Furthermore, the role of two-photon absorption in resonant absorbers is examined.

Chapter 5 presents an application of a semiconductor saturable absorber mirror as an all-optically driven modulator for synchronization of two mode-locked fiber lasers and for active mode locking.

2. REVIEW OF MODE-LOCKED FIBER LASERS

This chapter initially gives a short overview of the history of mode locking and reviews the concepts of active and passive mode locking with an emphasis on passively mode-locked fiber lasers. The modeling of passively mode-locked fiber lasers is reviewed, which includes the pulse propagation in saturable absorbers and fibers. Finally, this section reviews the theory of self-starting and discusses how to avoid Q-switching and Q-switched mode locking.

2.1 Mode-locking techniques

Several methods are used to achieve short pulse durations. With Q-switched lasers pulse durations can range from nanoseconds [7] to tens of picoseconds [8]. In order to achieve pulse durations in the *ps* or *fs* range mode-locking techniques must be used.

The first demonstration of mode locking was in the 1960s with Nd:glass as the active material [9]. Sub-picosecond pulses were first realized in dye lasers. In these lasers organic dyes served as the gain and as the saturable absorber medium. Remarkably, the generated pulses had a much shorter duration than the recovery times of the gain and absorber materials. The shortest pulse duration achieved directly from a dye laser was 27 *fs* [10]. Today the most popular gain medium to achieve ultrafast pulses is Titan-Sapphire. Five *fs*-pulses which consist of two-optical pulses were generated [11]. The pulse shortening mechanism in this case is a combination of Kerr-Lens mode-locking (KLML) [12] and Saturable Absorber Semiconductor Mirror (SESAM) mode locking. The SESAM reliably starts the laser and the KLML provides the fast pulse shortening to *fs* durations.

While the objective is to achieve as short as possible pulse durations, a conflicting requirement is to achieve compact, reliable, maintenance-free pulse generators. Today, a compact, low-cost, sub-picosecond high-energy system can only be realized with fiber technology. Fiber pigtailed, high-power, single-mode diode lasers [13] provide reliable, direct-electrically powered, pump sources. Fiber components provide as isolators, dichroic couplers, and output couplers the possibility to build all-fiber integrated setups [14, 15]. Rare-earth dopants enable mode locking at wavelengths from

900 *nm* using Neodymium [16] to 1900 *nm* using Thulium [17, 18]. Due to this wide wavelength range and their relatively easy implementation, fiber lasers are versatile pulsed sources.

2.1.1 Active mode locking

Active mode locking is a method of generating ultrashort pulses using an external signal. In its simplest case an actively mode-locked laser consists of two mirrors, which terminate the laser cavity, the gain material, and the modulator. The modulator can either be an amplitude or a phase modulator [19]. In a laser cavity with round-trip time T_R, different axial modes are separated by the frequency

$$\Delta\omega_e = 2\pi\frac{1}{T_R}. \tag{2.1}$$

In an actively mode-locked laser an amplitude or phase modulator is driven at a frequency ω_m, which is close to the frequency separation of the cavity modes.

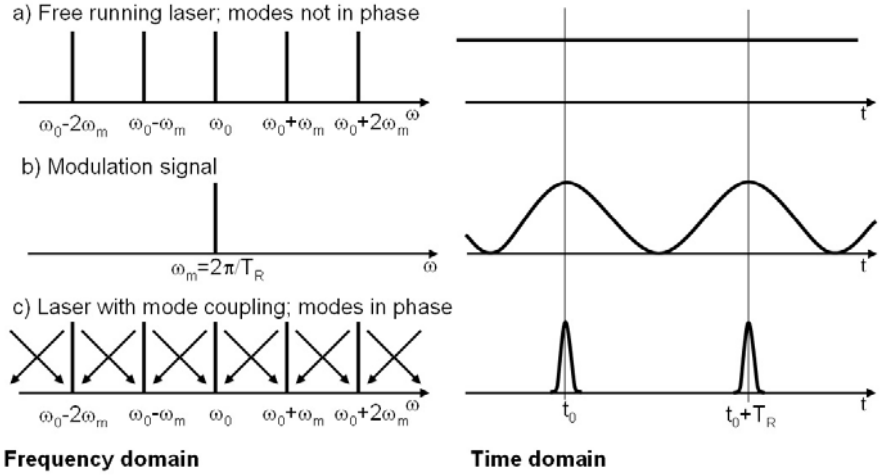

Fig. 2.1: *Illustration of the active mode-locking principle. The left side shows the frequency domain and the right side, the time domain. (a) Shows the amplitude of a free running laser, in the frequency domain different cavity-frequency modes have random phase and are spaced equally, separated by ω_M around a central frequency ω_0. In the time domain this results in a constant amplitude. (b) Shows the modulation signal with a single frequency component at ω_M, which corresponds to a sine-shaped modulation with a period equal to the round-trip time T_R. (c) When the modulation is applied, the cavity-frequency modes are locked to each other. In the time domain this results in the formation of short pulses.*

The term mode locking originates in the frequency domain description. The left side of Fig. 2.1 illustrates active mode locking in the frequency domain, whereas,

the right side illustrates the temporal structure of radiation [20]. In a continuous-wave laser, the different axial modes have random phase relation. If these modes are locked to each other, the energy will be concentrated around peaks separated by the round-trip time. When a laser is modulated at the frequency ω_M, the axial modes of the laser at frequency ω_e will acquire sidebands $\omega_e \pm n \cdot \omega_m$. The position of these sidebands is either exactly or very close to another axial mode of the laser. The axial modes communicate through these sidebands, and, therefore, become in phase with the modulator and couple together. If there are many spectral components coupled together in phase, they form a gaussian pulse. The minimum achievable pulse duration depends on the strength of the modulation; also, it depends on the gain bandwidth of the lasing material. A narrow gain bandwidth only supports a narrow spectrum and therefore it does not support very short pulses.

The active mode locking can be mathematically described by multiplicatives to the electric field E in the frequency and time domain. The gain profile can be described by a Lorentzian line-shape, which can be expanded to the second order around the center frequency ω_0 [21]. Then the gain perturbs an incident spectral amplitude $E(\omega)$ to

$$E'(\omega) = \left[1 + g\left(1 - \frac{(\omega-\omega_0)^2}{\omega_G^2}\right)\right] E(\omega), \tag{2.2}$$

where g is the gain and ω_G the gain bandwidth. The response for the slow varying amplitude $E(t)$ in the time domain is determined by the Fourier transform

$$E'(t) = \left[1 + g\left(1 + \frac{1}{\omega_G^2}\frac{d^2}{dt^2}\right)\right] E(t). \tag{2.3}$$

An amplitude modulator at fundamental repetition rate has typically a transmission of $1 - M(1 - cos(\omega_M t))$, where M is the modulation depth and ω_M the modulation frequency. It is also possible to drive the modulator at a multiple of the fundamental repetition rate to achieve harmonic mode locking [22]. Around the transmission peak maximum the modulation can be simplified to $1 - M(\omega_M t)^2/2$. For steady state operation $\{E'(t) = E(t)\}$ the amplitude is given by

$$\left[g\left(1 + \frac{1}{\omega_G^2}\frac{d^2}{dt^2}\right) - l - M\frac{(\omega_M t)^2}{2}\right] E(t) = 0, \tag{2.4}$$

where l represents the cavity losses. The solution of this equation is a pulse of Gaussian shape [23]:

$$E(t) = E_0 exp(-t^2/\tau_P^2). \tag{2.5}$$

Thus, the achievable pulse duration in an actively mode-locked laser is given by

$$\tau_P = \sqrt[4]{\frac{2g}{M\omega_M^2\omega_G^2}}. \tag{2.6}$$

This derivation does not take into account dispersion and self-phase modulation (SPM). Dispersion causes a pulse broadening and SPM a spectral broadening. In anomalous regime of dispersion, the limit given by Equation 2.6 can be overcome and subpicosecond operation can be achieved using soliton propagation [24]. 600 *fs* pulses have been generated using intra-cavity soliton pulse compression [25]. The drawback of the active mode locking is that the generation of shorter pulse durations depends on faster external modulation signals.

2.1.2 Passive mode locking

In contrast to active mode locking, the modulation in passive mode locking is not externally given but adapting to the duration of the pulse; therefore, passive mode locking enables the generation of shorter pulses than active mode locking. Passive mode locking is based on pulse formation using a nonlinear element. In the simplest case this is a saturable absorber material which has low loss for high and a high loss for small incident intensities. Since the low-intensity edges of the pulse get more attenuated and the peak becomes less attenuated, the pulse shortens with every pass through the absorber. Other methods of passive mode-locking are based on the use of artificial saturable absorbers generated by non-linear polarization rotation [26], self-phase modulation in loop mirrors [27], and interference in coupled cavities [28].

A description of mode locking in the time domain is more suitable for passive mode locking because the modulation is not sine-shaped as in active mode locking. The absorber response depends on the initial temporal pulse shape and would be very difficult to describe in the frequency domain. Thus, the pulse amplitude typically is described as a function of time. In a saturable absorber mode-locked laser the amplitude evolves with [21]

$$E'(t) = \left[g - l + \frac{1}{\omega_G^2}\frac{d^2}{dt^2} - q(t)\right] E(t), \tag{2.7}$$

where g is the saturated gain and $q(t)$ the saturable absorption. In case of a weakly saturated fast absorber, the absorber response can be approximated by

$$q(t) = q_0 - \frac{q_0}{P_a}|E(t)|^2. \tag{2.8}$$

q_0 is the modulation depth and P_a the saturation energy. Thus, the steady state re-

quires that

$$\left[g - l + \frac{1}{\omega_G^2}\frac{d^2}{dt^2} - q_0 + \frac{q_0}{P_a}|E(t)|^2\right] E(t) = 0. \tag{2.9}$$

The solution of this equation has the form

$$E(t) = E_0 sech(t/\tau_P). \tag{2.10}$$

It fulfills the equation if the pulse duration is

$$\tau_P = \frac{1}{\omega_G}\sqrt{\frac{2P_a}{|E_0|^2}} \tag{2.11}$$

and the saturated gain is

$$g = l + q_0 - \frac{1}{(\omega_G \tau_P)^2}. \tag{2.12}$$

The shortest pulse will be achieved if the absorber is completely saturated at the peak of the pulse. This is the case if $P_a = |E_0|^2$ [29]. The minimum achievable pulse duration is

$$\tau_P = \omega_G \sqrt{2/q_0}. \tag{2.13}$$

This equation can be quantitatively understood as an equilibrium between pulse shortening by an absorber at a rate of $\sqrt{q_0}$ and pulse broadening by the finite gain bandwidth ω_G.

2.2 Ultrafast Fiber Lasers

With the ability to build powerful, single-mode diode lasers, an efficient way was available to create population inversion in rare-earth doped optical fibers. Fig 2.2 shows the typical setup for an Ytterbium-doped fiber laser [30,31]. The gain material is pumped by a single-mode diode laser via a dichroic pump coupler. The length of the gain material typically varies between 5 cm to 1 m depending on the doping level of the fiber and the desired lasing wavelength. The output pulse train is detected via a fiber-tap coupler. Since glass has normal dispersion at wavelengths below 1300 *nm*, dispersion compensation is necessary to achieve overall anomalous cavity dispersion and to employ soliton propagation. The dispersion can be adjusted to be close to zero or to a negative value with grating pairs [32], tapers [S8], photonic crystal fibers [33], or photonic band-gap fibers [34, 35],[S9].

The lasing and pump wavelength of the fiber laser is determined by the fiber doping material. The most popular doping materials are erbium and ytterbium. Some optical properties of the gain media are listed in Table 2.1. Ytterbium has been employed as a gain material in most fiber lasers investigated in this thesis. Its wavelength range

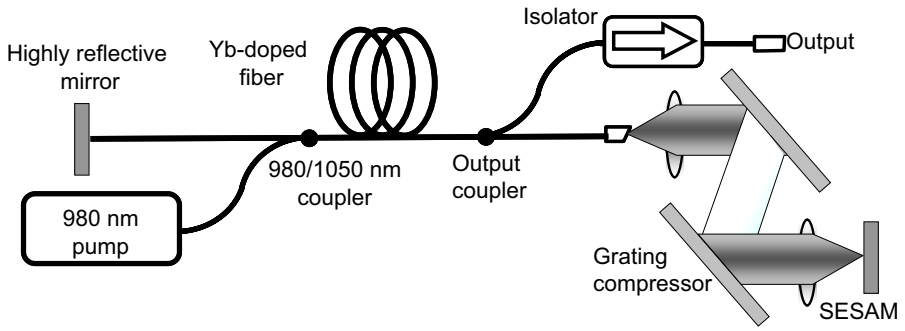

Fig. 2.2: *Typical setup of a mode locked fiber laser.*

cover 980 *nm* to 1160 *nm* [30, 36], which makes it suitable as a replacement for Nd:YAG lasers and for long-wavelength Ti:Sapphire solid-state lasers. Due to its large gain bandwidth, the generation of sub 50 *fs* pulses is possible [37]. The large saturation energy allows for extraction of high energy pulses in fiber amplifiers [38]. Erbium covers an emission wavelength between 1520 *nm* and 1600 *nm* [39], which is of special interest in telecommunication, because it lies in the low loss window of glass, and anomalous dispersion enables soliton transmission. The mode field diameters listed in Table 2.1 were calculated with the geometrical parameters given in the data sheets of the fibers INO Yb164 and INO Er123 using the fiber eigenvalue equation [40].

	Ytterbium	Erbium
Pump wavelength	920 *nm* or 980 *nm*	980 *nm* or 1480 *nm*
Typical lasing wavelengths	980 *nm* to 1160 *nm*	1520 *nm* to 1600 *nm*
Mode field diameter	5.3 μm	6.3 μm
Saturation energy	43 μJ [41]	10 μJ [42]
Recovery time	1.1 *ms* [41]	1.0 *ms* [43]

Table 2.1: *Typical parameters of ytterbium and erbium doped fibers.*

Fig. 2.3 shows the typical spectrum and autocorrelation of a mode-locked fiber laser. The solid line shows the experimental data and the dashed line simulation results. The simulation details are described in Section 2.3. The dotted graph in Fig. 2.3 (b) displays a simulated pulse shape. The fiber laser consisted of 50 *cm* Yb-doped fiber and 1 *m* of passive fiber. The out-coupling ratio is 10% and the laser delivers up to 10 *mW* output power. The dispersion compensation in this laser is provided by a transmission grating pair resulting in a total cavity dispersion of $-0.17\ ps^2$ with a grating separation of 18 *mm*. The gratings have a period of 0.8 μm. The laser emitted pulses with a spectral width of 2.1 *nm*. The pulse duration is 0.77 *ps* assuming a gaussian pulse shape. The time-bandwidth product of 0.46 indicates the soliton character of the pulse. The slight deviation from the transform-limited value of 0.44

is due to chirping in the output fiber. The soliton mode-locked fiber laser is a simple implementation of a sub-picosecond laser.

2.3 Numerical modeling of mode-locked fiber lasers

The Haus-master equation gives a compact description of passive mode locking. Assuming that the nonlinear and linear changes of the pulse within each round trip are small, the dynamics in a fiber laser can be described by [21]:

$$\frac{\partial A}{\partial z} = \frac{g-l-q}{2}A - \frac{\left((\omega_G)^2 + i\beta_2\right)}{2}\frac{\partial^2 A}{\partial T^2} + i\gamma|A|^2 A, \tag{2.14}$$

where β_2 is the second order fiber dispersion, q the saturable absorber loss per length, and g is the saturable fiber gain. This equation is useful for obtaining analytical solutions; however, it does not take into account the discreetness of the elements in a fiber laser.

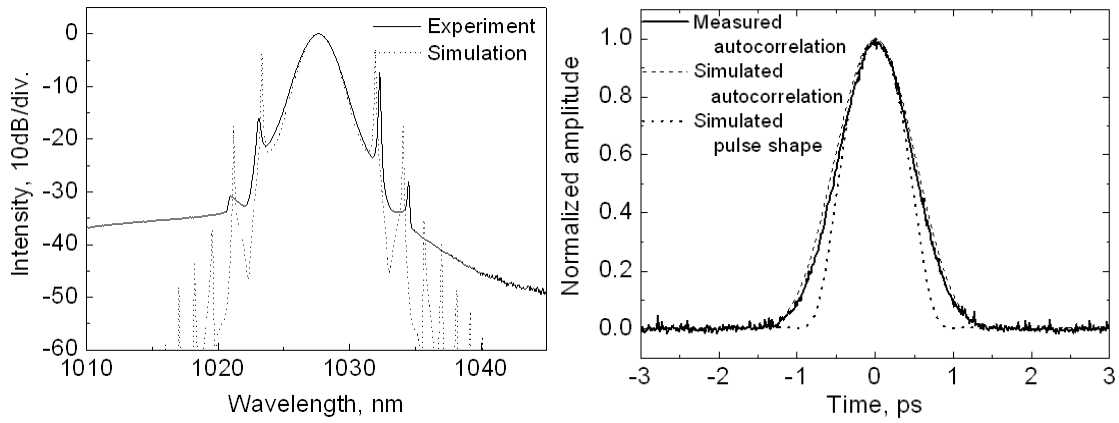

(a) (b)

Fig. 2.3: *(a) Spectrum of a mode-locked fiber laser (solid line: Experiment: dashed line: Simulation) (b) Pulse shape (solid line: Measured autocorrelation; dashed line: Simulated autocorrelation; dotted: Simulated pulse shape).*

For the numerical modeling of a fiber laser, the pulse should propagate through different elements consecutively. The fiber laser in Fig. 2.2 consists of an active fiber, a passive fiber, a grating pair, an output coupler, and the saturable absorber. This section describes how to numerically analyze these elements, particularly, the fiber and the saturable absorber.

2.3.1 Pulse Propagation in Fibers-Nonlinear Schrödinger Equation

The Nonlinear Schrödinger Equation (NLSE) [44] describes the propagation of the ultrashort pulse envelope A in a fiber. The form most commonly used for describing the pulse propagation in fiber lasers is

$$\frac{\partial A}{\partial z} = -\frac{i\beta_2}{2}\frac{\partial^2 A}{\partial T^2} + \frac{\beta_3}{6}\frac{\partial^3 A}{\partial T^3} + i\gamma|A|^2 A \tag{2.15}$$

where γ is the nonlinear parameter, β_2 the second order dispersion, and β_3 the third order dispersion. This equation includes a wide range of effects as pulse broadening due to dispersion, spectral broadening due to SPM, and soliton propagation. The equation can be easily extended to higher order nonlinear effects as self steepening and Raman shifting, which, however, proved to be negligible in fiber lasers.

Equation 2.15 can be numerically solved by the split-step Fourier method. For this purpose the propagation is divided into a nonlinear step and a dispersive step

$$\frac{\partial A}{\partial z} = (\hat{D} + \hat{N})A \tag{2.16}$$

with the operator

$$\hat{D} = -\frac{i\beta_2}{2}\frac{\partial^2}{\partial T^2} + \frac{\beta_3}{6}\frac{\partial^3}{\partial T^3} \tag{2.17}$$

and

$$\hat{N} = i\gamma|A|^2 . \tag{2.18}$$

The operator $\hat{D}$ describes the linear, dispersive propagation and the operator $\hat{N}$ nonlinear effects. The fiber is now divided into different sections. The propagation in each section is carried out in two steps: first the nonlinear step and then the dispersive step. A more accurate solution can be obtained by applying the nonlinear step in the center of the fiber section. Therefore, the propagation from point z to point $z+h$ can be approximated by

$$A(z+h,T) = exp(h/2\cdot\hat{D})exp(h\cdot\hat{N})exp(h/2\cdot\hat{D})A(z,T). \tag{2.19}$$

The nonlinear step is carried out with a multiplication in the time domain

$$exp(h\cdot\hat{N})A(z,t) = exp(ih\gamma|A(z,T)|^2)A(z,T) \tag{2.20}$$

and the dispersion step with a multiplication in the frequency domain

$$exp(h\cdot\hat{D})A(z,t) = \frac{1}{2\pi}\int_{-\infty}^{\infty}\tilde{A}(z,\omega)exp\left(\frac{i}{2}\beta_2\omega^2 h + \frac{i}{6}\beta_3\omega^3 h - i\omega T\right)d\omega \tag{2.21}$$

using the Fourier transform

$$\tilde{A}(z,\omega) = \int_{-\infty}^{\infty} A(z,T) exp\,(i\omega T)\,dT. \tag{2.22}$$

The Fast Fourier transform algorithm allows for an efficient solution of the NLSE. In this method the complex amplitudes of the pulse need to be sampled with 2^N points, with N being a positive integer.

When simulating active fibers in mode-locked lasers, gain saturation and gain filtering have to be taken into account. In a pulsed fiber laser it can be assumed that the gain saturation depends on the total pulse energy [45]:

$$g(P_{average}) = \frac{g_0}{1 + P_{average}/P_{sat,G}} \tag{2.23}$$

$P_{average} = E_P/T_R$ is the average power, g_0 the small signal gain, and $P_{sat,G} = E_{sat,G}/\tau_G$ the saturation power, where $E_{sat,G}$ is the gain-saturation energy and τ_G the gain recovery time. The wavelength dependence of the gain is implemented in the frequency domain step

$$\begin{aligned} \exp(\tilde{h}\cdot\hat{D})A(z,t) &= \frac{1}{2\pi}\int_{-\infty}^{\infty} \tilde{A}(z,\omega) exp\left(\frac{g\cdot\tilde{h}(\omega) - l}{2}\right. \\ &\quad \left. + \frac{i}{2}\beta_2\omega^2 h + \frac{i}{6}\beta_3\omega^3 h - i\omega T\right) d\omega, \end{aligned} \tag{2.24}$$

where g is the fiber gain calculated with equation 2.23, l the fiber loss, and $\tilde{h}$ the lineshape. The line shape can assumed to be Lorentzian because of the predominantly homogenous broadening mechanism in rare earth doped glasses [46]:

$$\tilde{h}(\omega) = \frac{1}{1 + \left(\frac{\omega-\omega_0}{\omega_G}\right)^2} \tag{2.25}$$

Equations 2.19, 2.20, 2.23, 2.24, and 2.25 describe the propagation in active and passive fibers needed for the simulation of fiber lasers.

2.3.2 Pulse interaction with saturable absorbers

A mathematical description of the absorber is necessary to model a passively mode-locked fiber laser. It is given by [21, 47]

$$\frac{dq}{dt} = -\frac{q - q_0}{\tau_A} - \frac{P}{E_{sat,A}}q, \tag{2.26}$$

where q_0 is the saturable loss, P the incident pulse power, τ_A the recovery time, and $E_{sat,A}$ the saturation energy. In case of a fast absorber, (i.e. the incident pulse is much longer than the recovery time), the saturable absorption recovers immediately when the pulse power decreases, as seen in Fig. 2.4 (a). In this case the solution of Equation 2.26 is

$$q(t) = \frac{q_0}{1 + \frac{P}{P_{sat,A}}}, \tag{2.27}$$

with the saturation power $P_{sat,A} = E_{sat,A}/\tau_A$. This solution is obtained by setting the derivative $dq/dt = 0$ and is also applicable for absorbers with incident continuous wave (cw)-radiation. When the recovery time is much longer than the pulse duration, the slow absorber saturates with the incident pulse energy, as seen in Fig. 2.4 (b):

$$q(t) = q_0 exp\left(-\frac{1}{E_{sat}}\int_{-\infty}^{t} P(t')dt'\right). \tag{2.28}$$

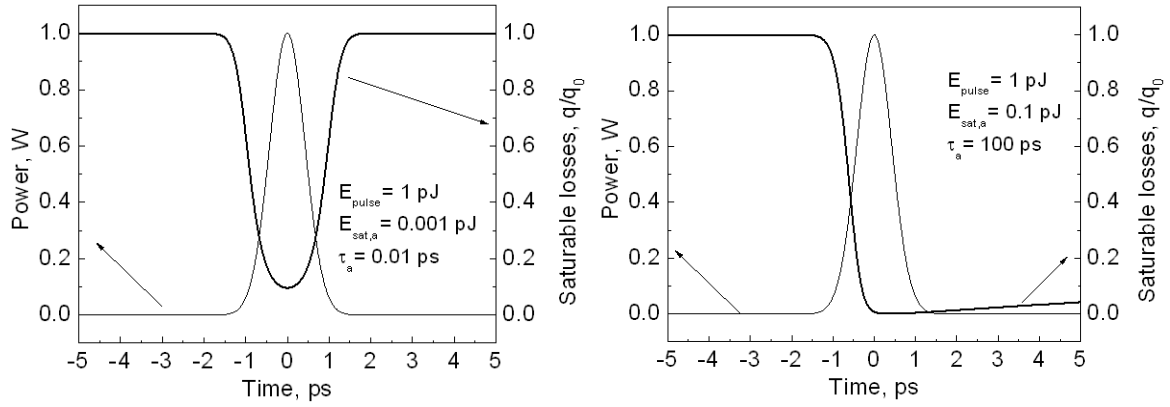

(a) (b)

Fig. 2.4: *Saturable absorbtion (right axis) for an incident gaussian pulse found by solving Equation 2.26 numerically for (a) a fast absorber and (b) a slow absorber. The left axis shows the temporal pulse power.*

The solutions for the slow and fast saturable absorber give an easy tool for approximate analytical consideration; however, for fiber laser simulations a numerical solution of Equation 2.26 has to be obtained. When solving the equation with numerical methods, such as the Runge-Kutta method [48], the solution might diverge when the pulse is sampled with relatively few sampling points; therefore, the pulse shape will be divided in piecewise constant sections and Equation 2.26 will be solved for the constant power of each of these sections.

For a constant incident power P the inhomogeneous linear differential Equation 2.26

can be solved analytically [49] resulting in the solution

$$q(t+t_0) = \left[q(t_0) - \frac{q_0 E_{sat,A}}{E_{sat,A} + P\tau_A}\right] exp\left[-\left(\frac{1}{\tau_A} + \frac{P}{E_{sat,A}}\right)t\right] + \frac{q_0 E_{sat,A}}{E_{sat,A} + P\tau_A}. \quad (2.29)$$

Therefore, the saturable absorption of a SESAM can be calculated with Equation 2.29 when approximating the pulse by a piecewise constant function.

2.3.3 Modeling the mode-locked fiber laser

In addition to an active fiber and a saturable absorber, a mode-locked fiber laser includes dispersive elements, such as grating pairs or hollow-core photonic-band-gap fibers that are described by Equation 2.24.

Element	Parameter	Value
Active fiber	Length	500 mm
	2nd order dispersion	20 ps^2/km
	3rd order dispersion	0.05 ps^3/km
	Nonlinear parameter	5 $/Wkm$
	Gain bandwidth	20 nm
	Saturation power	10 mW
Passive fiber	Length	1500 mm
	2nd order dispersion	20 ps^2/km
	3rd order dispersion	0.05 ps^3/km
	Nonlinear parameter	5 $/Wkm$
Saturable absorber	Modulation Depth	10%
	Nonsaturable losses	4%
	Recovery time	1 ps
	Saturation energy	1 pJ
Dispersion compensator (Grating pair)	2nd order dispersion	-0.126 ps^2
	3rd order dispersion	0.00035 ps^3
	Losses	18%
System	Output mirror reflectivity	20%
	Repetition rate	50 MHz
	Cavity type	Linear round trip cavity

Table 2.2: *Parameters of the elements for the mode-locked fiber-laser simulations*

The dotted lines in Fig. 2.3 show the results of the simulation of the fiber laser used in the experiment. The parameters used in the simulation are given in table 2.2. The simulation has a very good agreement with the experiment. It correctly predicts the pulse duration and the location of the soliton sidebands, which can be used to calculate the cavity dispersion of -0.172 ps^2 [50]. In conclusion, a complete numerical description of a mode-locked fiber laser has been given.

2.4 Self-starting mode locking, Q-switching, and Q-switched mode locking

Lasers that start passive mode locking without external perturbations are called self-starting lasers. The self-starting behavior is determined largely by the saturable absorber. Initial fluctuations have to be amplified by the absorber; the highest intensities undergo lower attenuation than the cw-background. The dominant mechanism for self-starting is the mode coupling. The mode coupling provides additional gain for side modes, which have the growth rate

$$\frac{1}{T_{buildup}} = \left[\frac{2q_0}{(1+P/P_{sat,A})^2+(2\pi m\tau_A)^2}\frac{P}{\tau_A} + \frac{2g_0}{(1+P/P_{sat,G})^2+(2\pi m\tau_G)^2}\frac{P}{\tau_G}\right]_{cw}, \tag{2.30}$$

where m is the mode separation in units of $2\pi/T_R$. If the growth rate is positive, neighboring modes grow until a steady state is reached. For short recovery times of absorption, long gain recovery time, and operation far above the mode-locking threshold, the startup-time can be simplified

$$\frac{1}{T_{buildup}} = \left[\frac{dq}{dP}\right]_{cw} P. \tag{2.31}$$

Fig. 2.5 (a) shows the saturable losses as a function of intensity with incident cw-light [51] . The slope of the loss determines the ability of the absorber to start the laser. This model ignores many effects that can influence self-starting as dispersion and SESAM saturation by amplified spontaneous emission, which will be further discussed in this thesis. The spurious reflection from fiber splices and fiber end faces, higher order modes in fibers [52], and spatial hole burning [53] may also prevent self-starting. Haus and Ippen [54] found a criterion that includes the scattering effects caused by these spurious reflections considering at a resonator with additional reflections:

$$\left|\sum r_i sin\Phi_i\right| < \frac{\tau_P}{T_R}, \tag{2.32}$$

where r_i are the scattering amplitudes, Φ_i the phase shifts experienced by the scattered waves, and τ_P/T_R the ratio of the pulse duration to the cavity round-trip time. Since this ratio is typically of the order of $10^{-3}...10^{-5}$, this constitutes a strong restriction on the tolerable spurious reflections. Fabry–Perot effects should be avoided by using angled cleaves of the fiber ends, using fiber isolators at the output and by antireflection coating of the cavity elements.

Equation 2.31 implies that as high as possible driving force Pdq/dP is desired; however, with a low value of the saturation power the laser tends to operate in the Q-

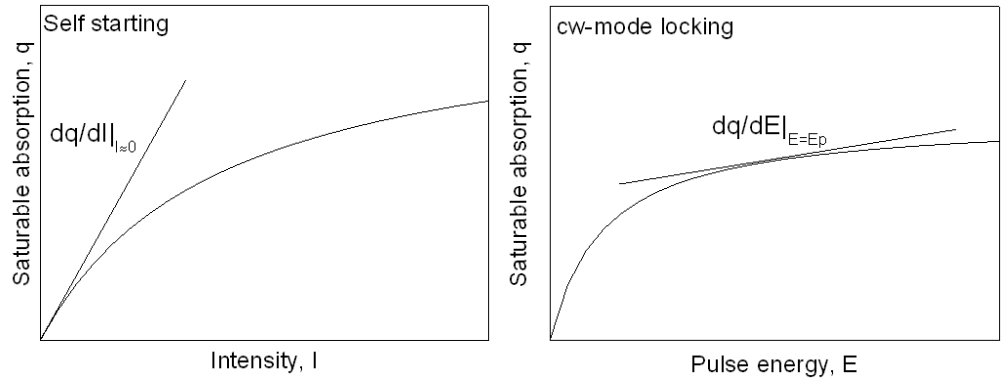

(a) (b)

Fig. 2.5: *Saturable absorption with incident (a) cw-radiation and (b) pulsed radiation, depending on cw-power and pulse energy, respectively [51].*

switched regime. The condition for stability against Q-switching is [51]:

$$\left[\frac{dq}{dP}\right]_{cw} P < r\frac{T_R}{\tau_G}, \tag{2.33}$$

where T_R is the round-trip time and r is the pumping rate normalized to the threshold. The left side of Equation 2.33 determines the reduction in losses for every pass of the light through the absorber. The right side determines how much the gain saturates per round trip. The saturation of the gain compensates for the decreased round-trip losses caused by the absorber. If the gain does not saturate sufficiently, Q-switched pulsing appears instead of the mode-locked operation.

Within the stability limits given by Equation 2.33, the mode-locked pulse train can still be modulated by a strong Q-switched envelope. This Q-switched mode locking (QSML) is not desirable in most applications because a train of constant energy pulses is required. Furthermore an exact control of the q-switched envelope is difficult to achieve and the high energy peaks can damage saturable absorber and pump diode laser. Analyzing the steady state in a mode-locked laser [55], it can be shown that the condition to prevent Q-switched mode locking is given by

$$E_P \left|\frac{dq}{dE_P}\right|_{cw} < \frac{T_R}{\tau_G} + \frac{E_P}{E_{sat,G}}. \tag{2.34}$$

The slope dq/dE_P should be minimized to avoid Q-switched mode-locking. The nonlinear reflectivity with incident pulsed radiation and the slope dq/dE_P is illustrated in Fig. 2.5.

Quantitatively, Equation 2.34 can be understood as follows: if the pulse energy rises slightly, due to noise or relaxation oscillations, these energy fluctuations grow expo-

nentially because of the higher absorber reflectivity. In order to prevent Q-switched mode locking, the gain saturation has to be strong enough to stop this exponential rise. With some approximations (the assumption of a small modulation depth, strong oversaturation of the saturable absorption, low out-coupling ratio and operation far above the threshold), the stability condition can be written as [56]

$$E_P^2 > E_{sat,G} E_{sat,A} q_0. \tag{2.35}$$

The derivation of this expression assumes a slow saturable absorber. When using a fast absorber, the degree of oversaturation decreases because the absorber partially recovers during the pulse exposure. This causes the necessity of a higher pulse energy to achieve stability without QSML. Equation 2.35 gives a very good guideline for designing a laser that is stable against QSML although not all of the above mentioned approximations (small modulation depth and small out-coupling) are valid in a fiber laser.

3. SESAM DESIGN

This chapter first gives a short overview about the effect of the SESAM parameters (saturation energy, recovery time, modulation depth and two photon absorption) on the mode-locked operation. The SESAM parameters can be adjusted using well-controlled techniques. In particular, the saturation energy can be controlled by exploiting quantum-well absorption. The recovery time can be decreased by low-temperature growth, heavy ion bombardment, or the use of quantum-dot structures. The use of resonant structures allows for additional control of the modulation depth, the saturation energy, and the strength of the two-photon absorption.

3.1 SESAM Parameters

SESAMs are described by the rate Equation 2.26. The parameters in this equation are the saturation energy $E_{sat,A}$, the modulation depth q_0 and the recovery time τ_A. Two-photon absorption (TPA) is another important effect, that is not included in Equation 2.26. It is a nonlinear process that causes absorption proportional to the incident intensity. This causes an additional loss

$$l_{TPA} = E_P/E_2 \tag{3.1}$$

for a pulse, where E_P is the pulse energy and E_2 is the inverse slope of the TPA. In order to build a fiber laser with easy self-starting, high pulse quality and stability against QSML, different, partially- contradicting requirements have to be fulfilled, as shown in table 3.1. Therefore, careful control of the SESAM parameters is needed to fulfil the requirements of the application.

3.2 Quantum-well absorbers

The simplest way of reducing the saturation energy is to focus the beam more tightly onto the absorber. Since the numerical aperture of the lens has to be very high, this method is limited, it only allows an improvement by an factor of about 4.

#	Preventing QSML	Achieving reliable self-starting	Achieving high pulse quality
$E_{sat,A}$ see chapter	Low 2.4	Low 4.2.1	High 4.1
q_0 see chapter	Low 2.4	High 4.2.1	High 4.1
τ_A see chapter	High 2.4	Balanced 4.2.2	Low 4.1
E_2 see chapter	Low 4.3	High 4.3	High 4.3

Table 3.1: *Requirements on the SESAM properties saturation energy $E_{sat,A}$, modulation depth q_0, recovery time τ_A and inverse TPA slope E_2 for preventing QSML, achieving easy self-starting and achieving high pulse quality. Furthermore the chapters in which the requirements are further discussed are listed.*

The saturation energy depends on quantum well absorption. A quantum well is a potential well, which confines electrons or holes. These wells are formed by sandwiching semiconductor layers between semiconductor materials with higher band gaps [57]. The absorption wavelength can easily be controlled by adjusting depth and width of the quantum wells. Nonlinear effects, as saturable absorption, are enhanced in quantum well structures. Fig. 3.1 shows the schematics of a multiple quantum-well structure working at a wavelength of about 1 μm.

The bottom distributed Bragg reflector (DBR), which consists of pairs of GaAs/AlAs layers, provides high reflectivity (typically higher than 99%) and broad bandwidth (larger than 100 *nm*). The DBR is followed by a spacer layer, which adjusts the position of the quantum wells to be in an antinode of the standing wave pattern of the Fabry–Perot cavity, which is formed between the bottom DBR and the top mirror. The top mirror locates at the surface between the surface cap layer and air or additional dielectric coatings.

The top spacer adjusts the thickness of the cavity to achieve resonant or anti-resonant operation. The number of quantum wells determines the modulation depth and saturation energy. A higher number of quantum wells leads to a higher modulation depth and a higher saturation energy. As seen in the band-gap diagram in Fig. 3.1, every material except for the GaInAs quantum wells has band-gap energies higher than the photon energy. Consequently, absorption occurs only in the quantum-well material.

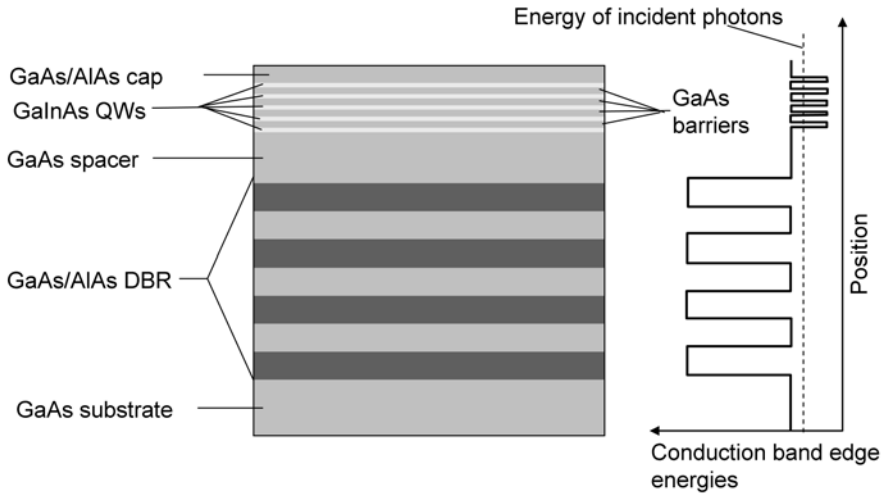

Fig. 3.1: *Schematics of a quantum well structure and conduction band diagram*

3.3 Absorbers with short recovery time

3.3.1 Metamorphic growth, low temperature growth, and ion implantation

The absorber recovery time in light emitting devices is usually determined by the radiative carrier-recombination time, which is in the range of few *ns*. This kind of recombination is dominant within semiconductors with a low number of defects. To decrease the recovery time more defects have to be introduced into the semiconductor. In a semiconductor, fast non-radiative recombination centers are typically responsible for a short recovery time [58]. Several methods are available to introduce defects.

Another method of recovery time reduction is the generation of lattice mismatched induced imperfections by metamophoric growth. When growing InP on GaAs the lattice mismatch causes a higher number of defects. This effect is exploited in an InGaAs-SESAM [S1] by growing a layer of InP between the bottom GaAs-based DBR and QW region. The InP layer plays the role of a “lattice-reformation” region. The thickness of this layer was varied between 75 *nm* and 480 *nm* to change number of defects. It was found out that there is a monotonic dependence between the thickness of the InP buffer and the recovery time of the quantum-well absorber. The recovery time measured with a pump-probe setup showed a recovery time decrease from 480 *ps* to 150 *ps*, when the buffer layer thickness decreased from 480 *nm* to 75 *nm*.

The bombardment of a quantum-well material with energetic ions can reduce the recovery by up to three orders of magnitude. Delpon et. al. [59] demonstrated the reduction in recovery time of InGaAs/InAlAs from 1.6 *ns* to 1.8 *ps*. They used O^+ and Ni^+ ions with energies ranging from 10 to 100 *MeV* to achieve large penetra-

tion depths into the material. The bombarding of the absorber, however, may cause a degradation of the modulation depth and increase non-saturable losses. Using rapid thermal annealing (RTA), the modulation depth of the absorber can be restored, while preserving a short recovery time [S2]. Irradiation with 6 MeV ions at the dose of $10^{12} cm^{-2}$ was shown to reduce the recovery time from 162 ps to 0.8 ps, while the modulation depth decreases from 18.3% to 14.0%, and the nonsaturable losses increase from 8.7% to 19.5%. When the absorber is placed in a nitrogen atmosphere and exposed for 1 s to 400°C, the nonsaturable losses decrease to 11.0%, and the modulation depth increases from 14.0% to 17.4%. The recovery time slightly increases to 1.1 ps due to the RTA process. In conclusion RTA improved the properties of the SESAMs by increasing the modulation depth and decreasing the nonsaturable losses while maintaining a short recovery time.

3.3.2 Quantum-dot absorbers

Saturable absorbers with short recovery times can be realized with quantum-dot absorbers. Quantum-dot absorbers can be grown using standard solid molecular-beam epitaxy (MBE) [P5]. Similar to the quantum-well SESAM, it contains a DBR sequence made of GaAs and AlGaAs layers. The absorber described in [P5] consists of eight multiple stacks of ten InGaAs-quantum-dot layers with 10 nm thick spacer layers of GaAs. Adjacent multiple stacks are separated by 23.7 nm layers of high-temperature grown GaAs to eliminate the effects of indium segregation and 13.7 nm layers of low-temperature grown GaAs to decrease the carrier lifetime. The recovery times have been investigated in a similar structure, where the quantum dots were formed by the deposition of nine periods of 0.075 nm of InAs and 0.1 nm of GaAs by a pump probe technique using 130 fs pulses [60]. The measurement showed a fast recovery time of $\sim$1 ps followed by a slower decay of $\sim$100 ps. It is believed that the fast recovery time corresponds to transitions in the quantum-dot layers, whereas, the slow decay corresponds to transitions back to the ground state [60]. Fig. 3.2 (a) shows the low intensity reflectivity of the quantum absorber used in [P5]. It clearly shows the resonant character of the structure. The nonlinear reflectivity of this structure is shown in Fig. 3.2 (b). The low saturation energy of 14.8 $\mu J/cm^2$ and the high nonlinear constrast of 17.6% make the quantum-dot absorber suitable for mode locking fiber lasers.

This quantum-dot absorber was used in a fiber laser without dispersion compensation. The light was focused onto the absorber using an objective with a numerical aperture of 0.5 and a focal length of 2 mm, resulting in an saturation energy of 0.2 pJ assuming a mode field area of 1.5 μm^2 on the absorber. Stable mode-locking has been obtained with a very low threshold pump power of 30 mW. A sequence of pulses with a repetition rate of 50 MHz and an average power of 5 mW was obtained for a pump power of 100 mW and 30% output coupling. The optical spectrum and auto-

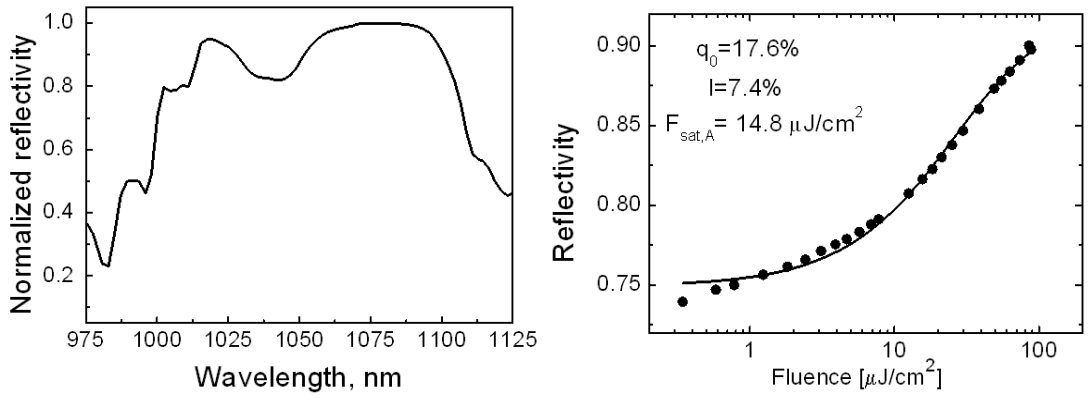

(a) (b)

Fig. 3.2: *(a) Low intensity reflectivity and (b) nonlinear reflectivity at 1042* nm *of the quantum-dot structure [P5].*

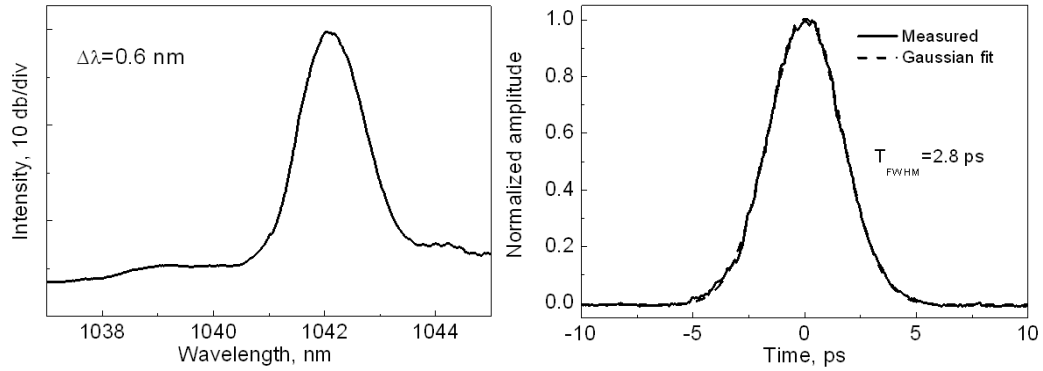

(a) (b)

Fig. 3.3: *(a) Intensity autocorrelation and (b) spectrum of the fiber laser mode-locked by a QD-absorber [P5].*

correlation are shown in Fig. 3.4 (a) and (b), respectively. A pulse duration of 2.8 *ps* was derived assuming a Gaussian fit. The time bandwidth product is 0.5 with a spectral width of 0.6 *nm*. The low value of the time bandwidth product, indicates the strong pulse shaping by the quantum-dot absorber despite the high cavity dispersion.

3.4 Resonant Saturable Absorbers

The modulation depth of a SESAM can be enhanced by increasing the number of quantum wells; however this also causes an increase in the saturation energy and might therefore prevent self-starting or cause QSML. A way to increase the modulation depth while maintaining a low saturation energy is to place the element in a resonant Fabry–Pérot cavity.

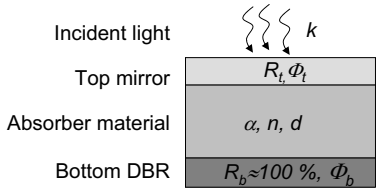

Fig. 3.4: *Schematics of a resonant absorber cavity.*

Fig. 3.4 shows the schematics of such a SESAM cavity. The reflectivity can be calculated with the Fabry–Perot model [20]:

$$R = \frac{\left(\sqrt{R_T} + exp(-2\alpha d)\right)^2 - 4\sqrt{R_T}exp(-2\alpha d)cos^2(\Phi_{rt}/2)}{\left(1 + \sqrt{R_T} + exp(-2\alpha d)\right)^2 - 4\sqrt{R_T}exp(-2\alpha d)cos^2(\Phi_{rt}/2)}, \tag{3.2}$$

where R_T is the top mirror reflectivity, α is the absorber amplitude absorbtion coefficient, d the cavity thickness, and Φ_{rt} the round trip cavity phase shift given by

$$\Phi_{rt} = 2nkd + \Phi_b + \Phi_t \tag{3.3}$$

with the refractive index n, the vacuum wave number k, the top mirror phaseshift Φ_t, and the bottom mirror phaseshift Φ_b. The bottom mirror reflectivity is assumed to be 100%. Φ_{rt} equals $m2\pi$ in a resonant cavity ($m = 1,2,3...$). The field intensity inside the cavity is enhanced by the factor ε [61] compared to an antireflection-coated structure I_0:

$$I = \varepsilon I_0 \tag{3.4}$$

with

$$\varepsilon = \frac{1 - R_T}{\left(1 + \sqrt{R_T}exp(-2\alpha d)\right)^2 - 4\sqrt{R_T}exp(-2\alpha d)cos^2(\Phi_{rt}/2)}. \tag{3.5}$$

This leads to decrease in the saturation energy compared to the saturation energy of the antireflection-coated structure $E^0_{sat,A}$ by a factor of $1/\varepsilon$.

$$E_{sat,A} = \frac{1}{\varepsilon}E^0_{sat,A} \tag{3.6}$$

Neglecting the non-saturable losses, the modulation depth achieves the value $1 - R$. Remarkably, the product

$$E_{sat,A}q_0 = E^0_{sat,A}(1 - R_s), \tag{3.7}$$

that defines the absorber contribution to the stability against Q-switched mode locking, does not depend on the detuning from the cavity resonance. R_s is the reflectivity of the antireflection coated structure. When the modulation depth is increased by moving closer to the resonant wavelength, the saturation energy decreases inversely proportional due to the field enhancement. The presence of nonlinear losses decreases

the product even when moving closer to the resonance, and, therefore, increases the stability against QSML.

A typical absorber [P1] used in this thesis consists of a bottom mirror with 30 pairs of AlAs-GaAs quarter-wave layers forming a distributed Bragg reflector. The stop band is centered around 1050 *nm* and has a bandwidth of approximately 120 *nm*. The quantum well structure consists of five 6 *nm* thick InGaAs quantum wells and of 16 *nm* thick GaAs barriers. The quantum well structure is sandwiched between a 0.1 μm GaAs-buffer layer and a 100 *nm* GaAs cap layer.

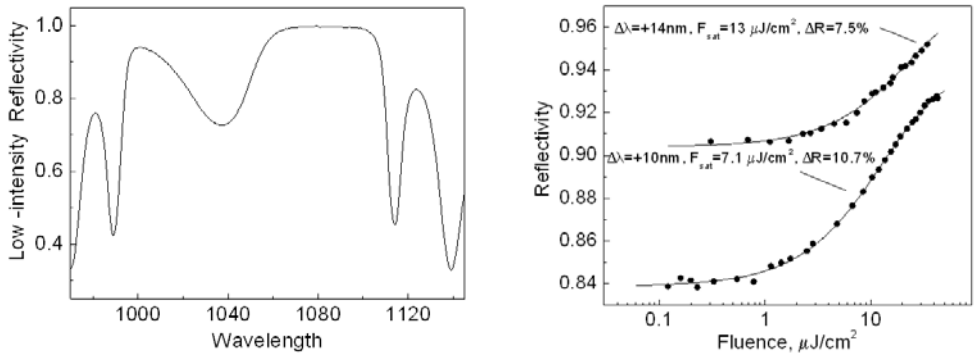

(a) (b)

Fig. 3.5: *(a) Linear reflectivity and (b) nonlinear reflectivity of a resonant SESAM for two different detunings.*

Fig. 3.5 (a) and (b) show the low intensity reflectivity and the nonlinear reflectivity of this resonant strucure, respectively. The saturation fluences (fluence $F = E/A$, where E is the pulse energy and A the mode field area; on the SESAM $F_{sat,A} = E_{sat,A}/A_A$ and in the gain material $F_{sat,L} = E_{sat,L}/A_L$) and the modulation depths found from the measurements were 13 J/cm^2 and 7.5% for 14 *nm* detuning from the resonance and 7.1 J/cm^2 and 11% for 10 *nm* detuning from the resonance. As expected from the analysis of the Fabry–Perot cavity, the modulation depth increases, while the saturation energy decreases when moving closer to the resonance. The value of the product $E_{sat,A}q_0$ is 0.97 $\mu J/cm^2$ and 0.78 $\mu J/cm^2$ for a detuning from the resonance of $\Delta\lambda = 14$ *nm* and $\Delta\lambda = 10$ *nm*, respectively. The lower product for smaller detunings from the resonance is due to the increased non-saturable loss of the material near the resonance. The highest value of the reflectivity change, close to the resonance, is estimated to be 20%.

It can be concluded that the use of resonant SESAMs is a way to increase the modulation depth while decreasing the saturation energy. The stability against QSML is not degraded using this approach, on the contrary, it is improved for proper near-resonance operation. It will be shown in Section 4.2.1 that this is an easy method to

achieve reliable self-starting.

4. INFLUENCE OF SESAM PARAMETERS ON A MODE-LOCKED FIBER LASER

The previous chapter presented the technology of SESAMs. This chapter discusses how the different SESAM parameters affect the properties of a fiber laser. Q-switched mode locking was previously discussed in Section 2.4. This chapter further investigates the effect of the saturation energy, modulation depth, recovery time, and two-photon absorption on the pulse quality and the self-starting mode-locking.

4.1 Pulse quality

For many applications the pulse quality and duration are crucial. Even in a reliably self-starting, cw-mode-locked laser, the pulse can be too long, too broad, and have too low energy to be used in applications as second harmonic generation [62], [S7], frequency conversion by Raman-soliton self shifting [S6], micromachining [6], and telecommunication [63]. Multiple pulsing and noise-like pulse shapes can also disturb the pulse quality.

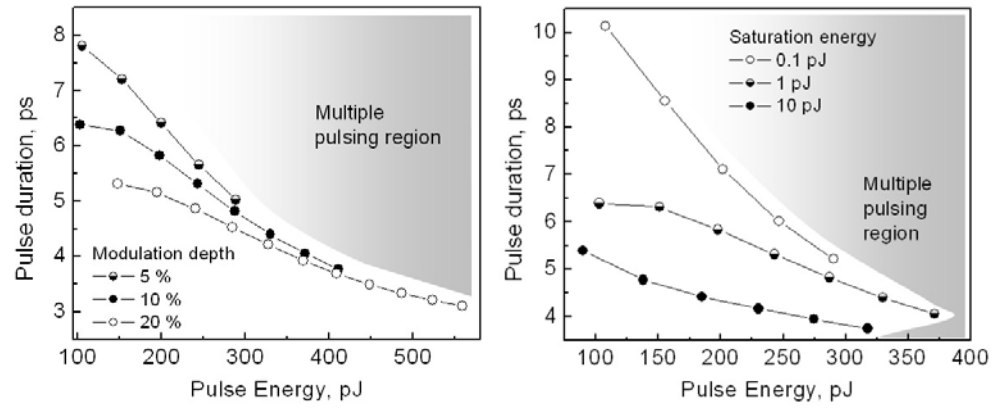

(a) (b)

Fig. 4.1: *Simulated pulse durations as a function of energy for different (a) modulation depths and (b) saturation energies in a simulated fiber laser.*

The pulse duration is an important criterion to assess the pulse quality. Equation 2.13 gives an estimate for the minimum pulse duration, depending on the modulation

depth of a fast absorber; however, this equation does not account for dispersion, self-phase modulation, and the discreetness of elements in fiber lasers. Their influence was investigated by simulating a fiber laser with the parameters listed in table 2.2. The total dispersion was changed to 0.014 ps^2 by adjusting the parameters of the dispersion compensating elements to exclude soliton effects.

The simulation results are presented in Fig. 4.1 (a), which shows the pulse duration as a function of pulse energy for different modulation depths. The pulse energy was changed by adjusting the fiber gain. As expected, a higher modulation depth enabled the generation of shorter pulses; however, the difference in the pulse durations depends on the pulse energies. There are deviations between the pulse durations estimated with Equation 2.13 and the simulated pulse durations. At a pulse energy of about 286 pJ, the simulated pulse durations between the 5% modulation-depth absorber and the 20% modulation-depth absorber differ by 10%, whereas, Equation 2.13 predicted a twice as long pulse duration for the 5% absorber compared to the 20% absorber. This indicates that the pulse shaping by SPM and dispersion strongly influences the pulse duration in a fiber laser.

A higher modulation depth also enables higher pulse energies. The pulse breakup occurs for the 20% modulation depth absorber at a pulse energy twice as high as for the 5% absorber.

In conclusion, a high modulation depth is desirable to achieve high pulse energy and short pulse durations; however, one has to take into account that the modulation depth cannot be increased arbitrarily since it could cause QSML and high, non-saturable losses; therefore, an absorber has to be chosen with a carefully balanced modulation depth.

The pulse quality is also strongly influenced by the saturation energy of the SESAM. Fig. 4.1 (b) shows the pulse duration as a function of pulse energy for different saturation energies. As expected, the pulse duration decreased with increasing pulse energy. When the pulse energy exceeds a certain critical value, the pulse broke up, and multiple pulsing occurred. This critical value is the highest for a saturation energy of 1 pJ. With the lower saturation energy of 0.1 pJ, the pulse oversaturated the absorber faster and the pulse breakup occurred earlier. For the higher saturation energy of 10 pJ, the higher peak power caused a stronger SPM and, therefore, pulse breakup at lower pulse energies. The higher peak power was caused by the stronger pulse shaping of the absorber at higher pulse energies compared to the lower-saturation energy absorber. With higher pulse energies the spectral broadening by SPM can partially overcome the spectral limitations of the gain material [64]. This caused the pulse to further shorten even though the absorber was already oversaturated. In conclusion, the saturation energy has to be carefully adjusted to achieve short pulse durations and high pulse energies.

The absorber recovery time is another absorber parameter that affects the pulse qual-

ity. Fast and slow absorbers differ in their pulse shaping mechanisms. The slow absorber attenuates the leading edge of the pulse much more than the trailing edge [65]; therefore, the pulse is shifted backwards in time with every propagation through the absorber. Behind the pulse there is a window of net gain because it takes a long time for the SESAM to recover its saturable absorption. Noise is amplified during this window. This noise grows due to its higher gain compared to the pulse. Since the pulse moves backwards, due to the slow absorber interaction, it is shifted on top of the growing noise, which causes noise to be suppressed. Simulations [65] showed that the absorber recovery τ_A time is limited by $\tau_A < 28\tau_P$ with regard to the pulse duration τ_P. When the recovery time exceeds this value the pulse-trailing-edge noise is amplified to significant levels and the pulse duration increases; However. when $\tau_A < 28\tau_P$ is maintained, pulse durations achieved with slow absorbers are only slightly longer than with fast absorbers. For example [29], if the absorber recovery time is increased from 50 *fs* to 10 *ps* the minimal achievable pulse duration increased only from 200 emphfs to 220 emphfs (using a q_0 of 0.005 and a $\omega_G = 8\pi$ *THz*). These estimations have been made for a solid state laser, ignoring dispersion, SPM, and the discreetness of the cavity elements.

Slow and fast absorbers have been used in a fiber laser to investigate the importance of the absorber recovery time. Fig. 4.2 and 4.3 show (a) the wavelength spectra and (b) the intensity autocorrelations of a slow and a fast SESAM, respectively, measured in a fiber laser. The fiber laser is similar to the one shown in Fig. 2.3: however, the grating separation has been decreased to 7 *mm* to achieve normal dispersion. During mode locking, the pulse durations were 9.4 *ps* and 7.4 *ps* for slow and fast SESAM, respectively. This is in agreement with the slight increase in the pulse width expected with a slow SESAM. We analyzed the dechirped pulses by assuming a linear phase over the spectrum. The laser mode locked with the fast absorber shows a pulse with duration of 300 *fs*. It was more compressible compared to the pulse obtained with the slow absorber with a duration of 500 *fs*.

Apart from the longer pulse duration, the mode locking was less stable and critical in alignment with the slow absorber compared to the mode locking achieved with the fast absorber. These instabilities have been further investigated by numerical simulations. A laser similar to the one presented in Section 2.3 has been simulated. The total cavity dispersion was chosen to be normal ($D_2 = 0.014$ ps^2) to analyze the effects of the pulse shaping by the absorber without the soliton-pulse shaping. Fig. 4.4 (a) and (b) show the evolution of the pulse shape for the slow and fast SESAM, respectively. The plots show the temporal pulse shape for successive round trips. In contrast to the fast SESAM, no steady state evolves for the slow SESAM. Fig. 4.5 (a) shows the pulse shapes for the slow and fast SESAMs. In the case of the slow absorber, the noise, which arises after the passing of the pulse, is amplified because the absorber did not recover completely. The fast absorber recovers quickly and, therefore, noise at the trailing edge of the absorber is efficiently suppressed. Since

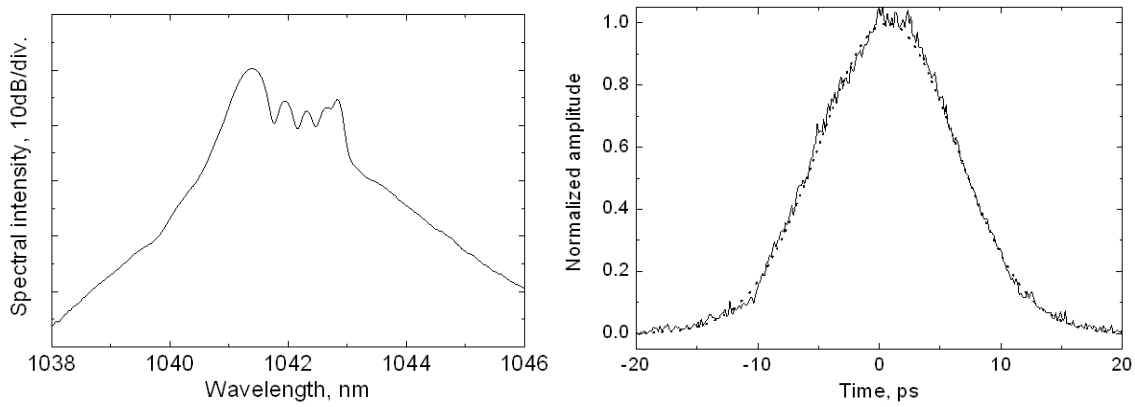

(a) (b)

Fig. 4.2: *Wavelength spectrum (a) and autocorrelation (b) of a pulse generated by fiber laser using a slow SESAM. The spectral width is 3 nm and the pulse duration derived from a gaussian fit is 9.4 ps.*

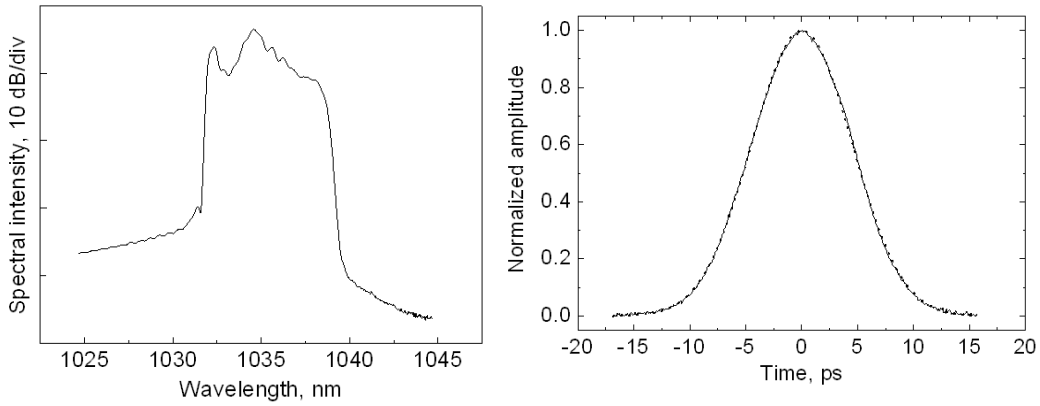

(a) (b)

Fig. 4.3: *Wavelength spectrum (a) and autocorrelation (b) of a pulse generated by fiber laser using a fast SESAM. The spectral width is 5* nm *and the pulse duration derived from a gaussian fit is 7.4 ps.*

the recovery time is in the range of the pulse duration, a slight asymmetry of the pulse arises because the trailing edge of the pulse is less absorbed in the SESAM; therefore, a fast absorber is preferable in order to avoid instabilities in the pulse shapes.

Wavelength shifting is another interesting effect caused by the slow recovery of a saturable absorber. The wavelength spectrum in Fig. 4.5 (b) shows the spectral shift. The wavelength spectrum shifts by 2 *nm* and 4 *nm* for the fast and slow absorber, respectively, towards shorter wavelengths away from the gain peak. This is caused by the interaction of SPM, normal dispersion, and slow absorber response [65]. SPM and normal dispersion cause positive chirp, which means that the long-wavelength components are more concentrated in the leading edge of the pulse. Since

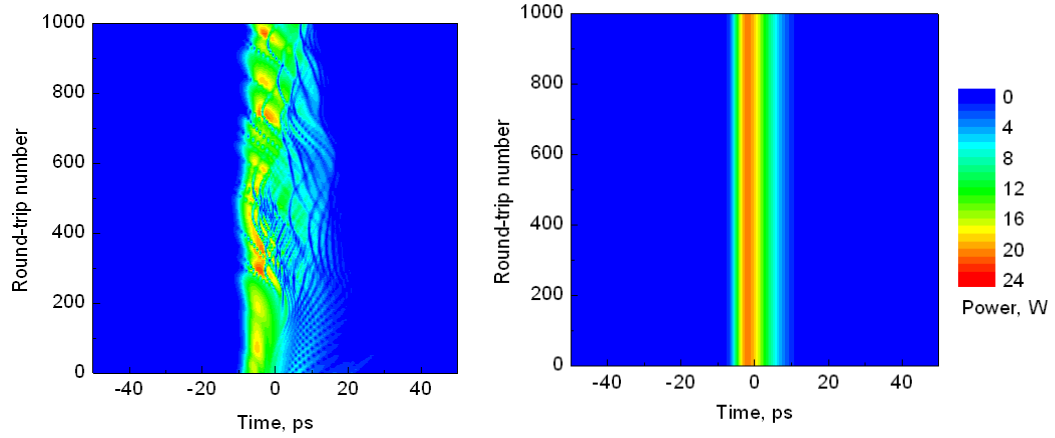

(a) (b)

Fig. 4.4: *Simulation of a fiber laser mode locked by a slow or a fast SESAM. Temporal pulse shape as a function of the round-trip number for (a) a slow absorber (b) a fast absorber.*

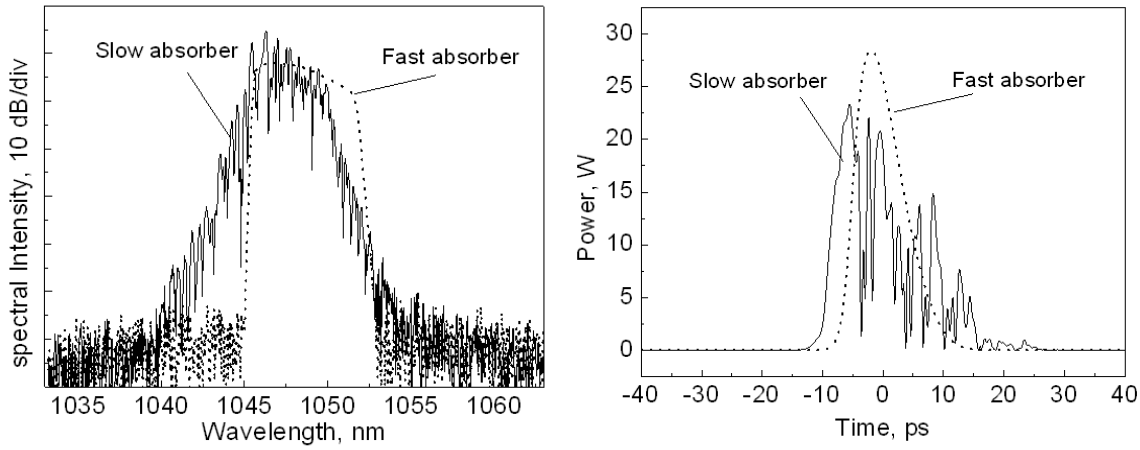

(a) (b)

Fig. 4.5: *Simulation of a fiber laser mode locked by a slow (solid line) or a fast SESAM (dashed line). (a) Wavelength spectrum (b) Temporal pulse shape.*

the slow saturable absorber has more absorption in this wing of the pulse, more long-wavelength components are extinguished, and the spectrum shifts towards shorter wavelengths for slower absorbers. The longer pulse duration is caused by the lower losses that a pulse experiences in the absorber, due to the longer recovery time; therefore, the overall gain-loss-balance with the gain filtering favors slightly longer pulses; furthermore, the pulse develops a trailing wing due to the smaller attenuation in the absorber. Thus, a fast absorber is preferable when the goal is to achieve clean pulse shapes because it causes more symmetrical pulse shapes and spectra.

4.2 Self-starting mode locking

The theory of self-starting mode locking was reviewed in Section 2.4. We extend the focus on specific issues in fiber lasers: the necessity of high modulation depth SESAMs and the importance of amplified spontaneous emission (ASE).

4.2.1 Modulation depth and saturation energy

High modulation depth of absorbers is a key parameter for stable mode locking in fiber lasers. We observed, that when using SESAMs with small modulation depth, only fiber lasers with anomalous dispersion could start mode locking. However, resonant SESAMs, as the one described in Section 3.4, could start mode locking without dispersion compensation [P1]. In particular, when using the SESAM with the resonant wavelength of 1036 *nm*, shown in Fig. 3.5, mode locking was obtained for wavelengths between 1030 *nm* and 1045 *nm*. Outside this range, only Q-switched mode locking was observed. The stability of the self-starting was studied by placing a chopper inside the cavity. Reliably self-starting operation was observed for several hours. We generated 11 *ps* pulses using the setup shown in Fig. 4.6 using a high modulation depth absorber. A loop mirror serves simultaneously as output coupler and as cavity end mirror in this setup.

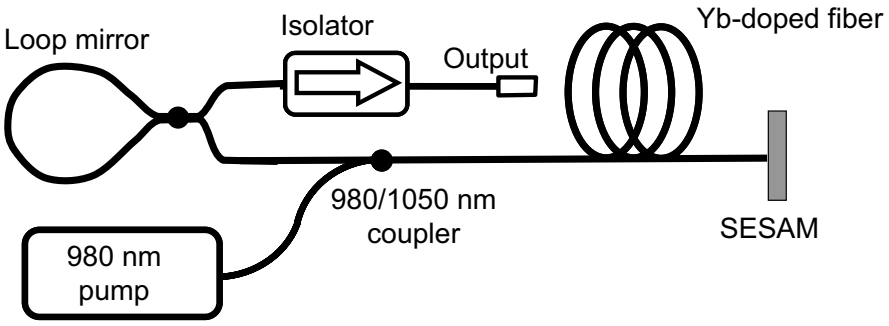

Fig. 4.6: *Setup of a dispersion-compensation-free fiber laser.*

The dominant role of the high-modulation-depth SESAM for the self- starting operation was further confirmed with numerical simulations. Fig. 4.7 (a) shows the number of roundtrips needed to reach a steady for cavity dispersions from –0.6 ps^2 to +0.6 ps^2. Modulation depths from 1% to 20% have been simulated. Because the properties of a resonant SESAM (see Section 3.4) the saturation energies were decreased with increased modulation depth to maintain $q_0 E_{sat,A} = const$. The simulation was started from white noise. The evolution of the pulse was observed up to 10 000 cavity round trips. For low-modulation-depth steady states have been observed only for anomalous dispersion of the cavity. Therefore, self-starting mode locking is only

possible with soliton-pulse shaping achieved by an intra cavity dispersion compensation. As seen from Fig. 4.7 (a), the number of rounds trips needed to reach a steady state is largely independent of the dispersion for high modulation depth and low saturation energy, i.e. the self-starting can be achieved for a large range of normal and anomalous dispersions.

In summary, a resonant SESAM provides nonlinear characteristics that enable easy self-starting operation, while maintaining stability against Q-switched mode locking.

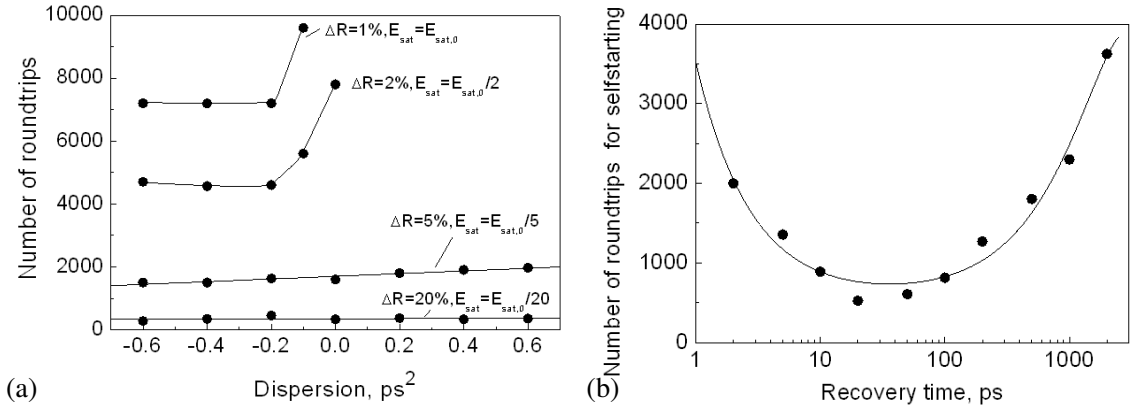

Fig. 4.7: *Simulation of the self-starting process in a fiber laser; shown is the number of roundtrips to achieve steady-state operation (a) for different cavity dispersions and modulation depths. (b) for different recovery times.*

4.2.2 Recovery time

Based on Equation 2.31, a long recovery is desirable for self-starting because it ensures a lower saturation power and, therefore, a higher response to low-power fluctuations. However, we observed that an as-grown SESAM could not start mode-locking in a SESAM, in contrast to the bombarded SESAM, which ensured reliable self-starting. Analysis [P2] shows that a cw-field in a laser, e.g. ASE from the active fiber, can saturate the absorber, and reduce the modulation depth thus prevent mode locking. The field incident onto the absorber can be separated in a time dependent part $P_{pulse}(t)$ and a time independent part P_0:

$$P(t) = P_{pulse}(t) + P_0. \tag{4.1}$$

By substituting this expression in Equation 2.26, we obtain an equation for the evolution of saturable absorption in the presence of a cw-background in a laser cavity. It is identical with the original expression 2.26; however, the modulation depth q_0 is

replaced by an effective modulation depth $q_{0,eff}$ given by

$$q_{0,eff} = q_0 \frac{1}{1 + P_0 \tau_{rec,A} / E_{sat}}. \tag{4.2}$$

This equation describes a decrease in modulation depth and a corresponding degradation in the starting capability of the SESAM.

The effect of the recovery time was further investigated by simulating the start up of a fiber laser from noise and varying the absorber recovery time. Other parameters used were a pulse energy of 80 pJ, a cw-background radiation of 4 mW, and a modulation depth of 20%. Fig. 4.7 (b) shows the numbers of roundtrips needed to achieve a steady state for different recovery times. The graph clearly shows that there is an optimal range for recovery times between 10 ps and 100 ps. At shorter recovery times, the absorber does not provide sufficient discrimination for the start up from low intensity fluctuations, and the number of roundtrips needed to achieve a steady state increases. When using absorber recovery times longer than 100 ps, the cw-radiation saturates the absorber and prevents a reliable self-starting operation.

In experiments the recovery time of the InGaAs quantum-well absorption has been changed using heavy-ion irradiation (see reference [P2] for further details). The irradiation with 10-MeV nickel ions was found to decrease the recovery time by 2 to 3 orders of magnitude. Fig. 4.8 (a) shows the nonlinear reflectivity of the as-grown and bombarded SESAMs. The other nonlinear properties are a saturation fluence of 3.3 J/cm^2 and 5.0 J/cm^2 and a modulation depth of 18.3% and 17.7% for the unbombarded and the bombarded SESAM, respectively. The non-saturable losses are increased from 8% to 16% after the ion irradiation, but still they are tolerable in a fiber laser cavity. A mode-locked fiber laser with the fast absorber could start mode

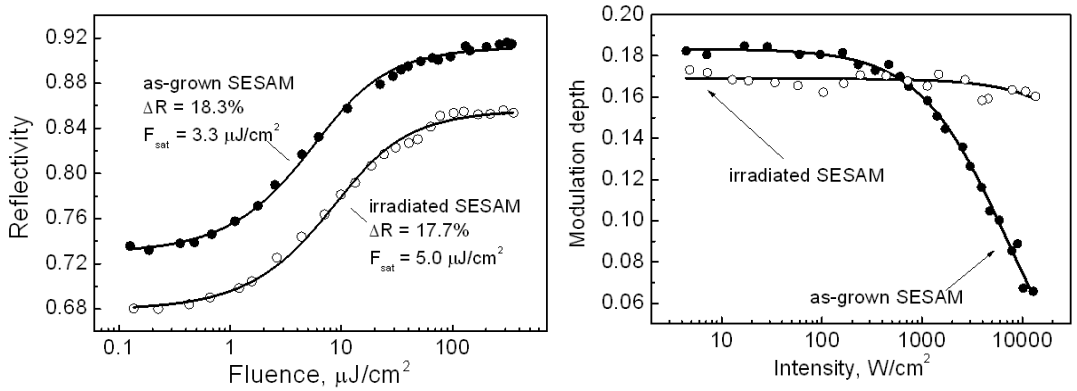

(a) (b)

Fig. 4.8: *(a) Nonlinear reflectivity measurements for unbombarded and bombarded SESAM (b) Effective modulation depth measured with incident cw-radiation for unbombarded and bombarded SESAM.*

locking, whereas, the unbombarded absorber remains in cw-mode. The reason was investigated by measuring the nonlinear reflectivity using cw-radiation. Fig. 4.8 (b) shows the effective modulation depth as a function of the incident cw-radiation for the unbombarded and bombarded SESAM. For the slow absorber, the incident cw-light degrades the modulation depth. Remarkably, with an intensity of 10000 W/cm^2, corresponding to a cw-power of 3 mW, the effective modulation depth decreases from 18 % to 6%, whereas, for the fast absorber this decrease is below 1 %.

It is interesting that the recovery time of the absorbers can be estimated using the combination of the pulsed and the cw-measurement. The fitting curve in Fig. 4.8 (b) using Equation 4.2 gives the saturation power $P_{sat,A} = E_{sat,A}/\tau_A$. We can estimate the recovery time to be around 200 ps for the slow absorber and 5 ps for the fast absorber with the saturation energy, derived from the measurement shown in Fig. 4.8 (a).

In conclusion, we found that the cw-background radiation can degrade the modulation depth of a saturable absorber. Fast absorbers prevent the undesirable effect of cw-background radiation, such as ASE, on the absorber.

4.3 Influence of two-photon absorption in resonant semiconductors

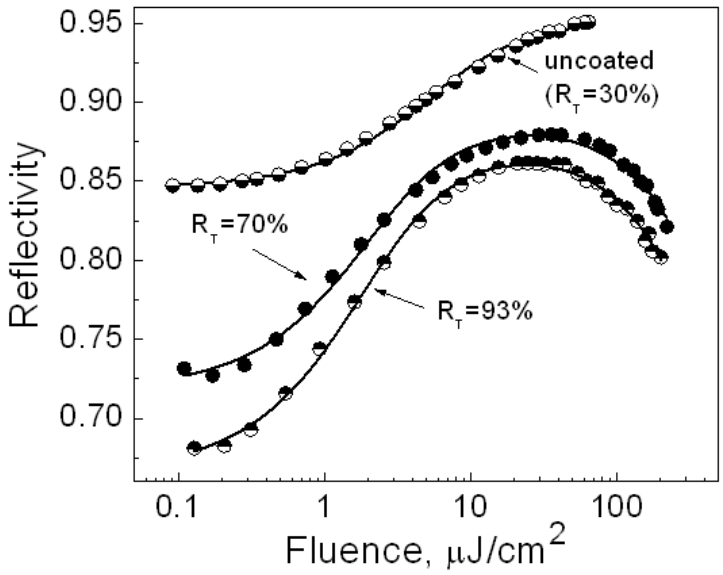

Fig. 4.9: *Nonlinear reflectivity of a quantum well absorber with an uncoated top surface and with top mirror reflectivities of 70% and 93%.*

Passive mode locking by saturable absorbers was shown to be a powerful technology for generating ultrashort pulses. For different lasers, various conditions, however, have to be maintained to achieve stable high quality mode-locking. To prevent Q-switched mode locking a careful balance between the saturable absorbtion and gain saturation has to be maintained. Inverse saturable absorption caused by TPA can be

exploited for preventing QSML in addition to the gain saturation [66]. This leads to a modified criterion for Q-switched mode locking [67]:

$$E_P^2 > \frac{q_0 E_{sat,A}}{1/E_{sat,L} + 1/E_2}, \tag{4.3}$$

where E_2 is the inverse slope of the induced two-photon absorption.

The analysis presented in Section 3.4 showed that the electric field in an absorber with cavity, as shown in Fig. 3.4, is enhanced by a factor ε compared to the cavity-free absorber, which is realized by an anti-reflection top mirror. The inverse nonlinear slope is consequently reduced by [P4]

$$E_2 = \frac{1}{\varepsilon^2} E_{2,0} \tag{4.4}$$

compared to the inverse nonlinear slope of the antireflection coated structure $E_{2,0}$. Since the saturation energy decreases linearly with $1/\varepsilon$, TPA can dominate the absorber response. Fig. 4.9 shows the nonlinear reflectivity of a saturable absorber mirrors with top mirror reflectivities of 30% (uncoated mirror), 70%, and 90%. More details about the experiment can be found in [P4]. The measurement data has been fitted with the function [68]:

$$R(F) = R_{ns} - [1 - exp(-F/F_{sat,A}] \frac{q_0}{F/F_{sat,A}} - \frac{F}{F_2}. \tag{4.5}$$

R_{ns} accounts for the nonsaturable loss of the structure and F_2 is the inverse slope of the induced two-photon-absorption. It is a measure for the threshold-fluence for two-photon absorption.

R_{top}	l	q_0	$F_{sat,A}$	F_2
30%	6%	10%	$3\mu J/cm^2$	n.a.
70%	10%	17%	$1.1\mu J/cm^2$	$3300\mu J/cm$
93%	11%	21%	$1.0\mu J/cm^2$	$2600\mu J/cm$

Table 4.1: *Parameters for different top-mirror reflectivities R_{top}, extracted from Fig. 4.9. Parameters: non saturable loss l, modulation depth q_0, saturation fluence $F_{sat,A}$ and inverse two-photon-absorption slope F_2 of the SESAM at resonance*

Table 4.1 shows the parameters deducted from the fitting curves in Fig. 4.9. For the uncoated sample no TPA could be detected. The modulation depths near the resonant wavelength of the absorber cavity increased from 17% to 21% when the top mirror reflectivities increase from 70% to 90%. The enhancement of the electric field caused an onset of the TPA at lower incident energies for the higher reflectivity mirror. The inverse slope drops from 3300 $\mu J/cm$ to 2600 $\mu J/cm$, whereas, the saturation energy decreased from 1.1 $\mu J/cm^2$ to 1.0 $\mu J/cm^2$. Fig. 4.9 indicates that the

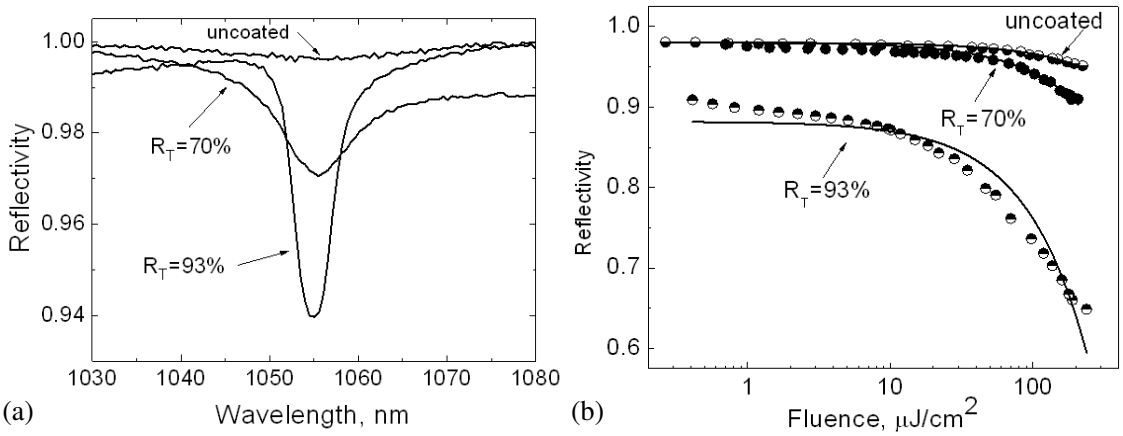

Fig. 4.10: *(a) Linear reflectivity and (b) nonlinear reflectivity of semiconductor mirrors. The top mirror reflectivies are 30% (uncoated), 70% and 93%.*

TPA-induced rollover may eventually decrease the effective modulation depth and, therefore, prevent mode locking. However, to a certain extent the saturation energy can be controlled independently by adjusting the number of quantum wells and the thickness of the spacer layer used as TPA-material.

The resonant TPA effect was further investigated using a bulk structure. Fig. 4.10 (a) shows the low intensity reflectivities and (b) the nonlinear reflectivities of a bulk structure with different top mirror reflectivities. The inverse slope F_2 of the TPA is 7600 $\mu J/cm^2$, 2600 $\mu J/cm^2$ and 800 $\mu J/cm^2$ for the uncoated, 70% and 93% top mirror reflectivity, respectively. Fig. 4.10 (b) clearly illustrates the enhancement of TPA with increasing top mirror reflectivity.

This study shows that the field enhancement in resonant cavities, which is commonly used for adjusting saturable absorber parameters, enhanced two-photon absorption as well. Thus in resonant absorbers the TPA effect can prevent QSML, whereas, the effective modulation depth might decrease and inhibit the self-starting mode locking. Therefore, a proper design of the resonant structure is required to exploit two photon absorption for preventing Q-switched mode-locking while maintaining the self-starting character of pulse operation.

5. SEMICONDUCTOR ALL-OPTICAL MODULATOR

In this chapter we demonstrate the use of saturable absorber mirrors as all-optical SEmiconductor Modulator Mirrors (SEMMs) to synchronize the repetition rate of a mode-locked ytterbium fiber laser at 1.05 μm to an mode-locked erbium fiber laser at 1.55 μm. Active mode-locking has also been achieved using an SEMM as an intra-cavity modulator.

5.1 Synchronization of independent, short-pulse fiber lasers

Applications like sum- and difference frequency generation, coherent anti-Stokes-Raman scattering microscopy, and two-color pump-probe investigation use pulse trains that are synchronized to each other with respect to their repetition rate. We demonstrated synchronization of outputs of two fiber lasers using cross-phase modulation in a fiber sharing a cavity [S3], synchronization of a master/slave configuration [S4], and synchronization of a fiber laser to a pulsed diode system[S5]. Synchronization of a passively mode-locked laser to a sine-modulation has been demonstrated by an amplitude modulator [69] and by modulation of the SESAM reflectivity by residual pump [70]. Synchronization by refractive index modulation due to free carrier generation has been demonstrated in solid state lasers [71]. In contrast to reference [71] we show synchronization using the amplitude modulation of the SEMM.

The synchronization is realized by focusing the pulse train from the master laser onto the SESAM that acts as a mode-locking element in the slave laser. Fig. 5.1 shows the the setup used for synchronization and active mode locking. The master laser is an Yb-doped fiber laser similar to the one described in Section 2.2. After amplification in a single clad fiber amplifier it delivers 2 *ps* pulses with an average power up to 30 *mW*. The amplifier consist of an ytterbium fiber pumped in counter-propagating direction by a 980 *nm* single-mode diode laser. Isolators where placed after the seed laser and the amplifier to protect the master laser system from feedback. The slave laser is an Er-doped fiber laser mode locked by a SESAM which also acts as the SEMM. The master pulse train is coupled into the slave laser cavity through an 1050 *nm*/ 1550 *nm* dichroic mirror. The repetition rates of master and slave laser are first coarsely equalized by adding an appropriate length of single-mode fiber in the master

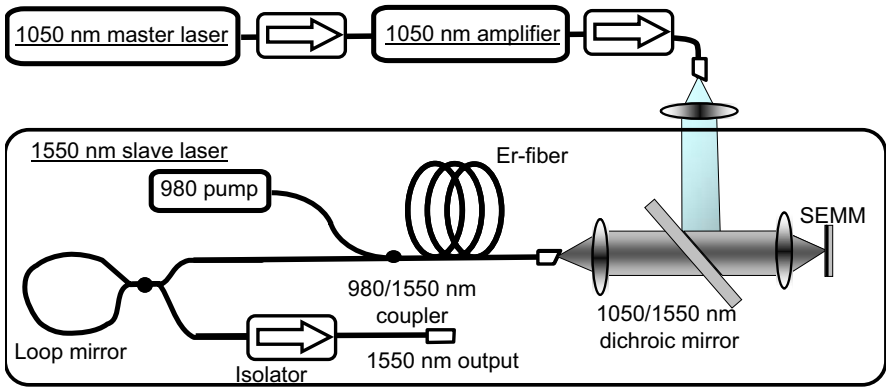

Fig. 5.1: *Setup for the SEMM synchronization experiments.*

laser cavity. By placing the SESAM-lens assembly of the master laser on a translation stage the repetition rate of the slave laser can be set closely to the rate of the master laser. The position was monitored using an inductive gauge with 0.5 μm precision.

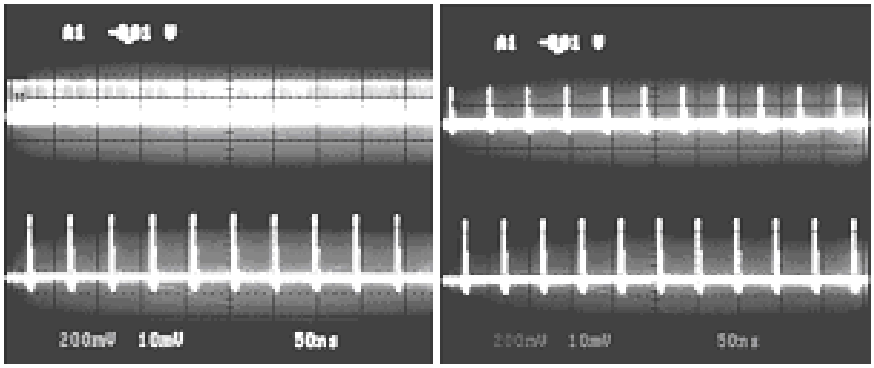

(a) (b)

Fig. 5.2: *Oscilloscope traces for mode locked pulse trains of the master laser (bottom trace) and the slave laser (top trace) triggered to the master pulse train (a) shows the unlocked state and (b) shows the locked state.*

The lasers could be easily locked together by setting the repetition rates close enough to each other using the translation stage of the master laser. The repetition rates of the master and the slave laser were measured using a microwave spectrum analyzer. Fig. 5.2 (a) shows a photograph from an analog scope showing the non-synchronized, free-running operation. In the non-synchronized regime only the master pulse train, used as trigger source, can be observed on the oscilloscope. In contrast, master and slave pulse trains could be seen clearly on the scope as shown in Fig. 5.2 (b) in the synchronized regime.

In Fig. 5.3 (a) the repetition rates of master and slave lasers are shown for different cavity displacements of the master laser. In the non-locking free-running regime

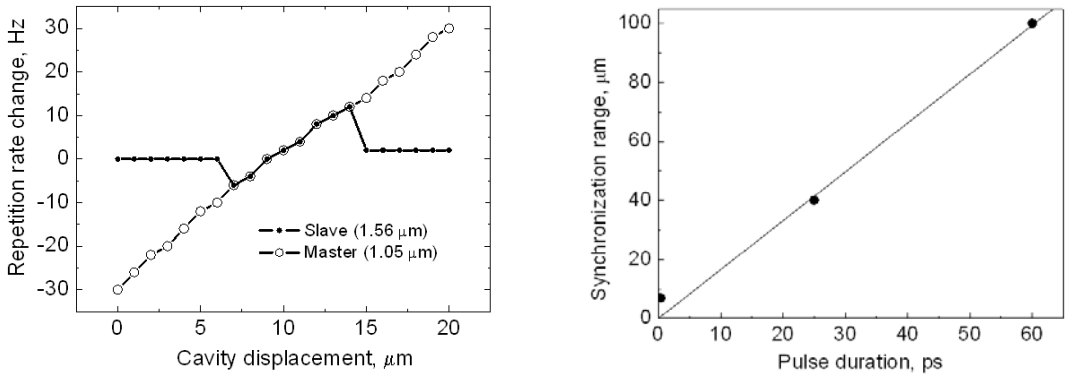

(a) (b)

Fig. 5.3: *(a) Repetition rates measured with a microwave spectrum analyzer of the master and slave laser as a function of the cavity displacement of the slave laser. (b) Synchronization range of the SEMM as a function of the slave laser pulse duration*

the master repetition rate changes linearly with the cavity displacement while the slave laser repetition rate stays constant. When both cavity lengths are brought close enough to each other the slave laser repetition rate jumps to the repetition of the master laser. For a cavity-tuning range of 7 μm, the slave laser repetition rate follows the master laser repetition rate. After exceeding the locking range the slave laser repetition rate stays again constant with the initial value.

In Fig. 5.3 (b) the dependence of the locking range on the pulse duration is presented. The pulse duration has been adjusted by using intra cavity filters with bandwidths between 1 *nm* and 10 *nm* and by changing the cavity dispersion. With a pulse duration of 60 *ps* a locking range of 100 μm could be reached compared to the locking range of 7 μm for the 0.8 *ps* pulse. The proportionality of the locking range to the pulse duration indicates the synchronization by amplitude modulation because the maximum achievable shift of a pulse by amplitude modulation is proportional to its duration.

We simulated the SEMM setup to achieve a deeper understanding of the locking process. The simulation is similar to that made for the fiber laser in Section 2.3.3. The saturable absorber, however, is saturated now by both the slave laser pulse with the saturation energy $E_{sat,slave}$ as in Equation 2.26 and by the master laser with a different saturation energy $E_{sat,master}$. The saturation dynamic is described by

$$\frac{dq_{slave}}{dt} = -\frac{q_{slave} - q_{0,slave}}{\tau_A} - \left(\frac{P_{slave}}{E_{sat,slave}} + \frac{P_{master}}{E_{sat,master}}\right) q_{slave}. \tag{5.1}$$

P_{slave} and P_{master} are the incident powers for the slave and master wavelength, respectively. q_{slave} is the saturable loss, $q_{0,slave}$ is the modulation depth for the slave pulse,

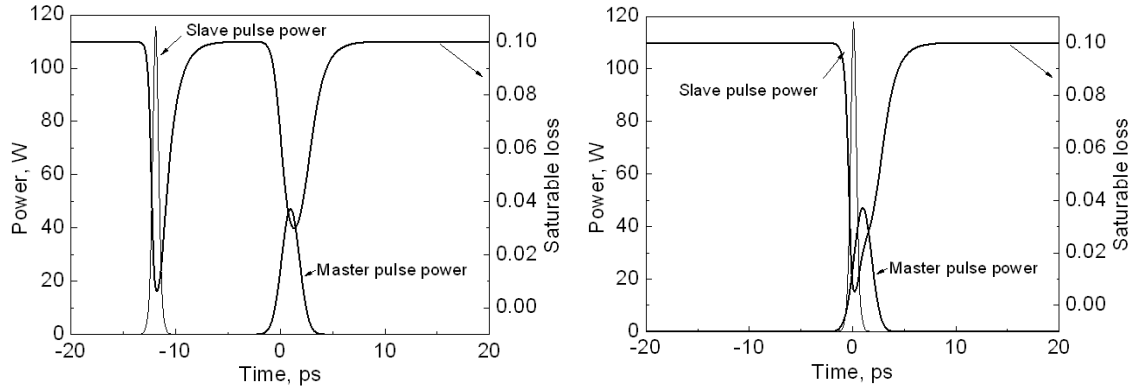

Fig. 5.4: *Simulation of the saturable absorption (left axis) for the slave pulse for (a) pulses are not intersecting on the SEMM (unlocked state) and (b) Pulses are intersecting on the SEMM (locked state). The right axis shows the pulse power for the master pulse and the slave pulse on (a) and (b).*

and τ_A is the recovery time of the SEMM structure. The modulation depth used in the simulation is 0.1, the saturation energy for the slave-laser wavelength is 10 pJ of the master-laser wavelength 40 pJ, the recovery time 10 ps and the pulse energy of the master pulse 200 pJ with a pulse duration of 2 ps. The simulated response of the absorber, when the SEMM is exposed to both the master and slave pulse is shown in Fig. 5.4. Fig. 5.4 (a) shows the pulses in the unlocked state, when pulses do not overlap in time on the SEMM. The fast recovery time guarantees a strong pulse shaping. The energy of the master pulse was chosen so, that it only partially saturated the SEMM; therefore, the SEMM provided enough pulse shaping to shift the slave pulse; however, a saturation reserve was necessary to mode lock the slave laser. This is in accordance with the experiment: with low saturation of the SEMM for low master pulse energy synchronization of the pulse trains was not possible. In contrast, strong saturation by the master pulse leads to a small modulation depth for the slave pulse, preventing slave-laser mode locking.

For the slave laser simulation an anomalous dispersion of –0.12 ps^2 has been chosen to employ soliton pulse shaping and to achieve sub-picosecond pulse duration. Fig. 5.5 shows the simulation results with these parameters. The simulated slave laser has a pulse duration of 0.8 ps. Fig. 5.5 (a) shows the master pulse train and the slave pulse train with a cavity-length offset from the master master pulse train of 9.0 μm. The slave pulse train initially shifts 0.03 ps per round trip with respect to the master pulse train, corresponding to a repetition rate difference of 33 Hz. When the two pulse trains collide on the absorber, the master pulse begins to modulate the slave pulse through the interaction in the SEMM. This causes the slave pulse train to shift in time by 0.03 ps per round trip and to equalize the repetition rates. In Fig. 5.5 (b) the offset of 10.5 μm is too high to be compensated by the SEMM. The lasers remain

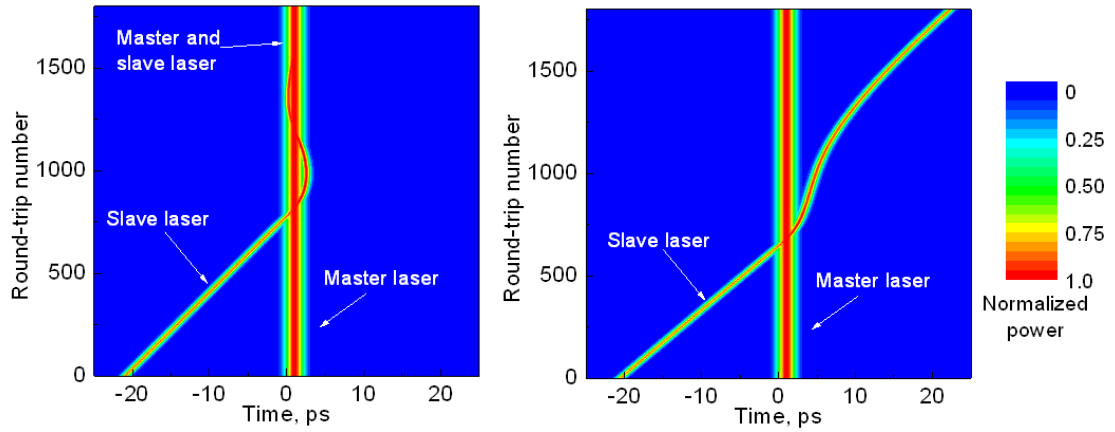

Fig. 5.5: *Simulation of SEMM locking; Normalized pulse shape intensity profile for different round trip numbers for (a) master laser at a repetition rate of 33.3 MHz and slave laser with a cavity offset of 9.0 µm, corresponding to a repetition rate difference of 33* Hz*, relative to the master laser (b) master laser at a repetition rate of 33.3 MHz and slave laser with a cavity offset of 10.5 µm, corresponding to a repetition rate difference of 38* Hz*, relative to the master laser (a) shows synchronization and (b) shows independent repetition rates.*

offset by 0.035 *ps* corresponding to a repetition rate difference of 38 *Hz*. Further simulations revealed high asymmetry regarding the sign of the repetition rate offset. Large offsets could only be compensated for slave laser repetition rates lower than the master laser repetition rate because of the asymmetry of the slow absorber response. In conclusion, the simulations confirmed the locking mechanism by pulse shifting through amplitude modulation.

5.2 Active mode locking

Self-starting passive mode locking of the slave laser should be avoided to achieve active mode locking by modulation of the SEMM. A fast absorber ensures the self-starting operation of the slave laser. When using an unbombarded SESAM, the slave laser cannot start mode locking, and it remains in a Q-switched regime. The Q-switching of the absorber is caused by the high modulation depth and the low saturation power of the SEMM. This mode of operation is shown in Fig. 5.6 (a). When driving the SEMM with the master laser, the amplitude modulation causes the slave laser to start mode locking actively as seen in Fig. 5.6 (b).

Active mode locking with an optically driven SEMM makes it possible to overcome the limitation Equation 2.6 regarding the pulse duration with respect to the modulation frequency ω_M. The pulse duration τ_P is proportional to the inverse square root

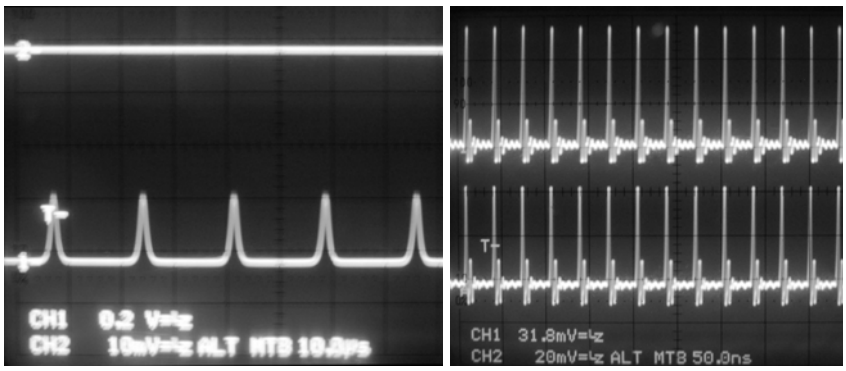

(a) (b)

Fig. 5.6: *Fully optically actively mode-locked slave laser. The top trace shows the 1.05 μm master laser and the bottom trace the 1.55μm slave laser (a) Master laser turned off, slave laser in Q-switched operation (time scale 10 μs/div) (b) Master laser mode locking, slave laser actively mode-locked (time scale 50 ns/div).*

of the modulation frequency, which is determined by the cavity-round trip time T_R; Therefore $\tau_P \sim \sqrt{T_R}$ [23]. In our setup the modulation strength depends on the detuning of the cavity. When the slave laser repetition rate is smaller than the master laser repetition rate the slave pulse coincides with the trailing edge of the master pulse. At the trailing pulse edge the absorber starts to recover at a rate inversely proportional to the absorber recovery time τ_A; therefore the modulation strength is determined by $\tau \sim \sqrt{\tau_A}$. When the slave laser repetition rate is higher than the master laser repetition rate, the slave pulse coincides with the leading edge of the master pulse. At the leading pulse edge the absorber starts to saturate at a rate inversely proportional to the pulse duration τ_{master}. Therefore the modulation strength is determined by the master pulse duration $\tau \sim \sqrt{\tau_{master}}$. Thus it is possible for a given repetition rate to achieve with active SEMM mode locking much shorter pulse durations compared with a sine-shaped modulator. For a given repetition rate of 50 *MHz* and a pulse duration of 2.5 *ps* a pulse shortening by a factor of 100 can be obtained using SEMM locking compared to sine-shaped amplitude mode locking.

The cavity-mismatch tolerance is dominated by the detuning effects in an actively mode-locked laser, which has a tolerance against cavity length detuning proportional to τ/N [20], where τ_P is the steady state pulse duration and N the number of round trips needed to shape and pull the pulse into synchronization; therefore it is expected that the tolerable cavity mismatch is proportional to the the pulse duration like in the case of synchronization. Stable active mode locking was reached for a cavity mismatch of 250 μm; however, it was found, that a large cavity mismatch results in a degradation of the mode-locking behavior. Due to the long loss window of the absorber, the laser showed wings and multiple pulse behavior for large cavity mismatches. For small cavity mismatches (< 100 μm) stable mode-locked operation

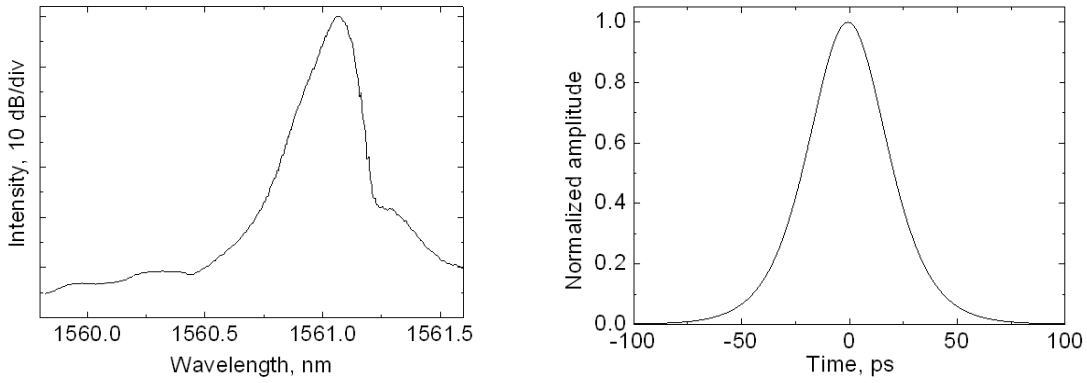

(a) (b)

Fig. 5.7: *(a) Spectrum and (b) autocorrelation of the actively mode-locked slave laser.*

with high pulse quality was maintained. Fig. 5.7 shows an actively mode-locked pulse spectrum (a) with a spectral width of 0.15 *nm* and the autocorrelation (b) corresponding to a pulse duration of 30 *ps*.

Using the same setup we achieved synchronization of two fiber lasers and all-optical active mode-locking. With careful selection of the absorber parameters, laser operation could be changed from synchronization to active mode locking.

6. CONCLUSIONS

This thesis dealt with the design of SESAMs and their properties. The primary focus was on the effect of SESAM parameters on mode-locked fiber lasers. The main achievements of this thesis are as follows:

A systematic investigation of resonant SESAMs. High-modulation-depth SESAMs produced by resonant Fabry–Perot cavities provide easy self-starting and maintain reliable suppression of Q-switched mode locking due to their low saturation energy.

The recovery time of SESAMs needs to be within a certain range to ensure reliable self-starting. When the absorber has a too-long recovery time, amplified spontaneous emission can saturate the absorber and, therefore, prevent self-starting.

We set up a fiber laser mode-locked by a quantum-dot absorber with a short recovery time. The high, nonlinear contrast and the low saturation energy of the SESAM, in combination with its low recovery time, enables self-starting picosecond-pulse generation.

The field enhancement in resonant semiconductor structures also increases the two photon absorption. This can improve the stability against Q-switched mode-locking, whereas the two-photon-absorption-induced rollover can degrade the modulation depth of a SESAM and, consequently, inhibit self-starting mode locking.

SESAMs can also be used as Semiconductor Modulator Mirrors (SEMMs). We demonstrated the simultaneous use of a SEMM as a mode-locking element in a 1.55 μm laser and as an element that provides the synchronization of the repetition rate to a 1.05 μm laser. Furthermore, we demonstrated all-optical active mode locking of a 1.55 μm laser driven with a SEMM.

In summary, we have thoroughly investigated ways to adjust the SESAM parameters for reliably self-starting, high-pulse-quality mode-locked fiber lasers.

BIBLIOGRAPHY

[1] T. Maiman, "Stimulated Optical Radiation in Ruby," *Nature*, vol. 187, pp. 493–494, 1960.

[2] J. Limpert, F. Röser, T. Schreiber, and A. Tünnermann, "High-Power Ultrafast Fiber Laser Systems," *Selected Topics in Quantum Electronics, IEEE Journal of*, vol. 12, p. 233, 2006.

[3] T. Juhasz, F. Loesel, R. Kurtz, C. Horvath, J. Bille, and G. Mourou, "Corneal refractive surgery with femtosecond lasers," *Selected Topics in Quantum Electronics, IEEE Journal of*, vol. 5, pp. 902–910, 1999.

[4] S. Konorov, V. Mitrokhin, A. Fedotov, D. Sidorov-Biryukov, V. Beloglazov, N. Skibina, A. Shcherbakov, E. Wintner, M. Scalora, and A. Zheltikov, "Laser Ablation of Dental Tissues with Picosecond Pulses of 1.06-μm Radiation Transmitted through a Hollow-Core Photonic-Crystal Fiber," *Applied Optics*, vol. 43, pp. 2251–2256, 2004.

[5] K. Kim, Z. Guo, J. Li, and S. Kumar, "Radiation heat transfer in tissue welding and soldering with ultrafast lasers," *Bioengineering Conference, 2003 IEEE 29th Annual, Proceedings of*, pp. 185–186, 2003.

[6] X. Liu, D. Du, and G. Mourou, "Laser ablation and micromachining with ultrashort laser pulses," *Quantum Electronics, IEEE Journal of*, vol. 33, pp. 1706–1716, 1997.

[7] Y. Kuo and M. Birnbaum, "Passive Q switching of the alexandrite laser with a Cr_4:Y_2SiO_5 solid-state saturable absorber," *Appl. Phys. Lett*, vol. 67, 1995.

[8] B. Braun, F. Kartner, G. Zhang, M. Moser, and U. Keller, "56-ps passively Q-switched diode-pumped microchip laser," *Optics Letters*, vol. 22, pp. 381–383, 1997.

[9] A. Demaria, H. Heynau, and D. Stetser, "Self mode-locking of lasers with saturable absorbers (Reversible bleachable dye-solutions for expander elements in laser)," *Applied Physics Letters*, vol. 8, pp. 174–176, 1966.

[10] J. Valdmanis, R. Fork, and J. Gordon, "Generation of optical pulses as short as 27 femtoseconds directly from a laser balancing self-phase modulation, group-velocity dispersion, saturable absorption, and saturable gain," *Optics Letters*, vol. 10, pp. 131–133, 1985.

[11] R. Ell, U. Morgner, F. Kärtner, J. Fujimoto, E. Ippen, V. Scheuer, G. Angelow, T. Tschudi, M. Lederer, A. Boiko, *et al.*, "Generation of 5-fs pulses and octave-spanning spectra directly from a Ti: sapphire laser," *Optics Letters*, vol. 26, pp. 373–375, 2001.

[12] H. Haus, J. Fujimoto, and E. Ippen, "Analytic theory of additive pulse and Kerr lens mode locking," *Quantum Electronics, IEEE Journal of*, vol. 28, pp. 2086–2096, 1992.

[13] D. Botez, "High-power single-mode semiconductor diode lasers," *1981 International Electron Devices Meeting*, vol. 27, 1981.

[14] K. Tamura, H. Haus, and E. Ippen, "Self-starting additive pulse mode-locked erbium fibre ring laser," *Electronics Letters*, vol. 28, pp. 2226–2228, 1992.

[15] I. Duling III, "Subpicosecond all-fibre erbium laser," *Electronics Letters*, vol. 27, pp. 544–545, 1991.

[16] M. Rusu, S. Karirinne, M. Guina, A. Grudinin, and O. Okhotnikov, "Femtosecond Neodymium-Doped Fiber Laser Operating in the 894–909-nm Spectral Range," *Photonics Technology Letters, IEEE*, vol. 16, p. 1029, 2004.

[17] R. Sharp, D. Spock, N. Pan, and J. Elliot, "190-fs passively mode-locked thulium fiber laser with a low threshold," *Optics Letters*, vol. 21, no. 12, pp. 881–883, 1996.

[18] L. Nelson, E. Ippen, and H. Haus, "Broadly tunable sub-500 fs pulses from an additive-pulse mode-locked thulium-doped fiber ring laser," *Applied Physics Letters*, vol. 67, pp. 19–21, 2006.

[19] I. Tomov, R. Fedosejevs, and M. Richardson, "Ultrashort pulse generation in lasers with active mode locking," *Quantum Electronics*, vol. 10, pp. 797–807, 1980.

[20] A. Siegman, *Lasers*. University Science Books, 1986.

[21] H. Haus, "Theory of mode locking with a fast saturable absorber," *Journal of Applied Physics*, vol. 46, pp. 3049–3058, 1975.

[22] M. Becker, D. Kuizenga, and A. Siegman, "Harmonic mode locking of the Nd: YAG laser," *Quantum Electronics, IEEE Journal of*, vol. 8, pp. 687–693, 1972.

[23] D. Kuizenga and A. Siegmann, "FM and AM mode locking of the homogeneous laser. I - Theory (Homogeneously broadened pulsed laser mode locking with internal frequency or amplitude modulation)," *Quantum Electronics, IEEE Journal of*, vol. 6, pp. 694–708, 1970.

[24] A. Hasegawa and Y. Kodama, "Signal transmission by optical solitons in monomode fiber," *Proceedings of the IEEE*, vol. 69, pp. 1145–1150, 1981.

[25] D. Jones, H. Haus, and E. Ippen, "Subpicosecond solitons in an actively mode-locked fiber laser," *Optics Letters*, vol. 21, pp. 1818–1820, 1996.

[26] V. Matsas, T. Newson, D. Richardson, and D. Payne, "Self starting passively mode-locked fibre ring soliton laser exploiting nonlinear polarisation rotation," *Electronics Letters*, vol. 28, p. 1391, 1992.

[27] I. Duling, "All-fiber ring soliton laser mode locked with a nonlinear mirror," *Optics Letters*, vol. 16, pp. 539–541, 1991.

[28] P. French, J. Williams, and J. Taylor, "Femtosecond pulse generation from a titanium-doped sapphire laser using nonlinear external cavity feedback," *Optics Letters*, vol. 14, pp. 686–688, 1989.

[29] F. Kärtner, J. der Au, and U. Keller, "Mode-locking with slow and fast saturable absorbers – What's the difference?" *IEEE J. Sel. Top. Quantum Electron*, vol. 4, pp. 159–168, 1998.

[30] O. Okhotnikov, L. Gomes, N. Xiang, T. Jouhti, and A. Grudinin, "Mode-locked ytterbium fiber laser tunable in the 980-1070-nm spectral range," *Optics Letters*, vol. 28, pp. 1522–1524, 2003.

[31] L. Orsila, L. Gomes, N. Xiang, T. Jouhti, and O. Okhotnikov, "Mode-Locked Ytterbium Fiber Lasers," *Applied Optics*, vol. 43, pp. 1902–1906, 2004.

[32] E. Treacy, "Optical pulse compression with diffraction gratings," *Quantum Electronics, IEEE Journal of*, vol. 5, pp. 454–458, 1969.

[33] H. Lim, F. Ilday, and F. Wise, "Femtosecond ytterbium fiber laser with photonic crystal fiber for dispersion control," *Optics Express*, vol. 10, pp. 1497–1502, 2002.

[34] H. Lim and F. Wise, "Control of dispersion in a femtosecond ytterbium laser by use of hollow-core photonic bandgap fiber," *Optics Express*, vol. 12, pp. 2231–2235, 2004.

[35] A. Isomäki and O. Okhotnikov, "All-fiber ytterbium soliton mode-locked laser with dispersion control by solid-core photonic bandgap fiber," *Optics Express*, vol. 14, pp. 4368–4373, 2006.

[36] D. Hanna, R. Percival, I. Perry, R. Smart, P. Suni, and A. Tropper, "An Ytterbium-doped Monomode Fibre Laser: Broadly Tunable Operation from 1.010 μm to 1.162 μm and Three-level Operation at 974 nm," *Journal of Modern Optics*, vol. 37, pp. 517–525, 1990.

[37] F. Ilday, J. Buckley, L. Kuznetsova, and F. Wise, "Generation of 36-femtosecond pulses from a ytterbium fiber laser," *Optics Express*, vol. 11, pp. 3550–3554, 2003.

[38] J. Limpert, S. Höfer, A. Liem, H. Zellmer, A. Tünnermann, S. Knoke, and H. Voelckel, "100-W average-power, high-energy nanosecond fiber amplifier," *Applied Physics B: Lasers and Optics*, vol. 75, pp. 477–479, 2002.

[39] S. Yamashita, "Widely tunable erbium-doped fiber ring laser covering both C-band and L-band," *Selected Topics in Quantum Electronics, IEEE Journal of*, vol. 7, pp. 41–43, 2001.

[40] A. Snyder and J. Love, "Optical waveguide theory," *J. Opt. Soc. Am. A*, vol. 3, p. 378, 1986.

[41] C. Hönninger, R. Paschotta, M. Graf, F. Morier-Genoud, G. Zhang, M. Moser, S. Biswal, J. Nees, A. Braun, G. Mourou, I. Johannsen, A. Giesen, W. Seeber, and U. Keller, "Ultrafast ytterbium-doped bulk lasers and laser amplifiers," *Applied Physics B: Lasers and Optics*, vol. 69, pp. 3–17, 1999.

[42] M. Jiang, G. Sucha, M. Fermann, J. Jimenez, D. Harter, M. Dagenais, S. Fox, and Y. Hu, "Nonlinearly limited saturable-absorber mode locking of an erbium fiber laser," *Optics Letters*, vol. 24, pp. 1074–1076, 1999.

[43] E. Desurvire, "Analysis of transient gain saturation and recovery in erbium-doped fiber amplifiers," *Photonics Technology Letters, IEEE*, vol. 1, pp. 196–199, 1989.

[44] G. Agrawal, *Nonlinear Fiber Optics*. Academic Press, 2001.

[45] H. Haus, "Mode-locking of lasers," *Selected Topics in Quantum Electronics, IEEE Journal of*, vol. 6, pp. 1173–1185, 2000.

[46] E. Desurvire, "Analysis of erbium-doped fiber amplifiers pumped in the 4 I 15/2-4 I 13/2 band," *Photonics Technology Letters, IEEE*, vol. 1, pp. 293–296, 1989.

[47] M. Hercher, "An analysis of saturable absorbers," *Appl. Opt*, vol. 6, p. 99, 1967.

[48] W. Press, S. Teukolsky, W. Vetterling, and B. Flannery, *Numerical Recipes in C*. Cambridge University Press Cambridge, 1992.

[49] I. Bronstein and K. Semendyayev, *Handbook of mathematics. Frankfurt/Main*. Van Nostrand Reinhold, 1979.

[50] S. Kelly, "Characteristic sideband instability of periodically amplified average soliton," *Electronics Letters*, vol. 28, pp. 806–807, 1992.

[51] U. Keller, K. Weingarten, F. Kärtner, D. Kopf, B. Braun, I. Jung, R. Fluck, C. Honninger, N. Matuschek, and J. aus der Au, "Semiconductor saturable absorber mirrors (SESAM's) for femtosecond to nanosecond pulse generation in solid-state lasers," *Selected Topics in Quantum Electronics, IEEE Journal of*, vol. 2, pp. 435–453, 1996.

[52] F. Krausz, C. Spielmann, T. Brabec, E. Wintner, and A. Schmidt, "Self-starting additive-pulse mode locking of a Nd:glass laser," *Optics Letters*, vol. 15, pp. 1082–1084, 1990.

[53] C. Flood, D. Walker, and H. van Driel, "Effect of spatial hole burning in a mode-locked diode end-pumped Nd: YAG laser," *Optics Letters*, vol. 20, pp. 58–60, 1995.

[54] H. Haus and E. Ippen, "Self-starting of passively mode-locked lasers," *Optics Letters*, vol. 16, pp. 1331–1333, 1991.

[55] F. Kaertner, L. Brovelli, D. Kopf, M. Kamp, I. Calasso, and U. Keller, "Control of solid state laser dynamics by semiconductor devices," *Optical Engineering (Bellingham, Washington)*, vol. 34, pp. 2024–2036, 1995.

[56] C. Hönninger, R. Paschotta, F. Morier-Genoud, M. Moser, and U. Keller, "Q-switching stability limits of continuous-wave passive mode locking," *J. Opt. Soc. Am. B*, vol. 16, pp. 46–56, 1999.

[57] U. Keller, D. Miller, G. Boyd, T. Chiu, J. Ferguson, and M. Asom, "Solid-state low-loss intracavity saturable absorber for Nd:YLF lasers – An antiresonant semiconductor Fabry-Perot saturable absorber," *Optics Letters*, vol. 17, pp. 505–507, 1992.

[58] S. Schmitt-Rink, D. Chemla, and D. Miller, "Theory of transient excitonic optical nonlinearities in semiconductor quantum-well structures," *Physical Review B*, vol. 32, pp. 6601–6609, 1985.

[59] E. L. Delpon, J. Oudar, N. Bouche, R. Raj, A. Shen, N. Stelmakh, and J. Lourtioz, "Ultrafast excitonic saturable absorption in ion-implanted InGaAs/InAlAs multiple quantum wells," *Applied Physics Letters*, vol. 72, pp. 759–761, 2006.

[60] E. Rafailov, S. White, A. Lagatsky, A. Miller, W. Sibbett, D. Livshits, A. Zhukov, and V. Ustinov, "Fast Quantum-Dot Saturable Absorber for Passive Mode-Locking of Solid-State Lasers," *Photonics Technology Letters, IEEE*, vol. 16, p. 2439, 2004.

[61] L. Brovelli, U. Keller, and T. Chiu, "Design and operation of antiresonant Fabry-Perot saturable semiconductor absorbers for mode-locked solid-state lasers," *J. Opt. Soc. Am. B*, vol. 12, pp. 311–322, 1995.

[62] W. Glenn, "Second-harmonic generation by picosecond optical pulses," *Quantum Electronics, IEEE Journal of*, vol. 5, pp. 284–290, 1969.

[63] M. Nakazawa, T. Yamamoto, and K. Tamura, "1.28 Tbit/s-70 km OTDM transmission using third- and fourth-order simultaneous dispersion compensation with a phase modulator," *Electronics Letters*, vol. 36, pp. 2027–2029, 2000.

[64] H. Haus and Y. Silberberg, "Laser mode locking with addition of nonlinear index," *Quantum Electronics, IEEE Journal of*, vol. 22, pp. 325–331, 1986.

[65] R. Paschotta and U. Keller, "Passive mode locking with slow saturable absorbers," *Applied Physics B: Lasers and Optics*, vol. 73, pp. 653–662, 2001.

[66] R. Grange, M. Haiml, R. Paschotta, G. Spühler, L. Krainer, M. Golling, O. Ostinelli, and U. Keller, "New regime of inverse saturable absorption for self-stabilizing passively mode-locked lasers," *Applied Physics B: Lasers and Optics*, vol. 80, pp. 151–158, 2005.

[67] T. Schibli, E. Thoen, F. Kärtner, and E. Ippen, "Suppression of Q-switched mode locking and break-up into multiple pulses by inverse saturable absorption," *Applied Physics B: Lasers and Optics*, vol. 70, pp. 41–49, 2000.

[68] M. Haiml, R. Grange, and U. Keller, "Optical characterization of semiconductor saturable absorbers," *Applied Physics B: Lasers and Optics*, vol. 79, pp. 331–339, 2004.

[69] O. Okhotnikov, M. Guina, and M. Pessa, "Stabilization of passive harmonic mode-locking by amplitude modulation," *Photonics Technology Letters, IEEE*, vol. 14, pp. 146–148, 2002.

[70] M. Guina and O. Okhotnikov, "Harmonic mode locking by synchronous optical pumping of a saturable absorber with the residual pump," *Optics Letters*, vol. 28, pp. 358–360, 2003.

[71] W. Seitz, R. Ell, U. Morgner, and F. Kärtner, "All-optical synchronization and mode locking of solid-state lasers with nonlinear semiconductor Fabry-Perot mirrors," *Selected Topics in Quantum Electronics, IEEE Journal of*, vol. 9, pp. 1093–1101, 2003.

Appendix 1

Publication 1

R. Herda and O. G. Okhotnikov, "Dispersion Compensation-Free Fiber Laser Mode-Locked and Stabilized by High-Contrast Saturable Absorber Mirror," *IEEE Journal of Quantum Electronics*, vol. 40, 2004, pp. 893–899.

Dispersion Compensation-Free Fiber Laser Mode-Locked and Stabilized by High-Contrast Saturable Absorber Mirror

Robert Herda and Oleg G. Okhotnikov

***Abstract*—We report here a compact diode-pumped fiber laser that represents a promising route to designing a portable and rugged picosecond light source. The laser presented in this paper is based on a high-contrast semiconductor saturable absorber mirror (SESAM) and targets reliable picosecond-range sources. The cavity is simple since no dispersion compensators are used, and the SESAM-based mode locking mechanism is robust and self-starting, resulting in low-maintenance turn-key operation. We investigated pulse formation in a short-length fiber cavity and found that nonlinear effects in a near-resonant SESAM in combination with large-cavity dispersion provide the predominant mechanism that causes pulse shaping. The role of a resonant high-contrast SESAM in preventing low-frequency Q-switching instability has been elucidated. The effect of the recovery time of the SESAM on the stretched pulse width and spectrum for resonant-type absorber mirrors was also studied.**

***Index Terms*—Fiber laser, mode-locked lasers, quantum wells, semiconductor devices, short pulse generation.**

I. Introduction

SHORT optical pulse generation has become an increasingly important technology in recent years in many applications including laser-based micromachining, thin-film formation, laser cleaning, medicine, and biology. Exciting results have been demonstrated with ultrashort pulses in ablation of a wide variety of materials with a minimum of thermal or shock damage to the surrounding materials. Examples include dielectrics, e.g., oxide ceramics, optical glasses, polymers, etc. Short pulses are also powerful instrumentals for surface patterning and microfabrication due to the noncontact character of material processing. In particular, higher spatial resolution can be achieved with short pulses by reducing the heat-affected zone and the shock-affected zone [1].

The requirements for simplicity, maintenance, and reliability, however, have not been met by conventional ultrafast technology currently based on solid-state lasers. Rapid progress in fiber laser technology has brought new opportunities and challenges with the development of the fiber optic components which are engineered to satisfy telecom requirements for operating conditions in severe environments. Another important technology that contributes essentially to the maintenance-free operation of the compact reliable ultrashort pulse lasers is the technology of semiconductor saturable absorber mirrors (SESAM). SESAMs have been used successfully to initiate and to sustain mode locking in a wide range of solid-state and fiber lasers [2]–[4]. The important aspect of using the SESAM in pulsed lasers is the flexibility in controlling the mirror parameters such as absorption recovery time, saturation fluence and insertion loss through the device design, growth conditions, and post-growth treatment, e.g., heavy ion implantation and thermal annealing. Exploiting the SESAM as a cavity mirror in the fiber laser results in compact size, and environmentally stable and simple ultrashort pulse lasers that can cover a wide wavelength range and generate optical pulses with durations from picoseconds to femtoseconds [4].

The broad fluorescence spectrum makes different fiber gain media attractive for building tunable and ultrashort pulse sources. For instance, ytterbium (Yb)-doped silica fibers having a broad gain bandwidth, high optical conversion efficiency, and large saturation fluence offer almost ideal gain medium for the generation and the amplification of wavelength-tunable ultrashort optical pulses. An additional interesting feature of Yb-doped fiber lasers is that under certain conditions those lasers can operate in the 977-nm spectral band, which makes them very attractive as a master source for frequency doubling to achieve 488 nm and, thus, to substitute bulky and inefficient Ar-ion lasers.

The main difficulty associated with pulse generation within Yb- and neodymium-doped fibers results from the high value of normal material dispersion for silica at wavelengths below 1.1 μm. Although waveguide dispersion has been used generally to balance the material dispersion at longer wavelength (> 1.3 μm), it does not appear feasible to achieve overall anomalous dispersion by this approach for shorter wavelengths using conventional wave-guiding mechanism. Dispersion compensation has been achieved by the use of a photonic crystal fiber, however, pulse quality degradation has been observed due to the high nonlinearity of the photonic fiber [5]. Photonic bandgap fiber based on air-core fiber could be an attractive solution for intracavity dispersion compensation in the near-infrared spectral region after low values of the back reflection and the splice loss with the gain fiber would be achieved [6]. The dispersion compensation by an intracavity prism sequence or a grating pair is still a widespread method used to offset the material dispersion. By use of these bulk dispersion-compensating elements within the cavity for controlling its total dispersion, which can be made either normal or anomalous, stretched-pulse or soliton-pulse regimes have been obtained

Manuscript received January 5, 2004; revised April 2, 2004.

The authors are with the Optoelectronics Research Centre, Tampere University of Technology, Tampere FIN-33101, Finland (e-mail: robert.herda@orc.tut.fi).

Digital Object Identifier 10.1109/JQE.2004.830194

[4]. In order to achieve compact picosecond lasers, the limiting factor that needs to be overcome is the sizeable and bulky grating-pair compensator or the large prism separation (>1 m) required for adequate control of dispersion in a fiber-based cavity. Alternatively, Gires–Tournois mirrors and chirped fiber Bragg gratings can be used to generate sufficient anomalous dispersion in a compact form, however, the practical value of these solutions is still to be evaluated. Negative dispersion generated by a Gires–Tournois interferometer (GTI) or chirped mirrors supplies sufficient compensation for solid-state lasers to balance the dispersion of the laser rod. Because the GTI mirror is based on a multiple-beam concept, higher dispersion required for fiber-based cavities can, in principle, be generated by increasing the finesse of the interferometer. In practice, however, the resonance sharpness of GTI strongly affects the usable bandwidth of the compensator. For this reason, in a typical fiber laser with a length of active medium of 1 m or longer, short pulse operation still requires a dispersion compensator such as a grating pair [4]. Bulk components, though, add to the complexity and maintenance, require alignment, and increase the physical size of the system, as mentioned above.

In order to achieve the self-starting mode locking, SESAMs are used to ensure self-starting character of the short-pulse operation [7], [8]. Especially with large net normal dispersion of the cavity, a high value of nonlinear reflectivity change ΔR (throughout this paper, the magnitude of the nonlinear reflectivity change ΔR is referred as a SESAM nonlinear contrast) of SESAM is desired for enhancement of the self-starting capability of mode locking [2], [3], [8], [9], [12]. However, increasing ΔR decreases the threshold for Q-switching instability [10].

In this paper, to cope with the difficulty in obtaining self-initiating short pulse generation from the cavity with large dispersion, semiconductor saturable absorber mirrors were optimized to ensure self-starting character of the mode locking in a laser with an arbitrary sign and a large value of dispersion. Using a Fabry–Perot (or a GTI) resonant absorber, we studied the starting properties of mode locking depending on the detuning from the resonance of the SESAM microcavity. Recently, we have used dispersive properties of near-resonant SESAMs for changing the cavity-average dispersion and forcing the erbium (Er)-doped fiber laser to operate in a stretched-pulse mode locking or soliton-assisted regime at 1.5- μm wavelength range [7], [8]. A dispersive GTI-type SESAM with negative group-velocity dispersion (GVD) was used for intracavity chirp compensation, giving rise to high-energy transform-limited pulses without the need for external pulse compression. Alternatively, a SESAM providing positive GVD was optimized for stretched-pulse regime, thus, avoiding the use of dispersion-compensating fiber and, therefore, reducing the nonlinear effects in the laser cavity. Here, we demonstrate that the use of near-resonant SESAMs with significantly increased magnitude of the reflectivity change ΔR (5%–20%) allows achieving reliably self-starting continuous wave (CW) mode locking with picosecond pulses for large dispersion of the laser cavity, either normal or anomalous, without implementing any dispersion-compensating technique and with no indication of the Q-switching instability. It was also confirmed experimentally that antiresonant absorbers with low value of ΔR (below 1%–2%) could not start mode locking without appropriate dispersion compensation provided by the intracavity dispersive delay line. We demonstrate that under certain conditions, the magnitude and recovery time of the SESAM nonlinearity provides a dominant mechanism for spectrum broadening and, therefore, for pulse shaping.

II. Model of Resonant Saturable Absorber Mirrors

From general analysis of the dynamic properties of the laser with nonlinear reflector, it is expected that large reflectivity change ΔR of the mirror improves the self-starting capability of passive mode locking. However, with an increase in the mirror absorption, e.g., by an increase in the number of quantum wells in the absorber layer, $E_{\mathrm{sat},A}\Delta R$— the product of saturation energy $E_{\mathrm{sat},A}$ and reflectivity change ΔR— the SESAM parameter that determines the stability limit of the CW mode locking, will also increase and eventually exceed the critical value. In the picosecond regime (without solitonic effect) the stability condition for CW mode locking against Q-switching can be written in the following form [10]:

$$E_p^2 > E_{\mathrm{sat},L}E_{\mathrm{sat},A}\Delta R$$

where E_p is the pulse energy and $E_{\mathrm{sat},L}$ is the saturation energy of the laser gain medium.

Therefore, with an increasing in the amount of the saturable absorption and, consequently, rising of the nonlinear reflectivity change, the condition for CW mode locking is more difficult to maintain.

For a given amount of the saturable absorption, a higher nonlinear contrast of the SESAM can be achieved by placing the absorber in the cavity, e.g., by applying a reflective coating on top of the absorber region. In addition, analysis of a Fabry–Perot structure shows [9] that the effective saturation energy of the resonant SESAM $E_{\mathrm{sat},A}^{\mathrm{eff}}$ decreases near a resonant wavelength. $E_{\mathrm{sat},A}^{\mathrm{eff}}$ is high out of the cavity resonance and it decreases by decreasing the cavity finesse (e.g., decreasing the top mirror reflectivity) or/and by tuning the operation wavelength closer to the cavity resonance. It can be shown that the effective saturation energy of the Fabry–Perot-based SESAM compared to the saturation energy of the absorber material is multiplied by factor η, or

$$E_{\mathrm{sat},A}^{\mathrm{eff}} = \eta E_{\mathrm{sat},A}^{0}$$

where

$$\eta = \frac{1}{1-R_T}\left[(1+\sqrt{R_T R_S})^2 - 4\sqrt{R_T R_S}\cos^2\left(\frac{\Phi_{rt}}{2}\right)\right].$$

Here R_T is the reflectivity of the top mirror and Φ_{rt} is the detuning from the resonance. $R_S = R_B\exp(-4\alpha d)$ is the reflectivity of the antireflection-coated absorber ($R_T = 0$). $R_B(\approx 1)$ is the reflectivity of the bottom mirror of the SESAM structure. Therefore, the product

$$E_{\mathrm{sat},A}^{\mathrm{eff}}\Delta R = E_{\mathrm{sat},A}^{0}(1-R_S)$$

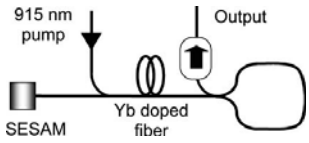

Fig. 1. Schematic of Yb fiber laser using resonant saturable absorber mirror.

that defines absorber contribution to the stability condition in the absence of nonsaturable loss does not depend on the detuning from the cavity resonance and the top mirror reflectivity. This is because an increase in the SESAM contrast ΔR near resonance is compensated by an equivalent decrease in the saturation energy $E_{\mathrm{sat},A}^{\mathrm{eff}}$, so that the product $E_{\mathrm{sat},A}^{\mathrm{eff}}\Delta R(\lambda)$ remains constant when tuning the laser wavelength around SESAM's resonant wavelength. The presence of nonsaturable losses additionally decreases the stability product. Therefore, near the resonant wavelength of the SESAM microcavity, both higher value of ΔR and lower value of $E_{\mathrm{sat},A}^{\mathrm{eff}}$ improve the self-starting capability of mode locking, in agreement with the conclusions made in [11] and [12]. It means that by operating the laser close to resonance it is feasible to facilitate reliable self-starting mode locking without violating the stability condition for CW mode locking.

III. Absorber Mirrors and Fiber Laser Details

In our experimental studies we used Yb-doped fibers as a gain medium placed in a linear cavity, shown in Fig. 1. The laser cavity contains a few centimeter-long pieces of Yb^{3+}-doped fiber with angled cleaved ends to suppress intracavity reflections, a wavelength-division multiplexer and a loop mirror, serving as a cavity mirror and an output coupler. The minimizing of the overall intracavity dispersion was accomplished by exploiting highly doped Yb fiber. A 15–35-cm-long Yb-doped silica fiber (NA = 0.13), cutoff wavelength ($\sim$ 920 nm) is pumped by a pigtailed single-mode laser diode operating at 915 nm with a maximum launched pump power of 200 mW. The unsaturated fiber absorption at 915 nm was $\sim$ 500 dB/m. The 915/1050 pump signal wavelength-selective coupler and the loop mirror were made of fiber with a cutoff wavelength of $\sim$910 nm. The cavity was terminated by a 55% reflectivity loop mirror from one end and by the SESAM structure from the other end. The short length of the fiber forming the loop mirror in a laser operating in a dispersion-stretched pulse regime excluded the nonlinear loop mirror action or nonlinear polarization rotation mode locking. A spectral filter was used on occasion in the cavity to provide tunable operation.

Resonant SESAMs used in this study were fabricated using solid-source molecular-beam epitaxy on n-type GaAs (100) substrates. The samples include a bottom mirror comprising 30 pairs of AlAs–GaAs quarter-wave layers forming a distributed Bragg reflector (DBR). The DBRs stopband had a center wavelength of 1050 nm and approximately 120-nm bandwidth (990–1110 nm).

Throughout this study, two types of quantum-well absorber materials were used.

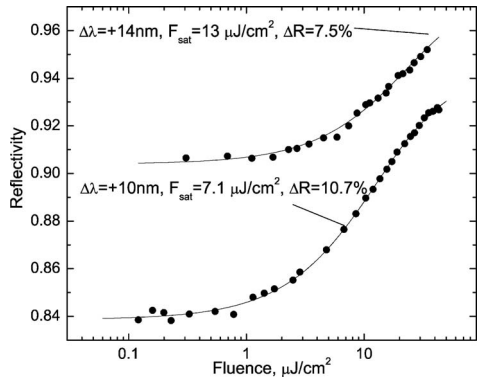

Fig. 2. Nonlinear reflectivity of a resonant SESAM for two different detunings from the SESAM resonance, $\Delta\lambda = +10$ nm and $\Delta\lambda + 14$ nm.

First, absorbers comprise five InGaAs quantum wells with 6-nm thickness and 16-nm GaAs barriers. The quantum well structure is sandwiched between a $\sim$0.1-μm GaAs buffer layer and a 100-nm GaAs cap layer. The photoluminescence emission from quantum wells was picked at 1.045 μm. To study the effect of the absorber speed on the mode locking performance, this SESAM was tested in the slow and fast versions — as grown and with post-growth implantation with heavy ions for decreasing its recovery time. The recovery time is expected to be reduced by two orders of magnitude resulting in picosecond range speed of the SESAM [13].

The second type of absorber studied consists of a five 5.8-nm-thick InGaAsN quantum wells separated by 17-nm GaAs barriers. The quantum wells are placed between a $\sim$0.1-μm GaAs buffer layer and a 90-nm GaAs cap layer. The photoluminescence peak from quantum wells was measured to be at 1.06 μm. Recently, InGaAsN-based absorber mirrors were successfully used in Er-doped fiber lasers operating in 1.55-μm wavelength range and in broadly tunable mode-locked Yb-fiber lasers [3], [4]. The reason of using the mixed group-III dilute nitride or substitutionally disordered $Ga_{1-x}In_xN_yAs_{1-y}$ based SESAMs in 1-μm wavelength range is that the recovery time of such a mirror can be easily controlled during epitaxial growth and by thermal annealing. It is well known that post-growth annealing modifies significantly optical properties of InGaAsN composition by changing the density of nonradiative defects [14]. The resonant wavelength of the SESAM cavity was positioned at $\sim$ 1036 nm by adjusting the thickness of the buffer layer.

The nonlinear reflectivity of the unbombarded SESAM is shown in Fig. 2. Although some degradation in the reflectivity may result from heavy-ion irradiation [14], we did not observe notable change in the SESAM nonlinear response. The saturation fluence and nonlinear reflectivity changes were measured to be $F_{\mathrm{sat},A}^{\mathrm{eff}} = 13\ \mu\mathrm{J/cm}^2$ and $\Delta R = 7.5\%$, respectively, for $\Delta\lambda = +14$ nm detuning from the SESAM cavity resonance and $F_{\mathrm{sat},A}^{\mathrm{eff}} = 7.1\ \mu\mathrm{J/cm}^2$ and $\Delta R = 11\%$ for smaller detuning $\Delta\lambda = +10$ nm. As expected from the above analysis, the reflectivity change decreases, whereas saturation fluence increases when tuning out of SESAM resonant wavelength. The value of

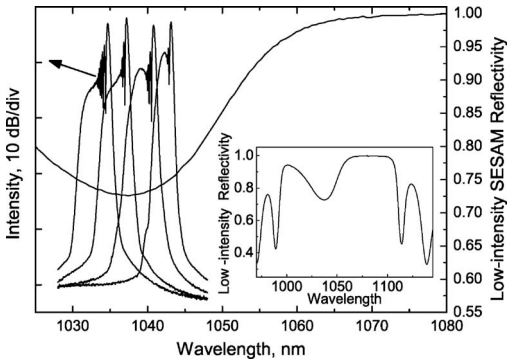

Fig. 3. Pulse spectra achieved for CW mode-locked operation by wavelength tuning using a spectral filter. Low-intensity reflectivity of the SESAM on a larger span is shown as an inset.

the product $F^{\text{eff}}_{\text{sat},A}\Delta R(\lambda)$ is 0.97 μJ/cm^2 and 0.78 μJ/cm^2 for $\Delta\lambda = +14$ nm and $\Delta\lambda = +10$ nm, respectively.

The lower value of the product $F^{\text{eff}}_{\text{sat},A}\Delta R(\lambda)$ for smaller detunings from the resonance is due to the increased nonsaturable loss of the absorber material. In turn, this feature leads to further increase in the stability against Q-switched mode locking, although decreasing the nonsaturable loss of the SESAM should clearly be an objective of the SESAM technology optimization. The highest value of the reflectivity change ΔR close to the resonant wavelength of the SESAM was estimated to be $\sim$20%.

IV. Experimental Results

It was mentioned above that near the resonant wavelength, the SESAM generates certain amount of an anomalous or normal dispersion for blue and red detunings, respectively. The tunable mode locking has revealed, however, no significant difference in the operation at the bands with anomalous and normal dispersion of the SESAM. It was confirmed by calculations that the dispersion generated by the resonant SESAM used in this study is significantly lower than the dispersion induced by the fiber. The overall normal cavity dispersion for the whole spectral range, therefore, was dominated by the fiber dispersion. Fig. 3 shows mode-locked spectra and low-intensity reflectivity of the SESAM near resonant wavelength of 1036 nm. Stable mode-locked operation has been obtained only for small detunings from the cavity resonance plotted in the figure. For large detunings, i.e., for antiresonant operation of the SESAM, CW mode locking was not achieved. In particularly, for wavelengths $\lambda < 1030$ nm and $\lambda > 1045$ nm, only Q-switched mode locking was observed. The obtained average output power of 5 mW corresponds to the pulse energy of 113 pJ in the cavity having repetition rate of 80 MHz. For a beam spot diameter at the absorber of 3 μm, this corresponds to the oversaturation factor of the SESAM of 110 at $\Delta\lambda = +14$ nm and 240 at $\Delta\lambda = +10$ nm.

The stability of the mode-locked operation and self-starting mechanism were tested using a chopper inside the laser cavity for several hours. Reliable startup of the short pulse operation was confirmed without any degradation in the performance observed.

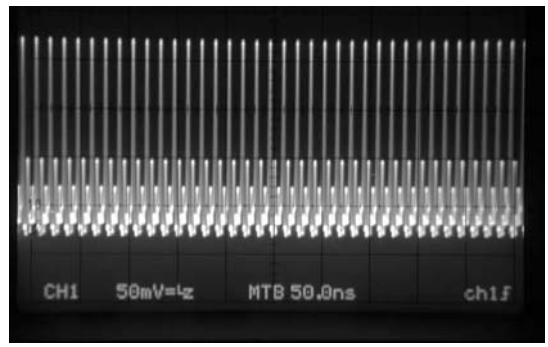

Fig. 4. Stable pulse train at the fundamental cavity frequency of 80 MHz.

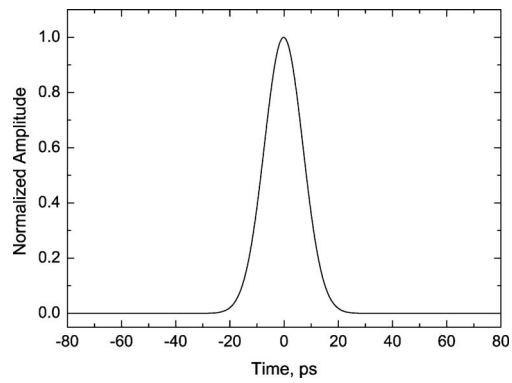

Fig. 5. Typical autocorrelation obtained without dispersion compensation. FWHM pulse width is 11 ps assuming Gaussian pulse shape.

Fig. 4 shows a stable pulse train at a repetition rate of 80 MHz. Typical autocorrelation, shown in Fig. 5, corresponds to $\sim$11-ps pulse with Gaussian shape. Pulse repetition rates for all laser configurations studied in this research was in a range of 80–140 MHz. A remarkable feature of using an absorber with high nonlinear response which can further be enhanced by exploiting near-resonant operation, is that under certain conditions, the absorber nonlinearity becomes significant and even dominant in the laser cavity. Indeed, in attempt to reduce the normal dispersion of the cavity, we minimize the length of the fiber, thus, reducing the contribution of its nonlinearity. Important consequences occur under these conditions. Particularly, the pulse-shaping mechanism is now determined mainly by the semiconductor mirror having slow-relaxation saturable nonlinearity compared to the ultrafast Kerr nonlinearity of the fiber. Fig. 6 shows broadened mode-locked pulse spectrum with a large downshifted Stokes asymmetry, similar to that observed in experiments with tunable pulse operation presented in Fig. 3. The asymmetry in a pulse spectrum is typical behavior for media with the finite (slow) relaxation time because a slow absorber provides significant pulse reshaping at the leading edge of the pulse [15], [16]. From this measurement showing remarkable asymmetry in the pulse spectrum, we confirmed that the nonlinearity of the semiconductor is essential in the laser cavity. The action of a slow saturable absorber results,

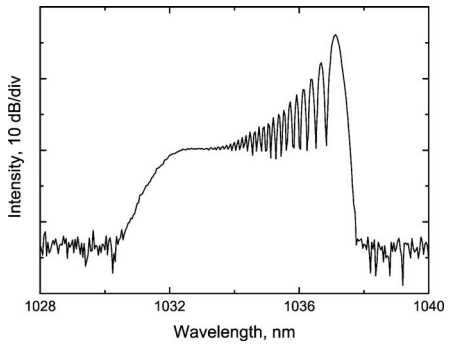

Fig. 6. Mode-locked spectrum with a large downshifted Stokes asymmetry.

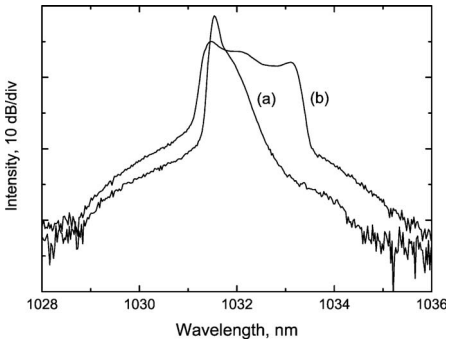

Fig. 7. Comparison of the mode-locked pulse spectra obtained using (a) slow and (b) fast absorbers. Spectra are plotted on log scale.

therefore, in a blue shift in the pulse spectrum as the interplay of self-phase modulation and rejection of the low-frequency components in the pulse spectrum [16], [17].

On the contrary, near-symmetrical pulse spectra are expected with fast absorbers providing the same losses for leading and trailing edges. Slow and fast SESAMs were obtained for the same InGaAs quantum-well structure both with and without 30-MeV heavy-ion irradiation with the dose of 10^{12} cm^{-2} that resulted in reduction in the recovery time of the absorber from hundreds of picoseconds down to a few picoseconds [18]. Keeping all parameters of the laser constant, we found that the ability of the laser to the self-startup of the mode-locked operation does not change notably with the change in the recovery time for resonant absorber mirrors. However, replacing the slow absorber with the fast one has resulted in the shortening of the mode-locked pulse by the factor of two, another indication that demonstrates the considerable role of the SESAM nonlinearity in the pulse shaping. Fig. 7 shows corresponding pulse spectra obtained from the same mode-locked laser using slow and fast absorbers, respectively. As expected from previous discussions, notable symmetry of the pulse spectrum was observed with the fast absorber as compared to the case of a slow SESAM.

This feature confirms the dominant effect of the high nonlinear response of the near-resonant SESAM on both pulse formation and the startup of the CW mode locking. This conclusion is further proved by a numerical simulation presented in Fig. 8

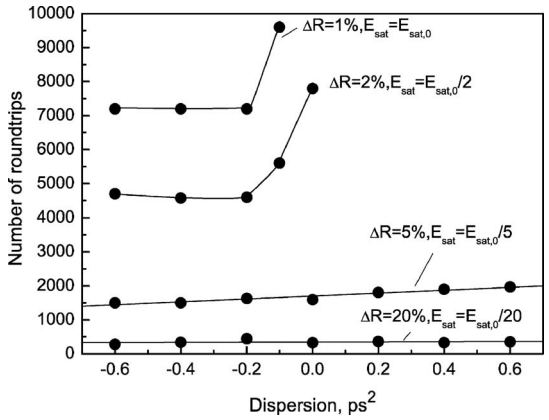

Fig. 8. Results of numerical simulation representing the number of cavity round trips necessary to achieve a steady-state operation for different nonlinear contrast ΔR of SESAM and for different values of net cavity dispersion.

that shows the number of cavity round trips required to reach steady-state CW mode-locked operation for different values of ΔR and, consequently, for different $E_{\mathrm{sat},A}^{\mathrm{eff}}$. The mode-locked fiber laser was modeled by subsequently calculating different elements. These include an output coupler, a dispersive element (a grating compressor or GTI), the active and passive fiber segments of the cavity, and a SESAM. The simulation takes into account amplification, second-order dispersion, and self-phase modulation. The propagation equation was solved by the split-step Fourier method [19].

These simulations show that with a SESAM having a high nonlinear contrast, the laser efficiently starts mode locking in a wide range of normal and anomalous dispersion values. On the contrary, for low-contrast absorbers, a reliable self-starting operation can be achieved only for low values of the total cavity dispersion. Although the anomalous dispersion provides better conditions for self-starting mode locking, it is obvious that the high nonlinear response is crucial for the reliable startup. In combination with the reduced magnitude of the saturation fluence of the SESAM near resonance, the above stability condition is satisfied and ensures the CW mode locking without Q-switching instability.

As it follows from the above analysis for the resonant SESAM, the saturation fluence increases significantly for large detunings from the cavity resonance, i.e., for antiresonant operation. This feature drives the transition from CW mode locking to Q-switched mode locking far from the cavity resonance. Another experimental confirmation of this phenomenon is shown in Fig. 9, where the pulse spectra are plotted for different pump powers. When no spectral filter was inserted into the laser cavity, with an increase in pump power, the pulse spectrum gradually shifts toward spectral range with higher saturation fluence $E_{\mathrm{sat},A}^{\mathrm{eff}}$, i.e., away from the cavity resonance located at $\lambda \sim$1036 nm. Another interesting feature observed with an increase in the output power is that the mode-locked pulse spectra acquires a large upshifted anti-Stokes asymmetry, as seen in Figs. 9 and 10. Therefore, with high pulse power, phase effects in the semiconductor absorber may cause a red

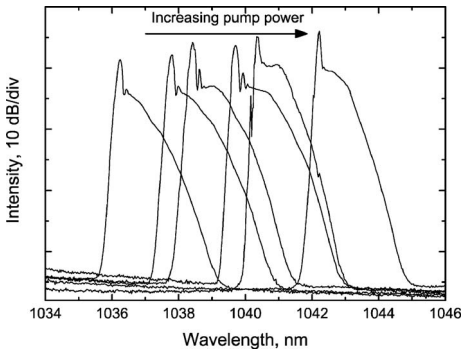

Fig. 9. Evolution (progressive out of resonance shifting) of mode-locked spectra with an increase in the pump power. SESAM resonant wavelength is positioned near 1035 nm.

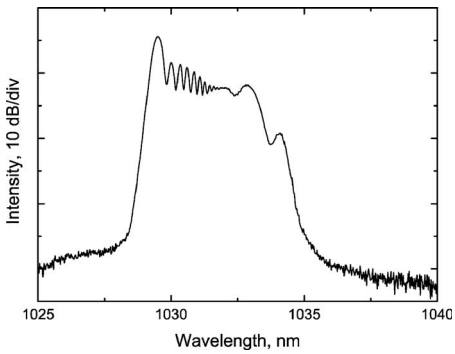

Fig. 10. Mode-locked spectrum with upshifted anti-Stokes asymmetry observed with an increased output power.

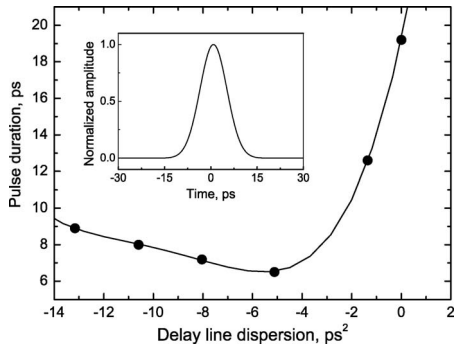

Fig. 11. Pulse width versus external delay line dispersion. Inset shows the intensity autocorrelation of the shortest 6.8-ps pulse obtained.

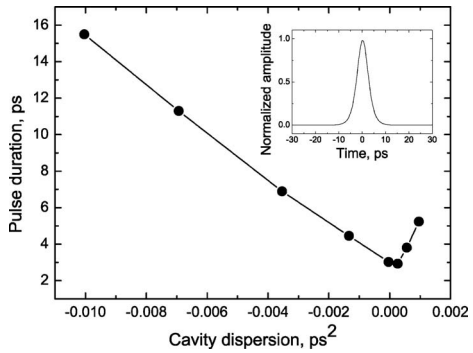

Fig. 12. Pulse width versus net cavity dispersion obtained using prism compensator. Intensity autocorrelation of the shortest pulse is shown as an inset.

shift in the pulse spectrum, contrary to the low-power behavior presented in Figs. 3 and 6, where expected upshift in frequency was observed. This phenomenon is still to be explored in detail.

The output pulses are highly chirped for the laser with large net normal dispersion of the cavity. To examine this, we used a grating-pair arrangement at the output of the laser to compensate the chirp on the pulses externally. Pulse durations as short as 6.8 ps have been achieved for the dispersion of the external delay line of -5 ps^2, as shown in Fig. 11.

The positive dispersion of the fiber of $\sim +0.0066$ ps^2 allows for dispersion compensation using intracavity prism pair. Two prisms consisting of SF 11-glass were employed providing an adjustable negative GVD. Fig. 12 shows the pulse duration as a function of the cavity dispersion. Pulses with durations as short as ~ 3 ps were obtained. The pulse shortening was mainly determined and limited by the nonlinearity and speed of the SESAM. It should, however, be noted that the useful bandwidth provided by the resonant absorbers with enhanced change in the nonlinear reflectivity can be made to support pulses well below 1 ps. The resonant ion-irradiated absorber used in these experiments was tested in a laser with fiber dispersion compensated by a grating pair. Pulses with sub-100 fs duration and a spectral bandwidth over 15 nm were obtained assisted by the nonlinear polarization rotation in a fiber.

V. Conclusion

In summary, we have identified major nonlinear mechanisms that provide spectrum formation in a laser with a high-contrast absorber mirror and no dispersion compensation. We have found that the combined action of the fiber dispersion and nonlinearity of the semiconductor mirror supply major pulse-shaping mechanisms. Our results suggest the use of short-fiber cavities free from dispersion compensators for compact picosecond mode-locked lasers stabilized by the SESAMs with large reflectivity change.

An appropriate dispersion-delay line at the output of the master source can be used for dechirping, resulting in high-quality pulses. Pulse width can be further reduced using amplification, nonlinear spectrum broadening, and pulse compression performed externally to the master oscillator, leading to a cost-effective femtosecond system.

Nonlinear effects in the near-resonant SESAM present a mechanism for picosecond pulse generation that is entirely self-starting for a wide range of the cavity dispersion. A reliable self-starting mode-locked laser has been demonstrated with a Yb-doped fiber as a gain medium and a saturable absorber that operates close to its cavity resonance. It was confirmed experimentally that large nonlinear response of the resonant

absorber combined with decreased saturation fluence maintains the stability against Q-switched mode locking.

It was also observed that using a slow saturable absorber in combination with nonlinear effects leads to a significant asymmetry in the mode-locked spectrum. The asymmetry occurs by removing the frequency components in the leading edge of the pulse, whereas the trailing edge of the pulse remains nearly unperturbed. With the self-phase modulation as a dominant nonlinear effect, red components get attenuated and the spectrum acquires a blue shift. In contrast, fast absorbers attenuate leading and trailing edges equally resulting in a near-symmetrical pulse spectrum.

ACKNOWLEDGMENT

The authors would like to thank Dr. A. Grudinin, Fianium-NewOptics Ltd., U.K., for valuable discussions.

REFERENCES

[1] X. Liu, D. Du, and G. Mourou, "Laser ablation and micromachining with ultrashort laser pulses," *IEEE J. Quantum Electron.*, vol. 33, pp. 1706–1716, Oct. 1997.

[2] U. Keller, K. J. Weingarten, F. X. Kärtner, D. Kopf, B. Braun, I. D. Jung, R. Fluck, C. Hönninger, N. Matuschek, and J. Aus der Au, "Semiconductor saturable absorber mirrors (SESAMs) for femtosecond to nanosecond pulse generation in solid-state lasers," *IEEE J. Select. Topics Quantum Electron.*, vol. 2, pp. 435–453, Sept. 1996.

[3] O. G. Okhotnikov, T. Jouhti, J. Konttinen, S. Karirinne, and M. Pessa, "1.5-μm monolithic GaInNAs semiconductor saturable absorber mode locking of an erbium fiber laser," *Opt. Lett.*, vol. 28, pp. 364–366, Mar. 2003.

[4] O. G. Okhotnikov, L. Gomes, N. Xiang, T. Jouhti, and A. B. Grudinin, "Mode-locked ytterbium fiber laser tunable in the 980–1070 nm spectral range," *Opt. Lett.*, vol. 28, pp. 1522–1524, Sept. 2003.

[5] H. Lim, F.Ö. Ilday, and F. W. Wise, "Femtosecond ytterbium fiber laser with photonic crystal fiber for dispersion control," *Opt. Express*, vol. 10, pp. 1497–1502, Dec. 2002.

[6] C. J. S. de Matos, J. R. Taylor, T. P. Hansen, K. P. Hansen, and J. Broeng, "All-fiber chirped pulse amplification using highly-dispersive air-core photonic bandgap fiber," *Opt. Express*, vol. 11, pp. 2832–2837, Nov. 2003.

[7] M. Guina, N. Xiang, A. Vainionpää, O. G. Okhotnikov, T. Sajavaara, and J. Keinonen, "Self-starting stretched-pulse fiber laser mode locked and stabilized with slow and fast semiconductor saturable absorbers," *Opt. Lett.*, vol. 26, pp. 1809–1811, Nov. 2001.

[8] M. Guina, N. Xiang, and O. G. Okhotnikov, "Stretched-pulse fiber lasers based on semiconductor saturable absorbers," *Appl. Phys. B. Photophys. Laser Chem.*, vol. 74, pp. S193–S200, June 2002.

[9] L. R. Brovelli, U. Keller, and T. H. Chiu, "Design and operation of antiresonant Fabry-Perot saturable semiconductor absorbers for mode-locked solid-state lasers," *J. Opt. Soc. Amer. B Opt. Phys.*, vol. 12, pp. 311–322, Feb. 1995.

[10] C. Hönninger, R. Paschotta, F. Morier-Genoud, M. Moser, and U. Keller, "Q-switching stability limits of continuous-wave passive mode locking," *J. Opt. Soc. Amer. B Opt. Phys.*, vol. 16, pp. 46–56, Jan. 1999.

[11] H. A. Haus, "Parameter ranges for CW passive mode locking," *IEEE J. Quantum Electron.*, vol. QE-12, pp. 169–176, Mar. 1976.

[12] F. X. Kärtner, L. R. Brovelli, D. Kopf, M. Kamp, I. Calasso, and U. Keller, "Control of solid-state laser dynamics by semiconductor devices," *Opt. Eng.*, vol. 34, pp. 2024–2036, July 1995.

[13] J. Mangeney, J. L. Oudar, J. C. Harmand, C. Mériadec, G. Patriarche, G. Aubin, N. Stelmakh, and J. M. Lourtioz, "Ultrafast saturable absorption at 1.55 μm in heavy-ion-irradiated quantum well vertical cavity," *Appl. Phys. Lett.*, vol. 76, pp. 1371–1373, Mar. 2000.

[14] M. Pessa, C. S. Peng, T. Youhti, E.-M. Pavelescu, W. Li, S. Karirinne, H. Liu, and O. G. Okhotnikov, "Toward high-performanve nitride lasers at 1.3 μm and beyond," *Proc. IEE Optoelectron.*, vol. 150, pp. 12–21, 2003.

[15] T. K. Gustafson, J. P. Taran, H. A. Haus, J. R. Lifsitz, and P. L. Kelley, "Self-modulation, self-steepening, and spectral development of light in small-scale trapped filaments," *Phys. Rev.*, vol. 177, pp. 306–313, Jan. 1969.

[16] R. Paschotta and U. Keller, "Passive mode locking with slow saturable absorbers," *Appl. Phys. B. Photophys. Laser Chem.*, vol. 73, pp. 653–662, Nov. 2001.

[17] N. Finlayson, E. M. Wright, and G. I. Stegeman, "Nonlinear optical pulse propagation in a semiconductor medium in the transient regime–I: Temporal and spectral effects," *IEEE J. Quantum Electron.*, vol. 26, pp. 770–777, Apr. 1990.

[18] A. Härkönen, T. Jouhti, N. V. Tkachenko, H. Lemmetyinen, B. Ryvkin, O. G. Okhotnikov, T. Sajavaara, and J. Keinonen, "Dynamics of photoluminescence in GaInNAs saturable absorber mirrors," *Appl. Phys. A. Solids Surf.*, vol. 77, pp. 861–863, Dec. 2003.

[19] G. P. Agrawal, *Nonlinear Fiber Optics*. New York: Academic, 2001.

Robert Herda was born in Jena, Germany, in 1977. He received the M.Sc. degree from the Institute of Applied Physics, Friedrich Schiller University, Jena, in 2003. He is currently working toward the Ph.D. degree at the Optoelectronics Research Centre, Tampere University of Technology, Tampere, Finland.

His current research is focused on experimental work and modeling the generation and amplification of ultrashort pulses.

Oleg G. Okhotnikov received the Ph.D. degree in laser physics from P. N. Lebedev Physical Institute, and the D.Sc. degree in laser physics from General Physics Institute, Russian Academy of Sciences, Moscow, Russia, in 1981 and 1992, respectively.

Since 1999, he has been a Full Professor at the Optoelectronics Research Centre, Tampere University of Technology, Tampere, Finland. He has published over 100 journal papers and holds six patents.

Appendix 2

Publication 2

R. Herda and O. G. Okhotnikov, "Effect of amplified spontaneous emission and absorber mirror recovery on the dynamics of mode-locked fiber lasers," *Applied Physics Letters*, vol. 86, 2005, pp. 0111131–0111133.

Effect of amplified spontaneous emission and absorber mirror recovery time on the dynamics of mode-locked fiber lasers

Robert Herda[a] and Oleg G. Okhotnikov
Optoelectronics Research Centre, Tampere University of Technology, P.O. Box 692, FIN-33101, Tampere, Finland

(Received 6 July 2004; accepted 1 November 2004; published online 27 December 2004)

The effect of the amplified spontaneous emission (ASE) on the performance of the semiconductor saturable absorber mirrors (SESAMs) in mode-locked fiber lasers has been investigated. We show that high level of ASE intensity typical for fiber lasers can saturate the absorption and degrade significantly the nonlinear response of the SESAM. We studied the effect of the absorber recovery time and demonstrated that the ion-irradiated SESAMs with fast nonlinear response are less affected by the ASE radiation and, consequently, in the presence of the high-power ASE they exhibit better self-starting capability compared with slow absorbers. © *2005 American Institute of Physics*. [DOI: 10.1063/1.1845589]

Optimization of semiconductor saturable absorber mirrors (SESAMs) for mode-locked fiber systems should address the specific features of fiber gain media that differ from other laser systems. Particularly, fiber lasers are characterized with the high level of intracavity spontaneous emission owing to the waveguiding geometry of the cavity. Intensity of the so-called amplified spontaneous emission (ASE) in a fiber cavity could be comparable with the level of the laser emission and, therefore, it can significantly affect mode-locking startup and stability. We have observed that the high degree of the absorber saturation provided by ASE may even prevent self-starting mode locking.

From a general analysis of the mode-locked laser with nonlinear mirror, it was concluded that without pulse shaping by soliton formation, an absorber with a fast response is desirable for enhancing the mechanism of the pulse narrowing. However, lasers mode locked by fast saturable absorbers have an intrinsic problem with self-starting from a continuous-wave (cw) operation due to insufficient pulse shaping for long pulses.[1–3] In particularly, it was shown that presence of a slow absorber has a remarkable impact on mode-locking stability.[3,4] Mode locking of the laser can be easily initiated and stabilized by the saturation dynamics of the slow absorber, although the pulses develop a trailing wing due to the slowly recovering absorption. The impact of a slow absorber becomes even more pronounced when the pulses have a large chirp as in the case of stretched-pulse mode-locked lasers.

Recently, we have analyzed the effect of the SESAM modulation depth ΔR on the self-starting characteristics of a mode-locked fiber laser.[4] We have shown that when using a SESAM having a high reflectivity change, the laser efficiently starts mode locking in a wide range of normal and anomalous dispersion values. To the contrary, with low modulation depth absorbers, a reliable self-starting operation can be achieved only for low values of the total cavity dispersion.

Motivation for this study is based on an unexpected observation: With different erbium, ytterbium, and neodymium fiber that lasers we have explored, the ability of the mode locked laser to operate self-starting was clearly improved with an increase in the speed of the absorber mirror. Moreover, with many slow absorbers, the self-starting regime could not be achieved at all, whereas, the same absorbers after heavy-ion irradiation demonstrate excellent self-starting potential.

The analysis of the absorber dynamics in a fiber laser developed here is based on the rate equation. The saturable loss of a SESAM is given by

$$\frac{\partial \delta_s(t)}{\partial t} = \frac{\delta_s(t) - \Delta R}{\tau_{\mathrm{rec}}} \frac{|\psi(t)|^2}{E_{\mathrm{sat}}} \delta_s, \tag{1}$$

where ΔR is the nonlinear contrast of the absorber, $|\psi|^2$ is the power of the optical field, τ_{rec} is the absorption recovery time, and E_{sat} is the absorber saturation energy. Analysis shows that when the optical field circulating inside the laser cavity contains a significant fraction of the ASE, the modulation depth of the SESAM decreases noticeably. In this case, the total field intensity can be expressed in the form that includes a time-dependent (optical pulse) and a time-independent component P_0 representing background ASE radiation

$$|\psi(t)|^2 = |\psi_{\mathrm{pulse}}(t)|^2 + P_0. \tag{2}$$

By substituting this expression for the optical field in Eq. (1), we obtain a modified rate equation that describes the evolution of the absorption in the presence of the ASE in the laser cavity

$$\frac{\partial \delta_s(t)}{\partial t} = \frac{\delta_s(t) - \Delta R_{\mathrm{eff}}}{\tau_{\mathrm{rec,eff}}} \frac{|\psi(t)_{\mathrm{pulse}}|^2}{E_{\mathrm{sat}}} \delta_s. \tag{3}$$

The effective nonlinear modulation depth ΔR_{eff} of the SESAM decreases owing to absorption saturation by the ASE as

$$\Delta R_{\mathrm{eff}} = \Delta R \frac{1}{1 + P_0 \tau_{\mathrm{rec}}/E_{\mathrm{sat}}}, \tag{4}$$

and, consequently, degrades the starting capability of the SESAM.

The effect of the absorber speed is further clarified in Fig. 1 by plotting the ratio $\Delta R_{\mathrm{eff}}/\Delta R$, which is a measure of

[a]Electronic mail: robert.herda@orc.tut.

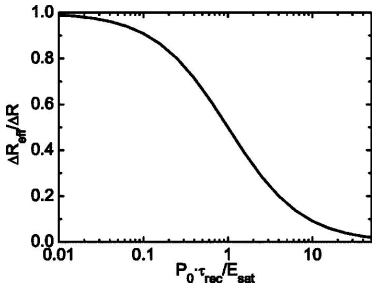

FIG. 1. The normalized effective modulation depth of the SESAM including the effect of ASE radiation as a function of the SESAM parameter $P_0\tau_{\mathrm{rec}}/E_{\mathrm{sat}}$. ΔR_{eff} and ΔR are the modulation depths of the absorber mirror with and without saturation induced by ASE, respectively.

modulation depth degradation due to presence of the ASE, as a function of $P_0\tau_{\mathrm{rec}}/E_{\mathrm{sat}}$. Figure 1 also suggests that the decrease in the absorber recovery time can ef ciently prevent the ASE-induced degradation of the SESAM nonlinear response due to absorption saturation. It should be noted here that the saturation energy E_{sat} does not change notably with the decrease in the absorber recovery time for $\tau_{\mathrm{pulse}} < \tau_{\mathrm{rec}}$ in agreement with the observations reported earlier.[5] As will be shown below, the saturation uence F_{sat} increases only slightly after ion irradiation, e.g. from 3.3 to 5.0 $\mu\mathrm{J/cm}^2$ for the typical sample studied here.

The in uence of the saturation by ASE has been further investigated by simulation of a ber laser dynamics. Figure 2 shows the number of roundtrips needed for the startup process for different recovery times of the absorption. This simulation takes into account ampli cation, second-order dispersion, self-phase modulation and is started from a cw background. The propagation equation was solved by the split-step-Fourier method. The values used in the simulation are typical for core-pumped ber lasers; pulse energy—80 pJ, average power of the background radiation—4 mW, absorber saturation energy—0.5 pJ, and modulation depth—20%. The gure shows that there is an optimum value for the recovery time of an absorber. For very small recovery times, long pulses are insuf ciently shaped and start-up time increases dramatically with an increase in the SESAM speed. For very long recovery times, the quasi-cw spontaneous radiation starts to saturate an absorber, thus decreasing its effective modulation depth and degrading the self-starting capability.

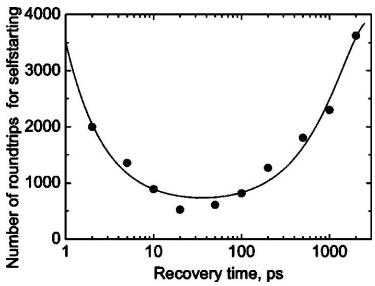

FIG. 2. Results of numerical simulation representing the number of cavity roundtrips required for the startup of the mode-locked operation versus SESAM recovery time.

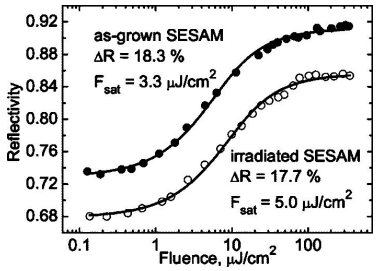

FIG. 3. Measured nonlinear re ectivity change of the absorber mirror prior and after heavy-ion irradiation versus pulse energy density and theoretical ts (solid lines).

SESAMs used in this study were fabricated by the solid-source molecular-beam epitaxy on an *n*-type GaAs (100) substrate. The samples include a bottom mirror comprising 30 pairs of AlAs/GaAs quarter-wave layers forming a distributed Bragg re ector (DBR). The DBR's stop band had a center wavelength of 1050 nm and 120 nm bandwidth. The absorbers are comprised of ve InGaAs quantum wells with 6 nm thickness and 16 nm GaAs barriers. The quantum-well structure is sandwiched between a $\sim$0.1 μm GaAs buffer layer and a 100 nm GaAs cap layer. The photoluminescence emission from quantum wells was picked at 1.045 μm. To study the effect of the absorber speed on the mode-locking performance, the SESAMs were tested in the slow and fast versions—as grown and with postgrowth irradiation with heavy ions for decreasing the recovery time. The samples were irradiated with 10 MeV nickel ions, with a dose of $2-5\times10^{11}$ cm^{-2}.[6–8] The recovery time was reduced by approximately two orders of magnitude, from 150–250 ps down to 2–8 ps. The absorber mirrors studied and optimized here for operation with ber lasers have low value of the saturation uence in a range of $\sim$1–10 $\mu\mathrm{J/cm}^2$. Indeed, it is expected that using a SESAM with a low value of the saturation uence effectively prevents *Q*-switching instability.[9] Typical re ectivity changes with the incident pulse energy for as-grown mirrors and for mirrors after heavy-ion irradiation are shown in Fig. 3. Low intensity re ectivity measurements showed no signi cant changes in the resonant wavelength of the SESAM after postgrowth irradiation. The SESAM modulation depth and saturation uence extracted from this measurement are ΔR=18.3% and F_{sat} =3.3 $\mu\mathrm{J/cm}^2$ respectively, for the as-grown sample and ΔR =17.7% and F_{sat}=5.0 $\mu\mathrm{J/cm}^2$ after implantation. It can also be seen from the Fig. 3 that 10 MeV irradiation increased the nonsaturable loss by $\sim$5%. The nonsaturable loss can further be reduced by thermal annealing.[10]

The effect of ASE on modulation depth of the absorber was investigated by measuring the nonlinear response of the SESAM varying the intensity of the cw radiation that exposes the absorber. Figure 4 shows the modulation depth of the slow and fast SESAMs with the recovery times τ_{rec} $\approx$200 ps and $\tau_{\mathrm{rec}}\approx$5 ps, respectively, as a function of the broadband cw radiation intensity illuminated the sample. In agreement with the analysis, the degradation in the nonlinear response of the mirror by $\sim$9% was observed with the slow SESAM for the power levels that are typical for the ber lasers, while no measurable change in the fast SESAM re ectivity was found.

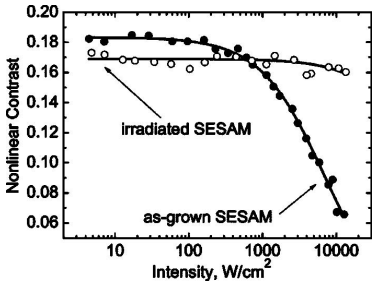

FIG. 4. Effective modulation depth for slow and fast SESAMs exposed to a cw radiation.

Contrary to the predictions based on the early analysis,[1,3] after the postgrowth heavy-ion irradiation, the absorber mirrors have shown an improved start-up performance. This phenomenon has been attributed to the effect of the ASE on the mirror characteristics. It is known that the SESAM action is based on the circumstance that the pulses with durations shorter than the absorber recovery time experience lower loss than the low-intensity quasi-cw radiation. Using absorber mirrors with a fast recovery time prevents absorber saturation by quasi-cw spontaneous noise and, consequently, precludes the degradation of the absorber modulation depth. Clearly, the discrimination against noiselike ASE radiation increases with an increase in the speed of the absorber.

In summary, we have found that ASE may severely affect the performance of the semiconductor saturable absorber mirrors in mode-locked ber laser and, therefore, should be taken into consideration when constructing ultrafast ber systems. We have found that high level of ASE intensity typical for ber lasers can saturate the absorption and degrade signi cantly the nonlinear response of the SESAM. In turn, this severely affects the starting mechanism. Because of the fast response time of the ion-irradiated SESAMs, these absorbers are less affected by the slowly varying ASE radiation and, consequently, demonstrate better self-starting capability compared with slow absorbers. This feature was not predicted by the earlier theories stated that slow absorbers are always preferable for the reliable self-start of the passive mode locking.

[1]E. P. Ippen, Appl. Phys. B: Lasers Opt. **58**, 159 (1994).
[2]H. A. Haus, IEEE J. Quantum Electron. **12**, 169 (1976).
[3]M. Guina, N. Xiang, A. Vainionpää, O. G. Okhotnikov, T. Sajavaara, and J. Keinonen, Opt. Lett. **26**, 1809 (2001).
[4]R. Herda and O. G. Okhotnikov, IEEE J. Quantum Electron. **40**, 893 (2004).
[5]J. Mangeney, J. L. Oudar, J. C. Harmand, C. Meriadec, G. Patriarche, G. Aubin, N. Stelmakh, and J. M. Loutioz, Appl. Phys. Lett. **76**, 1371 (2000).
[6]A. Härkönen, T. Jouhti, N. V. Tkachenko, H. Lemmetyinen, B. Ryvkin, O. G. Okhotnikov, T. Sajavaara, and J. Keinonen, Appl. Phys. A: Mater. Sci. Process. **77**, 861 (2003).
[7]E. Lugagne Delpon, J. L. Oudar, N. Bouché, R. Raj, A. Shen, N. Stelmakh, and J. M. Lourtioz, Appl. Phys. Lett. **72**, 759 (1998).
[8]M. J. Lederer, B. Luther-Davis, H. H. Tan, and C. Jagadish, IEEE J. Quantum Electron. **34**, 2150 (1998).
[9]C. Hönninger, R. Paschotta, F. Morier-Genoud, M. Moser, and U. Keller, J. Opt. Soc. Am. B **16**, 46 (1999).
[10]M. J. Lederer, B. Luther-Davies, H. H. Tan, and C. Jagadish, Appl. Phys. Lett. **70**, 3428 (1997).

Appendix 3

Publication 3

R. Herda, M. Rusu, A. Vainionpää, S. Suomalainen, O. Tengvall, and O. G. Okhotnikov, "Semiconductor All-Optical Modulator for Synchronization of Independent Fiber Laser Oscillators and Active Mode-Locking," *IEEE Journal of Quantum Electronics*, vol. 41, 2005, pp. 774–778.

Semiconductor All-Optical Modulator for Synchronization of Independent Fiber Laser Oscillators and Active Mode-Locking

Robert Herda, Matei Rusu, Anne Vainionpää, Soile Suomalainen, Olli Tengvall, and Oleg G. Okhotnikov

***Abstract*—Using an optically driven nonlinear semiconductor mirror, we have synchronized a 1.56-μm mode-locked erbium fiber laser to the pulse train from a mode-locked ytterbium fiber laser operating at 1.05 μm. We demonstrate that a robust active or passive mode-locked picosecond pulse operation and tight control of the repetition rate can be obtained resulting in a large value of the locking tolerance for the slave laser cavity mismatch exceeding 250 μm.**

***Index Terms*—Mode-locked lasers, nonlinear optics, optical fiber lasers, quantum-well devices, ultrafast optics.**

I. Introduction

SEMICONDUCTOR saturable absorber mirror (SESAM) technology has greatly pushed the development of passively mode-locked fiber lasers. Recently, pulse trains covering the vast wavelength range from 895 to 1560 nm were reported using neodymium, ytterbium and erbium mode-locked fiber lasers [1]–[4]. Essential improvement in the performance of passively mode-locked lasers needed for a variety of applications can be realized when the pulse train is stabilized or locked to an external clock. This requires several active or hybrid mode-locking techniques to be implemented. Different fields of science and technology have also a strong need to pursue research using ultrafast lasers in an arrangement called two-color experiment. Two-color sources are valuable instruments for ultrafast research including difference-, harmonic- and sum-frequency generation, coherent anti-Stokes Raman scattering microscopy, and two-color pump-probe investigations. For most applications, the relative jitter between the laser pulses is a crucial factor severely limiting the performance of the system. Various schemes for synchronization of ultrafast solid-state lasers with different wavelengths have been the objective of a number of studies [5]–[7]. Recently, we demonstrated passive synchronization between two fiber lasers using cross-phase modulation (XPM) in optical fiber [8]–[10]. Due to the long interaction length and good spatial overlap of the fields in the single-mode fiber, two laser oscillators with central wavelengths around 1.56 and 1.05 μm were firmly synchronized with a locking range larger by an order of magnitude than previously reported results in solid-state systems.

Manuscript received December 13, 2004; revised February 17, 2005.

The authors are with the Optoelectronics Research Centre, Tampere University of Technology, Tampere FIN-33720, Finland (e-mail: robert.herda@orc.tut.fi).

Digital Object Identifier 10.1109/JQE.2005.846687

Although the large normal group-velocity dispersion of the 1-μm Yb-fiber and the overall cavity dispersion of the 1.56-μm Er-fiber laser were compensated, it is, however, obvious that when the cavity frequencies of both lasers are equalized, the local cavity dispersion and the group velocities are still different at different wavelengths. Therefore, the interaction through XPM is strongly influenced by the pulse walk-off time. Hence, the walk-off length for 1.05- and 1.56-μm pulses in the "two-color" interaction section of the slave laser cavity is a factor that eventually limits the achievable modulation depth.

Here, we demonstrate a technique for mode-locked fiber laser stabilization based on nonlinearity of the semiconductor modulator mirror (SEMM) [11]–[14]. Short interaction length and high nonlinearity of the semiconductor material allow for enhanced modulation depth and, consequently, tight laser synchronization. Moreover, we found that the 1.56-μm slave laser can be actively mode-locked by the 1.05-μm master pulse train that drives optically the semiconductor mirror. This provides a complete control of the dynamics of the slave laser, including the start-up of the pulse operation.

The stabilization technique we demonstrate here should be applicable to different types of mode-locked fiber lasers used in the systems that require low-jitter ultrashort pulse oscillators.

Contrary to the locking technique demonstrated in [14], we exploit in our modulator saturable absorption and, therefore, cross-amplitude modulation as a nonlinear effect [11] rather than refractivity change due to free-carrier generation. Particularly, tuning the wavelength of the laser did not result in notable change in the modulator performance as expected with a Fabry–Pérot modulator based on refractive effects.

It was shown that to reliably start and operate a fiber laser in a mode-locking regime, it is desirable to have a quite high modulation depth [15], and a resonant absorptive nonlinearity is a convenient way to achieve a highly nonlinear response of the semiconductor reflector.

II. Experimental Setup and Semiconductor Modulator Characteristics

The experimental setup for a two-color mode-locked fiber source is illustrated in Fig. 1. Laser synchronization is performed by optical injection of the master source signal into the slave cavity through a 1050/1560 dichroic beam splitter. The master source was protected against back-reflections or coupling with the captured slave oscillator.

The slave erbium laser has a linear cavity terminated by the SEMM at one end and a short length fiber loop mirror at the

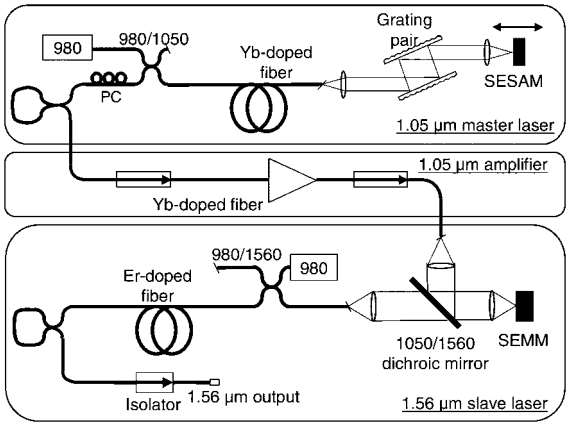

Fig. 1. Two-color laser system setup.

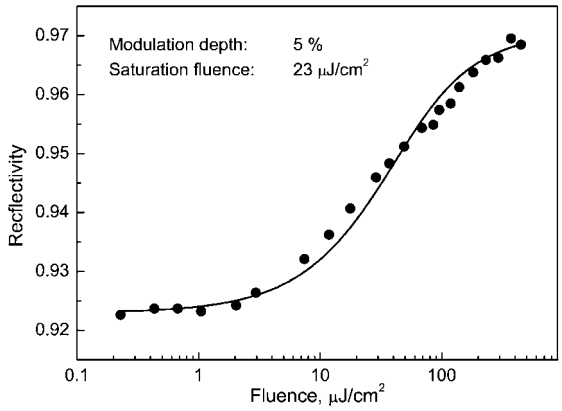

Fig. 2. Typical nonlinear reflectivity curve of SEMM used for all-optical synchronization.

other. Optical gain was provided by a 2-m-long erbium-doped fiber with 26-dB/m absorption at 980 nm.

The master laser is a stable, linear cavity laser passively mode-locked by a SESAM [1]. The gain medium consisted of a 70-cm-long piece of Yb-doped fiber with 434-dB/m absorption at 980 nm. The 1200-mm^{-1} grating pair placed in the free space section of the cavity compensated for the large normal dispersion of the intracavity fiber. A core-pumped fiber amplifier was employed to boost the average power of the master oscillator up to 30 mW. SESAM-based self-starting passive mode-locking was achieved in the master laser, resulting in 2-ps pulses with sech^2 shape. To ensure master laser protection against back reflections from the slave cavity, two optical isolators were placed at the input of the amplifier and before beam combiner to achieve one-way coupling from the master to the slave laser. The SESAM-lens assembly terminating the master laser cavity at one end can be translated axially, thus allowing for cavity length and, therefore, laser repetition rate control. The loop mirrors in both lasers served as an output coupler. The master laser repetition rate was measured to be around 30 MHz. By changing the fiber length and shifting the SEMM-lens holder, the cavity length of the master laser was tuned to be close to the cavity length of the slave oscillator. When sufficient modulation depth was achieved by maximizing the spatial overlap of the 1.56- and 1.05-μm incident fields, laser synchronization sets up.

The locking behavior was then investigated by fine-tuning the master cavity length using the translation stage. Movement of the SESAM-lens assembly was monitored using an inductive gauge with reading precision of 0.5 μm. The outputs of the master and slave lasers were detected and fed to the input of an electrical spectrum analyzer that allows for simultaneous monitoring the repetition rates of both oscillators.

The 1.05-μm SESAM and 1.56-μm SEMMs are grown with solid-source molecular-beam epitaxy (MBE) and details were given elsewhere [1]–[4]. In this study we have used GaAs-based technology for both 1- and 1.56-μm spectral ranges, as described in [4]. It was demonstrated that mode-locked fiber lasers operating in a broad spectral range covering 0.9–1.6 μm wavelengths can be built on GaAs substrates using excellent characteristics of AlAs–GaAs distributed Bragg reflectors. The key component is the multiple-quantum-well absorber mirror, notably, a dilute nitride SESAM. The absorption regions of SESAMs are made of compressively strained GaInAs–GaAs or novel GaInNAs–GaAs quantum wells grown monolithically by MBE on GaAs substrates, covering the entire spectral range from 0.9 to 1.6 μm. These SESAMs supply a strong mechanism for picosecond pulse generation that is entirely self-starting for a wide range of cavity dispersion and ensures stability against Q-switched mode-locking. Throughout the experiments, the mirror structures with different recovery times have been tested as a SEMM. Although it was well established that fast recovery time is an important issue in achieving a reliable self-starting pulse operation, particularly in fiber lasers [16], we have found that optimal speed of the SEMM used as a locking instrument represents a tradeoff between pulse duration and tolerance for cavity-length mismatch.

To determine the characteristics of the SEMM, we measured the reflectivity change of the device at operation wavelength for various pump powers. The modulation depth of the SEMMs we studied was in all cases between 2% and 5%. Typical nonlinear response of the modulator mirror is shown in Fig. 2.

The SEMM absorption was well saturated with an average fluence of 3000 μJ/cm^2 at 1 μm, which we used in the locking experiments.

III. All-Optical Synchronization of Passively Mode-Locked Lasers

Two different operation regimes have been distinguished depending on the characteristics of the SEMM. Mirrors with fast recovery time of the absorption of $\tau_{\mathrm{rt}} < 50$ ps achieved by ion irradiation could efficiently start and stabilize the passive mode-locking of the slave laser. Slow SEMMs comprising an as-grown structure could not initiate passive mode-locking and, therefore, supported only quasi-continuous wave (CW) or Q-switched operation of the slave laser. In both cases, however, synchronized mode-locked operation was achieved by injecting the control signal from the master oscillator provided that the cavity-length mismatch approached the locking tolerance. In the latter case

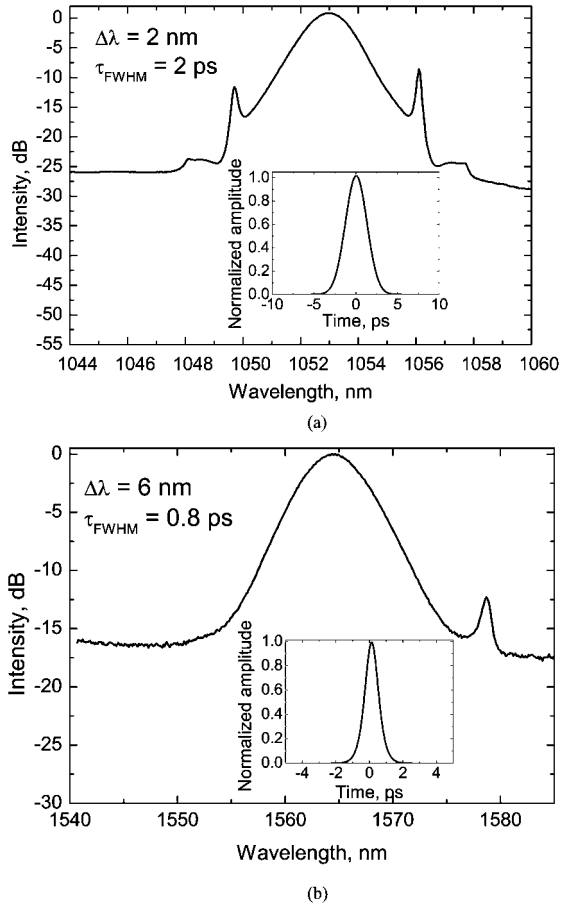

Fig. 3. Wavelength spectra and intensity autocorrelations (inset) for (a) master laser and (b) slave laser in locked state.

of a slow SEMM, the appearance of the synchronized state corresponded to the onset of the active mode-locking. Obviously, the synchronization mechanism and, consequently, the cavity-length mismatch tolerance are dependent on the character of mode-locking in the slave laser.

It should also be noted here that in the present experiments contrary to the laser configuration described in [14], the SEMM can start passive mode-locking of the slave laser and lock the oscillator to the master source, simultaneously. In turn, this results in a simple and robust laser cavity that does not require two semiconductor reflectors to be used in the slave laser cavity.

When the SEMM acts as a trigger for passive mode-locking, the duration of the nearly transform-limited pulses was usually ranging from a few picoseconds to subpicosecond values due to the efficient pulse shaping mechanism provided by the fast mirror.

The pulse widths of 2 ps for the master and 0.8 ps for the slave oscillator were deduced from the intensity autocorrelation measurements, assuming a sech^2 shape. The intensity autocorrelations and corresponding spectra are shown in Fig. 3(a) and (b).

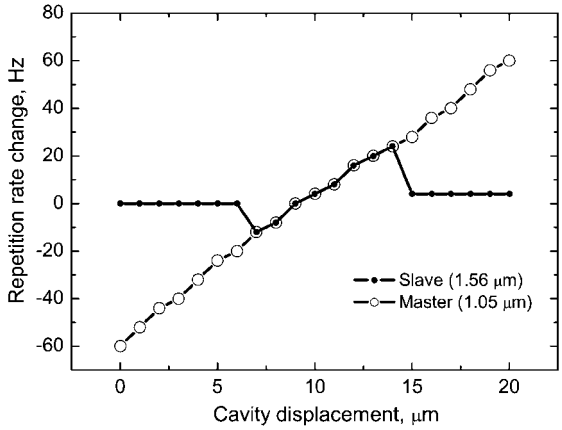

Fig. 4. Master and slave laser repetition rates versus master cavity-length detuning.

By changing the slave laser cavity length, while recording the cavity elongation together with repetition rate for both lasers, the slave laser pulse train could be easily set to be locked to the master pulses. Fig. 4 shows the repetition rate of the slave and maser lasers as a function of the SESAM-assembly displacement. When master and slave laser are synchronized their repetition rate stays equal despite a change in the master laser repetition rate.

Stable synchronization was maintained within the locking range even under continuous changing of the slave cavity length. As shown in Fig. 4, a slave cavity-length mismatch of 7 μm is tolerable without losing the locking state. In these measurements, the average power of the modulation signal at the output of the amplifier was 30 mW, whereas the slave laser average power was about 10 mW.

The synchronized two-color operation of the master-slave system was independently explored by monitoring the master and slave pulse trains on an analogue scope, as shown in Fig. 5, where the oscilloscope was triggered with the signal from master source. In nonsynchronized (free-running) operation, shown in Fig. 5(a), the pulse train from the slave laser (top trace) cannot be clearly seen on the scope. In contrast seeding the SEMM with the master pulse train initiated synchronized operation mode and allowed the slave laser train to be clearly viewed on the scope, as shown in Fig. 5(b).

It is expected that the cavity-length tolerance that ensures synchronization increases for mode-locked lasers with longer pulses [17]. The cavity mismatch was measured when the pulsewidth of the slave laser was increased with a bandwidth-limited optical filter inserted in the slave laser cavity. The spectral width of pulses was reduced down to 0.3 nm resulting in pulse duration of 10 ps. The cavity-length tolerance was measured to increase up to 40 μm.

IV. Active Mode-Locking by All-Optical Modulation

With a slow absorber mirror that cannot start passive mode-locking the support of active mode-locking is possible when it is driven optically by the pulse train from master laser.

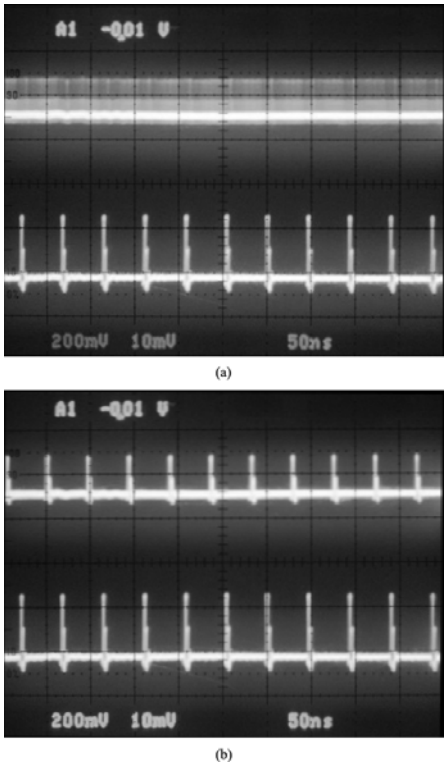

Fig. 5. Oscilloscope traces of (a) unlocked and (b) locked pulse trains. Top traces show the 1.56-μm pulse train from the slave oscillator and the bottom trace the 1.05-μm pulse train from the master laser. The oscilloscope is triggered to the master laser pulse train.

The cavity-length mismatch tolerance is based on a phenomenon that relates to the detuning effects in actively modes-locked lasers [17]. With the SEMM initiating active mode-locking, it is expected that the cavity-length mismatch limitations are much relaxed. Indeed, we could obtain a cavity-length mismatch up to 400 μm, when the slave laser was forced to operate actively in the mode-locked regime by injecting the control signal from master source. It should be noted, however, that detuning effects cause some deterioration in the mode-locked behavior. It was found that although a slow SEMM ensures reliable active mode-locked operation with large cavity-length tolerance, the autocorrelation shows wings or multiple-subpulse behavior due to long low-loss window in the SEMM reflectivity opened by the driving pulse from the master oscillator. In attempts to optimize the system performance, we have achieved clean pulses with duration of 30 ps, as shown in Fig. 6, using SEMM irradiated with low dose of ions to keep the recovery time $\tau_{\rm rt} \geq 100$ ps.

With the large cavity-length tolerance of the locking state of ≥ 250 μm obtained in this configuration, it was possible to maintain the synchronization state for long time without any cavity stabilization.

The active mode-locking nature of the slave laser operation is illustrated by the oscilloscope traces presented in Fig. 7(a) and (b).

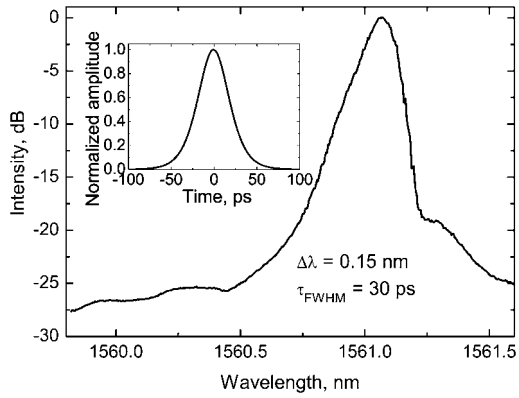

Fig. 6. Optical spectra and autocorrelation trace (inset) of the actively mode-locked slave laser.

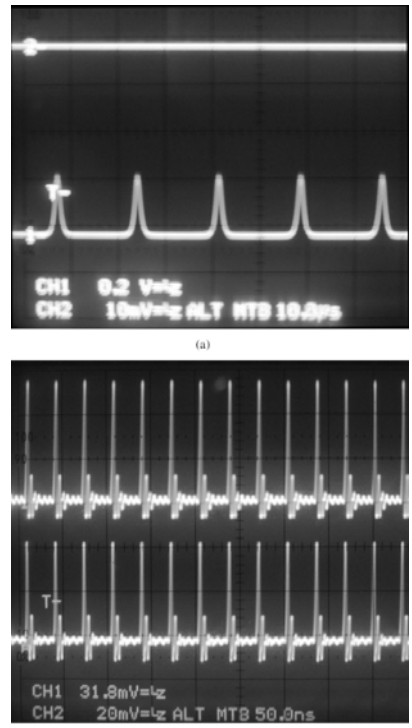

Fig. 7. Active mode-locking of the 1.56-μm slave laser using all optical SEMM. (a) Without 1.05-μm control signal (top trace); bottom trace shows 1.56-μm output (time scale -10 μs/div). (b) With control signal; top trace shows 1.05-μm seed signal. Bottom trace corresponds to active mode-locking regime of 1.56-μm slave oscillator (time scale -50 ns/div).

Without a control signal from the master laser, the slave laser did not start mode-locking and exhibited a passively Q-switched operation, as illustrated in Fig. 7(a). The passively Q-switched operation is caused by the high modulation depth of the absorber in combination with a high value of the saturation energy [18]. In contrast all-optical modulation provided by the SEMM,

driven with the signal from the mode-locked master source saturates synchronously the SEMM absorption and prevents the slave laser from passive Q-switching. Actively mode-locked operation of the slave laser achieved with the control signal from the master source is shown in Fig. 7(b).

V. Conclusion

We demonstrate that the absorptive nonlinearity of a semiconductor reflector controlled optically by the seed signal from a pulsed master oscillator can efficiently stabilize the subpicosecond pulse train from passively mode-locked slave laser. For a modulation depth of $<5\%$ and an average power of the control signal below 30 mW, the cavity-length mismatch tolerance $\sim 10\ \mu$m was achieved with a pulse duration of 0.8 ps and a mismatch of 40 μm with a pulse duration of 10 ps.

The capability of the modulator mirror allows for active mode-locking of the slave oscillator. Using a modulator with an optimized recovery time, clean 30-ps pulses were generated with a large cavity-length mismatch tolerance of $\sim 250\ \mu$m synchronized to the control signal.

References

[1] O. G. Okhotnikov, L. Gomes, N. Xiang, T. Jouhti, and A. B. Grudinin, "Mode-locked ytterbium fiber laser tunable in the 980–1070-nm spectral range," *Opt. Lett.*, vol. 28, pp. 1522–1524, 2003.

[2] O. G. Okhotnikov, T. Jouhti, J. Konttinen, S. Karirinne, and M. Pessa, "1.5-μm monolithic GaInNAs semiconductor saturable-absorber mode locking of an erbium fiber laser," *Opt. Lett.*, vol. 28, pp. 364–366, 2003.

[3] M. Rusu, S. Karirinne, M. Guina, A. B. Grudinin, and O. G. Okhotnikov, "Femtosecond neodymium-doped fiber laser operating in the 894–909 nm spectral range," *IEEE Photon Technol. Lett.*, vol. 16, no. 4, pp. 1029–1031, Apr. 2004.

[4] O. G. Okhotnikov, A. B. Grudinin, and M. Pessa, "Ultra-fast fiber systems based on sesam technology: New horizons and applications," *New J. Phys.*, vol. 6, pp. 177–177, Nov. 2004.

[5] R. J. Jones and J. C. Diels, "Stabilization of femtosecond lasers for optical frequency metrology and direct optical to radio frequency synthesis," *Phys. Rev. Lett.*, vol. 86, pp. 3288–3291, 2001.

[6] S. T. Cundiff, "Phase stabilization of ultrashort optical pulses," *J. Phys. D.*, vol. 35, pp. R43–R43, 2002.

[7] J. Rauschenberger, T. M. Fortier, D. J. Jones, J. Ye, and S. T. Cundiff, "Control of the frequency comb from a mode-locked erbium-doped fiber laser," *Opt. Exp.*, vol. 10, pp. 1404–1410, 2002.

[8] M. Rusu, R. Herda, and O. G. Okhotnikov, "Passively synchronized erbium (1550 nm) and ytterbium (1040 nm) mode-locked fiber lasers sharing the cavity," *Opt. Lett.*, vol. 29, pp. 2246–2248, 2004.

[9] ——, "Passively synchronized two-color mode-locked fiber system based on master-slave lasers geometry," *Opt. Exp.*, vol. 12, pp. 4719–4724, 2004.

[10] ——, "1.05-μm mode-locked ytterbium fiber laser stabilized with the pulse train from a 1.54-μm laser diode," *Opt. Exp.*, vol. 12, pp. 5258–5262, 2004.

[11] N. H. Bonadeo, W. H. Knox, J. M. Roth, and K. Bergman, "Passive harmonic mode-locked soliton fiber laser stabilized by an optically pumped saturable bragg reflector," *Opt. Lett.*, vol. 25, pp. 1421–1423, 2000.

[12] M. Guina and O. G. Okhotnikov, "Harmonically mode-locked laser stabilized by semiconductor saturable absorber modulated with the residual pump," *Appl. Phys. B.*, vol. 75, pp. 127–130, 2002.

[13] ——, "Harmonic mode-locking by synchronous optical pumping of a saturable absorber with the residual pump," *Opt. Lett.*, vol. 28, pp. 358–360, 2003.

[14] W. Seitz, R. Ell, U. Morgner, and F. X. Kärtner, "All-optical synchronization and mode locking of solid-statelasers with nonlinear semiconductor Fabry-Pérot mirrors," *IEEE J. Sel. Topics Quantum Electron.*, vol. 9, no. 4, pp. 1093–1101, Jul./Aug. 2003.

[15] R. Herda and O. G. Okhotnikov, "Dispersion compensation-free fiber laser mode-locked and stabilized by high-contrast saturable absorber mirror," *IEEE J. Quantum Electron.*, vol. 40, no. 7, pp. 893–899, Jul. 2004.

[16] ——, "Effect of amplified spontaneous emission and absorber mirror recovery time on the dynamics of the mode-locked fiber lasers," *Appl. Phys. Lett.*, vol. 86, pp. 011 113–011 113, Jan. 2005.

[17] A. E. Siegman, *Lasers*. Sausalito, CA: Univ. Science Books, 1986.

[18] C. Hönninger, R. Paschotta, F. Morier-Genoud, M. Moser, and U. Keller, "*Q*-switching stability limits of continuous-wave passive mode locking," *J. Opt. Soc. Amer. B*, vol. 16, pp. 46–56, 1999.

Robert Herda was born in Jena, Germany, in 1977. He received the M.Sc. degree at the Institute of Applied Physics, Friedrich Schiller University, Jena, Germany, in 2003. He is currently working toward the Ph.D. degree at the Optoelectronics Research Centre, Tampere University of Technology, Tampere, Finland.

His current research focuses on the experimental work and the modeling of the generation and nonlinear interaction of ultrashort pulses.

Matei Rusu received the M.Sc. degree in electronics engineering from the Tampere University of Technology, Tampere, Finland, in 2002, where he is currently working toward the Ph.D. degree in technical physics.

His doctoral research concerns applications of ultrafast fiber lasers.

Anne-Maria Vainionpää was born in Pirkkala, Finland, in 1976. She received the M.Sc. degree in electrical engineering from the Tampere University of Technology, Tampere, Finland, in 2000. She is currently working toward the Ph.D. degree at the Optoelectronics Research Centre, Tampere University of Technology.

Her current research is focused on the molecular beam epitaxy of III–V compound semiconductor devices for generating ultrashort pulses for optical communication.

Soile Suomalainen received the M.Sc. degree from the Optoelectronics Research Centre (ORC), Tampere University of Technology, Tampere, Finland, in 2003, where she is currently working toward the Ph.D. degree.

Her doctoral research concerns implementation and characterization of novel III–V semiconductor devices grown by molecular beam epitaxy.

Olli Tengvall was born in 1980. He is currently working toward the M.Sc. degree at the Optoelectronics Research Centre, Tampere University of Technology, Tampere, Finland.

His studies involve fabrication and design of delicate III–V semiconductor optoelectronical devices, particularly SESAMs.

Oleg G. Okhotnikov received the Ph.D. degree from P.N. Lebedev Physical Institute, Moscow, Russia, and the D.Sc. degree from General Physics Institute, Russian Academy of Sciences, Moscow, in 1981 and 1992, respectively, both in laser physics.

Since 1999, he has been a Full Professor at the the Optoelectronics Research Centre, Tampere University of Technology, Tampere, Finland. He has published over 100 journal papers and holds six patents.

Appendix 4

Publication 4

R. Herda, T. Hakulinen, S. Suomalainen, and O. G. Okhotnikov, "Cavity-enhanced saturable and two-photon absorption in semiconductors," *Applied Physics Letters*, vol. 87, 2005, pp. 21111051–21111053.

Cavity-enhanced saturable and two-photon absorption in semiconductors

Robert Herda, Tommi Hakulinen, Soile Suomalainen, and Oleg G. Okhotnikov
Optoelectronics Research Centre, Tampere University of Technology, P.O. Box 692, FIN-33101, Tampere, Finland

(Received 15 July 2005; accepted 27 September 2005; published online 14 November 2005)

Two-photon and saturable absorption are studied by placing GaAs and InGaAs materials in a microcavity. We show that field enhancement occurring due to the cavity influences the threshold and dynamic range of rollover in the nonlinear response. This approach can be used in semiconductor laser mirrors with improved capabilities for self-starting passive mode locking with suppressed tendency to Q-switching instability. © *2005 American Institute of Physics*.
[DOI: 10.1063/1.2133924]

Optical limiters or reverse saturable absorbers are devices designed to have high transmittance for low level inputs while blocking the signals with high intensities. The first optical limiters for cw lasers were based on thermal lensing in absorbing liquids, i.e., heating reduced the index causing thermal blooming resulting in a beam that was no longer focused in an imaging system. Then, two-photon absorption, self-focusing in Kerr liquids, nonlinear scattering from carbon particle suspensions and other processes have been suggested for pulsed laser light.[1,2]

The reverse saturable absorber development includes both searching for new limiting materials and nonlinear effects, as well as new optical geometries that improve their performance. Materials with nonlinear optical transmission resulting from two-photon absorption (TPA) are attractive for optical limiting, owing to their high transparency at low input energies.[3] The limiting mechanism is based on the intensity-dependent origin of TPA. For majority of semiconductor materials, the two-photon absorption is small and it becomes significant only at high intensities. For example, for GaAs the two-photon absorption coefficient is 23 cm/GW at $\lambda = 1.06\ \mu$m for 10 ns pulses, consequently, the two-photon absorption in GaAs becomes significant only for intensities higher than 10 MW/cm^2. The efficient limiting caused by TPA in semiconductors could be observed at relatively low average powers only for (sub)picosecond pulses with sufficient pulse peak powers.

Passive mode-locking using semiconductor saturable absorbers have been shown to be a powerful technology for producing ultrashort pulses from various lasers. The stability of the mode-locked operation can, however, be degraded because of low-frequency Q-switching instability provoked by the saturable absorption placed into the laser cavity. Avoiding the low-frequency instabilities is possible by using semiconductor saturable absorber mirrors (SESAMs) with reduced modulation depth; however, this solution is not applied to fiber lasers since low modulation in the reflectivity response would not ensure a reliable start of the mode locking.[4] Using optical limiting combined with saturable absorption may be a practical solution for noise suppression and prevent optical damage of the cavity elements.[5–7] The stable operation, though, requires the proper balance between saturable absorption and optical limiting. It is then obvious that fiber lasers requiring SESAMs with high modulation depth for mode-locked operation also need large roll-over in the reflectivity to stabilize the short pulse operation. It should be noted that strong rollover in the SESAM reflectivity for femtosecond pulses is expected with TPA as an instantaneous second-order process. However, the optical limiting due to TPA for picosecond pulses would be too weak to suppress the Q-switching instability. Since TPA effect scales linearly with the interaction length, the boosting of the two-photon absorption simply by increasing the volume of the material may not always be an acceptable solution.

In this paper, we show that the threshold and dynamic range of optical limiting can be improved by placing the TPA material in optical microcavity and adjusted by changing the finesse of the cavity.

Typical saturable absorber mirrors comprise a distributed Bragg reflector (DBR), an absorber usually in a form of quantum-well layers, spacer and cap layers. The semiconductor/air interface, when no antireflection coating is applied, forms together with DBR the microcavity that incorporates saturable absorber and TPA material. In a resonant structure the field intensity I is enhanced by the factor ε compared to the intensity of an antireflection-coated (cavity-free) structure I_0,

$$I = \varepsilon \cdot I_0. \tag{1}$$

The factor ε is given by

$$\varepsilon = \frac{1 - R_T}{(1 + \sqrt{R_T R_S})^2 - 4\sqrt{R_T R_S}\cos^2(\Phi_{rt}/2)}. \tag{2}$$

Here R_t is the reflectivity of the top mirror and Φ_{rt} is the detuning from the resonance. $R_S = R_B \exp(-4\alpha d)$ is the reflectivity of the antireflection-coated structure ($R_T = 0$). $R_B (\approx 1)$ is the reflectivity of the bottom DBR, α is the absorption coefficient, and d is the thickness of the absorber. The reflectivity of the SESAM for the incident pulse with fluence F and duration much shorter than the recovery time of the absorption can be written as

$$R(F) = R_{\mathrm{ns}} - \left[1 - \exp(-F/F_{\mathrm{sat}})\right]\frac{\Delta R}{F/F_{\mathrm{sat}}} - \frac{F}{F_2} \tag{3}$$

(Ref. 8). Here R_{ns} accounts for the nonsaturable loss in the structure, ΔR is the modulation depth of the absorber, F_{sat} is the saturation fluence, and F_2 is the inverse slope of the induced two-photon absorption. The saturation fluence of the absorber placed into the cavity becomes

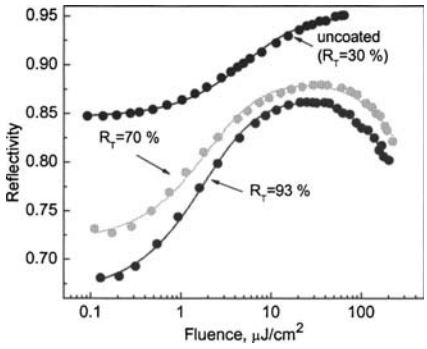

FIG. 1. Nonlinear reflectivity of quantum well absorber mirrors with uncoated top surface, with a top mirror reflectivity of 70% and of 93%.

$$F_{\mathrm{sat}} = \frac{1}{\varepsilon} \cdot F_{\mathrm{sat},0}, \tag{4}$$

while the nonlinear slope is given by

$$F_2 = \frac{1}{\varepsilon^2} \cdot F_{2,0}. \tag{5}$$

The subscript "0" in $F_{\mathrm{sat},0}F_{2,0}$, and ΔR_0 refers to the case of the antireflection-coated structure ($R_t=0$). The reflectivity of the absorber may then be expressed as

$$1 - R_{\mathrm{ns}} + \Delta R = \varepsilon \cdot (1 - R_{ns,0} + \Delta R_0). \tag{6}$$

It can be seen from this expression that the nonlinear contrast of the SESAM can be significantly enhanced with an increase in R_T. For a high-finesse cavity, the two-photon absorption can prevail over the linear absorption because the nonlinear slope scales quadratically with ε. For high values of R_T, the nonlinear reflectivity versus pulse fluence demonstrates a significant inverse saturable absorption feature, i.e., rollover.

The semiconductor reflectors presented here were grown by all-solid-source molecular beam epitaxy. The samples use bottom mirrors comprising 25 pairs of AlAs and GaAs quarter-wave layers forming a DBR with a center wavelength of 1055 nm. The absorber comprises a five 8 nm thick InGaAs quantum well structure placed into a $\lambda/4$ cavity made of GaAs. The GaAs spacer layer provides the dominant contribution to the TPA.

The saturable absorption and optical limiting measurements were carried out using a tunable (1.03–1.06 μm) mode-locked ytterbium fiber laser as a pump source. The laser produces 2 ps pulses with an average power up to 10 mW. The output beam passes the variable attenuator and then it is focused onto the sample using a microscope objective. Figure 1 shows the nonlinear reflectivity of a semiconductor mirror as a function of energy fluence and top mirror reflectivity R_T. The modulation depths of 10%, 17%, and 21% and corresponding saturation fluences of 3, 1.1, and 1.0 μJ/cm^2 were measured for the uncoated, $R_T=70\%$ and $R_T=93\%$ samples, respectively. The inverse nonlinear slope used as a measure of the limiting strength decreases from 3300 μJ/cm^2 for $R_T=70\%$ to 2600 μJ/cm^2 for $R_T=93\%$, revealing significant cavity enhancement of the TPA effect. For the uncoated sample, TPA could not be detected. This figure indicates that TPA-induced rollover in the reflectivity

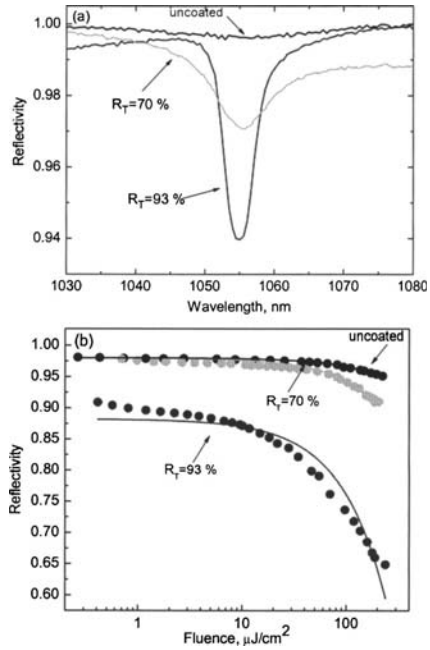

FIG. 2. (a) Spectra of low-intensity reflectivity and (b) nonlinear reflectivity versus pulse fluence for TPA limiting reflectors without saturable absorption. The cavity of the TPA reflectors are formed by the bottom DBR and the top mirror provided by an uncoated semiconductor/air interface or dielectric mirrors with reflectivity of 70% and 93%.

response may decrease the effective modulation depth and may eventually inhibit the self-starting operation. The stability condition for mode-locking against Q switching should, therefore, avoid excessive TPA, thus preventing a significant increase in nonsaturable loss. It is understood that saturation fluence of the linear absorption and the onset of the TPA effect could be to some extent adjusted independently by changing the number of absorbing quantum wells and the thickness of the spacer layer used as a TPA material. Meanwhile, the strength of both effects could be changed by varying the reflectivity R_T of the microcavity top mirror, resulting in field-assisted enhancement of the absorption.

The TPA effect has been further investigated in a similar reflector but without a quantum well absorber, therefore, only two-photon absorption contributes to the nonlinear reflectivity response of the semiconductor reflector. The DBR and spacer layer were identical to those used in the experiments with saturable absorption described above. The optical limiting due to the two-photon absorption was studied in an uncoated sample and structures with $R_T=70\%$ and a $R_T=93\%$. Figures 2(a) and 2(b) show lowintensity and the nonlinear reflectivities, respectively. The nonlinear response of the samples was measured near the resonant wavelength of 1055 nm, seen from the small-signal spectral response presented in Fig. 2(a). Without saturable absorption, the reflectivity gradually decreases with increasing the incident fluence, as seen from Fig. 2(b), owing to the TPA coefficient that increases quadratically with the pulse fluence. The inverse TPA slopes are 7100, 2600, and 800 μJ/cm^2 for the uncoated, 70% and 93% top mirror reflectivity, respectively. The limiting threshold defined as the fluence at which the

transmission begins to deviate from the linear transmission is proportional to the inverse nonlinear slope. Figure 2(b) clearly illustrates the influence of microcavity finesse on the limiting threshold and the strength of rollover. As expected, the strength of rollover increases with the increasing top mirror reflectivity. With shorter pulses, the limiting effect will be significantly enhanced.

In conclusion, in this paper we study the TPA-induced rollover in the saturable mirror reflectivity using field enhancement in semiconductors placed in a microcavity. The results show that the cavity effect commonly used for increasing the modulation depth of saturable absorber influences strongly the two-photon absorption as well. Placing saturable absorber and TPA material into the same microcavity provides additional flexibility in setting up the strength and threshold of two nonlinear effects. Particularly, such a semiconductor structure, when used as a laser mirror, would ensure robust self-staring mode-locked operation with protection against Q-switching instability and optical damage. Otherwise, excessive TPA could decrease significantly the absorber modulation depth, increase effective losses of the SESAM based on such a structure and, eventually, inhibit the self-starting passive mode locking. These features are primarily essential for fiber lasers that typically require high modulation depth and, in turn, strong rollover in the reflectivity at high pulse energies.

The authors gratefully acknowledge the support of the Academy of Finland (No 68580, No 201153, No 108821) and the European Commission (EU FP6 IST STREP, No 511406).

[1]D. J. Hagan, in *Handbook of Optics*, edited by M. Bass (2000), Vol. IV.
[2]C. R. Giuliano and L. D. Hess, IEEE J. Quantum Electron. **3**, 358 (1967).
[3]E. W. Van Stryland, H. Vanherzeele, M. A. Woodall, M. J. Soileau, A. L. Smirl, S. Guha, and T. F. Boggess, Opt. Eng. **24**, 613 (1985).
[4]R. Herda and O. G. Okhotnikov, IEEE J. Quantum Electron. **40**, 893 (2004).
[5]K. P. Komarov and V. D. Ugozhaev, Opt. Spektrosk. **55**, 564 (1983).
[6]A. Del Corno, G. Gabetta, G. C. Reali, V. Kubecek, and J. Marek, Opt. Lett. **15**, 734 (1990).
[7]T. R. Schibli, E. R. Thoen, F. X. Kärtner, and E. P. Ippen, Appl. Phys. B **70**, S41 (2000).
[8]R. Grange, M. Haiml, R. Paschotta, G. J. Spuehler, L. Krainer, M. Golling, O. Ostinelli, and U. Keller, Appl. Phys. B **80**, 151 (2005).

Appendix 5

Publication 5

R. Herda, O. G. Okhotnikov, E. U. Rafailov, W. Sibbett, P. Crittenden, and A. Starodumov, "Semiconductor Quantum-Dot Saturable Absorber Mode-Locked Fiber Laser," *IEEE Photonics Technology Letters*, vol. 18, 2006, pp. 157–159.

Semiconductor Quantum-Dot Saturable Absorber Mode-Locked Fiber Laser

Robert Herda, Oleg G. Okhotnikov, Edik U. Rafailov, *Senior Member, IEEE*, Wilson Sibbett, Paul Crittenden, and Andrei Starodumov

***Abstract*—We demonstrate self-starting passive mode-locking of an ytterbium fiber laser by using a multilayer quantum-dot saturable absorber mirror. A high modulation depth of the absorber ensures robust pulse operation of the fiber laser with a threshold pump power of 30 mW. The 2.8-ps pulses with an average power of 5 mW have been generated at 1042 nm.**

***Index Terms*—Lasers and laser optics, quantum dots (QDs), ultrafast lasers.**

I. Introduction

SIGNIFICANT progress in the fabrication of quantum-dot (QD) lasers using molecular beam epitaxy (MBE) has enabled the realization of both edge-emitting lasers and vertical-cavity surface-emitting lasers that produce relatively high continuous-wave powers [1]. Notably, devices based on QD structures are gaining interest in the generation and amplification of femtosecond pulses because emission/absorption spectra and the optical gain in QD material have an enhanced spectral latitude associated with the distribution of dot sizes [2], [3].

Recent progress in ultrafast laser science and technology has been enhanced by the further development of semiconductor saturable absorber mirrors (SESAMs) that take advantage of advanced bandgap engineering and semiconductor growth technology. The designs of SESAMs demonstrated so far are based predominantly on quantum-well (QW) materials.

It was shown that the absorber recovery time has tremendous effect of the start-up of the mode-locking in fiber lasers [4]. Particularly, the SESAMs with fast nonlinear response are less affected by high-intensity amplified spontaneous emission typical for fiber lasers. Consequently, fast absorbers exhibit better self-starting capability compared with slow absorbers.

The use of QD absorbers is a promising approach to achieve fast structures without additional actions related to the post-growth processes needed to reduced the recovery time of the absorption.

Manuscript received July 11, 2005; revised September 25, 2005.

R. Herda and O. G. Okhotnikov are with the Optoelectronics Research Centre, Tampere University of Technology, FIN-333101 Tampere, Finland (e-mail: robert.herda@tut.fi).

E. U. Rafailov is with the Electronic Engineering and Physics Division, University of Dundee, Dundee DD1 4HN5, U.K. (e-mail: e.u.rafailov@dundee.ac.uk).

W. Sibbett is with the School of Physics and Astronomy, University of St. Andrews, St. Andrews, Fife KY16 9SS, U.K. (e-mail: ws@st-and.ac.uk).

P. Crittenden and A. Starodumov are with Coherent Inc., Santa Clara, CA, 95054 USA (e-mail: andrei.starodoumov@coherent.com).

Digital Object Identifier 10.1109/LPT.2005.860376

In this connection, the potential of QD semiconductors when incorporated into ultrashort-pulse lasers has yet to be explored and documented.

The fast carrier dynamics of QD structures facilitate the deployment of such materials as fast saturable absorbers in mode-locked lasers. This approach was successfully demonstrated in solid-state lasers [5]. The SESAM technology has also led to advances in mode-locked fiber lasers. The main features of these—high efficiency, reliability, small footprint, and the option for all-fiber design—make them promising candidates for applications traditionally covered by ultrafast solid-state lasers. In addition, the broad fluorescence spectrum makes different fiber-based gain media attractive for tunable and ultrashort pulse sources. Recently, pulse sequences covering the impressive wavelength range from 895 to 1560 nm were reported using neodymium, ytterbium- and erbium-doped, mode-locked, fiber lasers [6]–[8]. In this letter we present, for the first time, experimental data that demonstrate passive mode-locking of an Yb-doped fiber laser initiated and stabilized by using a saturable absorber mirror comprising an 80-layer QD structure within a distributed Bragg reflector.

II. Absorber Mirror Structure and Parameters

The QD absorber mirror studied in this work was grown by MBE (NL Nanosemiconductor GmbH) on a GaAs (100) substrate. The mirror consists of 33 pairs of $Al_{0.9}Ga_{0.1}As$–GaAs quarterwave layers forming a Bragg reflector having a center wavelength of 1060 nm and approximately 100-nm bandwidth. The absorber section of the structure consisted of eight multiple stacks of ten InGaAs QD layers with 10-nm-thick spacer layers of GaAs. Adjacent multiple stacks were separated by 23.7 nm of high-temperature grown GaAs to eliminate the effects of indium segregation and 13.7 nm of low-temperature grown GaAs to decrease the carrier lifetime. The linear and nonlinear reflectivities of the 80-layer SESAM are shown in Fig. 1(a) and 1(b), respectively.

The modulation depth of the QD SESAM and the saturation fluence measured at 1042 nm were 17.6% and 14.8 μJ/cm^2, respectively. The unsaturated low-intensity reflectivity shown in Fig. 1(a) reveals the resonant character of QD absorber mirror. It should be noted that the high modulation depth of the nonlinear response is expected near 1042 nm because this corresponds to the spectral "hole" in the unsaturated reflectivity. Indeed, the highest modulation depth in the intensity-dependent response (above 17%) was measured at this wavelength, as shown in Fig. 1(b). Consequently, the modulation depth gradually decreases with detuning from the resonant wavelength.

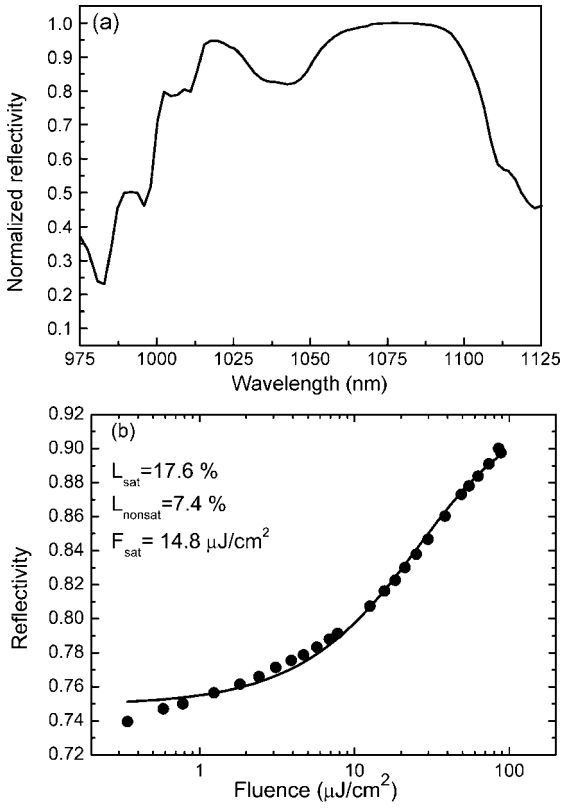

Fig. 1. (a) Low intensity reflectivity spectrum of the QD SESAM structure and (b) reflectivity change versus pulse energy density measured at 1042 nm. The absorption parameters derived from the fitting of the experimental data are: the saturable loss $L_{\rm sat}$; the nonsaturable loss $L_{\rm nonsat}$; the saturation fluence $F_{\rm sat}$.

III. Ytterbium Fiber Laser Mode-Locked With a QD Saturable Absorber Mirror

The performance of the absorber mirror was studied in a laser using Yb-doped fiber as a gain medium within the cavity configuration shown in Fig. 2.

The laser cavity contains a 75-cm-long piece of Yb-doped fiber with absorption of 434 dB/m at 980 nm. The active fiber was pumped through a 980/1050 nm wavelength-selective coupler. The output coupler was provided by a tap coupler.

The cavity was terminated by a broad-band high-reflectivity mirror and the QD absorber mirror. The light was focused onto the absorber by an antireflection-coated objective with a numerical aperture of 0.5. A tunable intracavity 3-nm bandwidth filter was used to optimize the mode-locked operation.

Optimum focusing of the laser beam onto an absorber mirror resulted in self-starting mode-locking at 1042 nm and it was clearly evident that this was initiated and stabilized by the saturation dynamics of the QD structure. Stable mode-locking has been obtained at 1040 nm with a very low threshold pump power of 30 mW at 980 nm for an output coupler of 7%. Fig. 3 shows

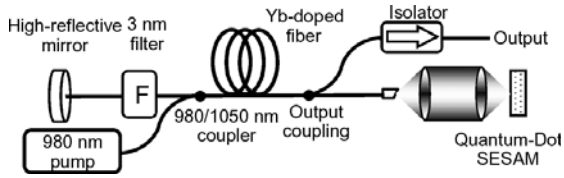

Fig. 2. Setup of the laser used to test the absorber. The overall dispersion of the cavity is estimated to be -0.1 ps/nm.

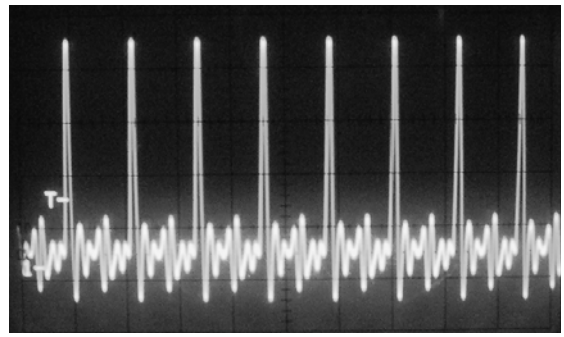

Fig. 3. Oscilloscope trace of mode-locked pulse sequence.

the stable pulse sequence displayed on using an analogue oscilloscope. A sequence of pulses at 50-MHz repetition rate with an average output power of 5 mW was obtained for a pump power of 100 mW and 30% output coupling.

The optical spectrum and the intensity autocorrelation are included as Fig. 4(a), (b). The spectral bandwidth and the pulse duration, assuming a Gaussian pulse shape, are 0.6 nm and 2.8 ps, respectively, with a time-bandwidth product of 0.5. The low value of time-bandwidth product despite the high normal dispersion of the laser cavity indicates a strong pulse shaping provided by an SESAM having a high modulation contrast and a short recovery time. It is important to note that owing to the high modulation depth of the nonlinear reflectivity, stable mode-locking was achieved without using any dispersion compensation inside the laser cavity.

The significance of the high modulation depth in the multilayer QD SESAM nonlinear response for achieving self-starting mode-locked operation from fiber lasers was further confirmed through the spectral tuning. It was found that while mode-locking around 1042 nm could be obtained at very low pump powers, the pulse operation at 1064 nm required a much higher pump power above that exceeded 150 mW. The pulse duration at this wavelength increased and the pulse train exhibited some low-frequency instability. This observation is in agreement with results on QW-based SESAMs presented in [4], [9] and implies that high modulation depth absorbers are appropriate for lasers having high cavity dispersion and high levels of spontaneous emission. In this respect, an especially important result of this study is the demonstration that a sufficiently high modulation depth is achievable in the response of multilayered QD semiconductor SESAMs and is sufficient for the self-started mode-locking of fiber lasers.

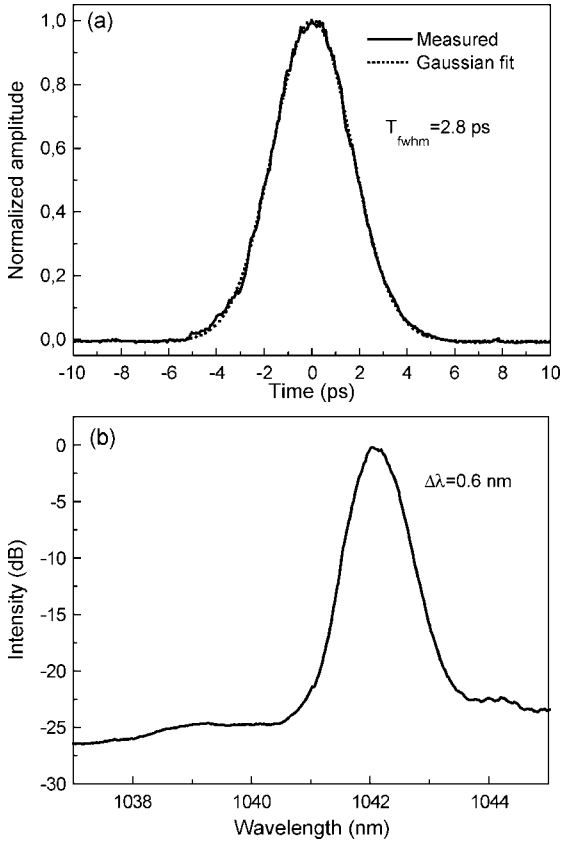

Fig. 4. (a) Intensity autocorrelation and (b) optical spectrum of the mode-locked Yb-doped fiber laser. The time-bandwidth product is 0.5 assuming a Gaussian pulse shape.

IV. Conclusion

We have demonstrated a passively mode-locked fiber laser using a high modulation depth absorber using a multilayer QD SESAM. A low-threshold self-starting mode-locked operation has been obtained with a simple laser cavity that operates well even without dispersion compensation. Sequences of sub-3-ps pulses at repetition rates of ∼50 MHz with an average output power of 5 mW at wavelengths around 1040 nm were obtained.

Acknowledgment

The authors thank NL Nanosemiconductor GmbH for providing the QD structure.

References

[1] A. R. Kovsh, N. N. Ledentsov, A. E. Zhukov, D. A. Livshits, N. A. Maleev, M. V. Maximov, V. M. Ustinov, J.-S. Wang, J. Y. Chi, D. N. Ouyang, D. Bimberg, and J. A. Lott, "Long-wavelength (1.3 to 1.5 μm) quantum dot lasers based on GaAs," in *Proc. SPIE 2004*, San Jose, CA, 2004, Paper 5349-06.

[2] P. Borri, W. Langbein, J. M. Hvam, F. Heinrichsdorff, M.-H. Mao, and D. Bimberg, "Spectral hole-burning and carrier-heating dynamics in In-GaAs quantum-dot amplifiers," *IEEE J. Sel. Topics Quantum Electron.*, vol. 28, no. 3, pp. 544–551, May/Jun. 2000.

[3] E. U. Rafailov, P. Loza-Alvarez, W. Sibbett, G. S. Sokolovskii, D. A. Livshits, A. E. Zhukov, and V. M. Ustinov, "Amplification of femtosecond pulses over by 18 dB in quantum-dot semiconductor optical amplifier," *IEEE Photon. Technol. Lett.*, vol. 15, no. 8, pp. 1023–1025, Aug. 2003.

[4] R. Herda and O. G. Okhotnikov, "Effect of amplified spontaneous emission and absorber mirror recovery time on the dynamics of the mode-locked fiber lasers," *Appl. Phys. Lett.*, vol. 86, p. 011 113, 2005.

[5] E. U. Rafailov, S. J. White, A. A. Lagatsky, A. Miller, W. Sibbett, D. A. Livshits, A. E. Zhukov, and V. M. Ustinov, "Fast quantum-dot saturable absorber for passive mode-locking of solid-state lasers," *IEEE Photon. Technol. Lett.*, vol. 16, no. 11, pp. 2439–2441, Nov. 2004.

[6] O. G. Okhotnikov, L. Gomes, N. Xiang, T. Jouhti, and A. B. Grudinin, "Mode-locked ytterbium fiber laser tunable in the 980–1070-nm spectral range," *Opt. Lett.*, vol. 28, pp. 1522–1524, 2003.

[7] O. G. Okhotnikov, T. Jouhti, J. Konttinen, S. Karirinne, and M. Pessa, "1.5-μm monolithic GaInNAs semiconductor saturable-absorber mode-locking of an erbium fiber laser," *Opt. Lett.*, vol. 28, pp. 364–366, 2003.

[8] M. Rusu, S. Karirinne, M. Guina, A. B. Grudinin, and O. G. Okhotnikov, "Femtosecond neodymium-doped fiber laser operating in the 894–909-nm spectral range," *IEEE Photon. Technol. Lett.*, vol. 16, no. 4, pp. 1029–1031, Apr. 2004.

[9] R. Herda and O. G. Okhotnikov, "Dispersion compensation-free fiber laser mode-locked and stabilized by high-contrast saturable absorber mirror," *IEEE J. Quantum Electron.*, vol. 40, no. 7, pp. 893–899, Jul. 2004.

Tampereen teknillinen yliopisto
PL 527
33101 Tampere

Tampere University of Technology
P.O. Box 527
FIN-33101 Tampere, Finland